

Advanced oxidation processes applied to mineralize paracetamol, chloroxylenol, ibuprofen and diclofenac in aqueous medium

Mètodes d'oxidació avançada aplicats a la mineralització del paracetamol, cloroxilenol, ibuprofè i diclofenac en medi aquós

Marcel Skoumal i Canals

ADVERTIMENT. La consulta d'aquesta tesi queda condicionada a l'acceptació de les següents condicions d'ús: La difusió d'aquesta tesi per mitjà del servei TDX (www.tesisenxarxa.net) ha estat autoritzada pels titulars dels drets de propietat intel·lectual únicament per a usos privats emmarcats en activitats d'investigació i docència. No s'autoritza la seva reproducció amb finalitats de lucre ni la seva difusió i posada a disposició des d'un lloc aliè al servei TDX. No s'autoritza la presentació del seu contingut en una finestra o marc aliè a TDX (framing). Aquesta reserva de drets afecta tant al resum de presentació de la tesi com als seus continguts. En la utilització o cita de parts de la tesi és obligat indicar el nom de la persona autora.

ADVERTENCIA. La consulta de esta tesis queda condicionada a la aceptación de las siguientes condiciones de uso: La difusión de esta tesis por medio del servicio TDR (www.tesisenred.net) ha sido autorizada por los titulares de los derechos de propiedad intelectual únicamente para usos privados enmarcados en actividades de investigación y docencia. No se autoriza su reproducción con finalidades de lucro ni su difusión y puesta a disposición desde un sitio ajeno al servicio TDR. No se autoriza la presentación de su contenido en una ventana o marco ajeno a TDR (framing). Esta reserva de derechos afecta tanto al resumen de presentación de la tesis como a sus contenidos. En la utilización o cita de partes de la tesis es obligado indicar el nombre de la persona autora.

WARNING. On having consulted this thesis you're accepting the following use conditions: Spreading this thesis by the TDX (www.tesisenxarxa.net) service has been authorized by the titular of the intellectual property rights only for private uses placed in investigation and teaching activities. Reproduction with lucrative aims is not authorized neither its spreading and availability from a site foreign to the TDX service. Introducing its content in a window or frame foreign to the TDX service is not authorized (framing). This rights affect to the presentation summary of the thesis as well as to its contents. In the using or citation of parts of the thesis it's obliged to indicate the name of the author.

**ADVANCED OXIDATION PROCESSES APPLIED TO MINERALIZE
PARACETAMOL, CHLOROXYLENOL, IBUPROFEN AND DICLOFENAC
IN AQUEOUS MEDIUM**

Doctoral Dissertation

Marcel Skoumal i Canals

Universitat de Barcelona

Departament de Química Física



UNIVERSITAT DE BARCELONA



Laboratori d'Electroquímica de
Materials i del Medi Ambient

6 RESULTS AND DISCUSSION /

RESULTATS I DISCUSSIÓ

6.1 Study of Paracetamol mineralization by means of ozonation / *Estudi de la mineralització del paracetamol mitjançant ozonització*

In this section, the mineralization of paracetamol will be thoroughly studied and discussed. The effect of several factors on the mineralization rate such as the ozone flow, temperature, pH, irradiance and initial concentration value of paracetamol will be analyzed. After that, the study of the occurring intermediates during the mineralization of this analgesic will follow. Several intermediates will be monitored and their evolution with time during several of the applied oxidation treatments will be discussed.

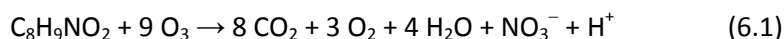
6.1.1 Effect of experimental parameters on paracetamol mineralization / *Efecte de paràmetres experimentals a la mineralització del paracetamol*

The effect of the infused ozone flow and irradiance on the mineralization rate will be studied first. Afterwards, the effect of temperature and the medium pH will be considered. The influence of metal cation catalysts and the initial concentration of the pharmaceutical will finally be studied.

- Influence of ozone flow and irradiance on paracetamol mineralization / *Influència del flux d'ozó i de la irradiància a la mineralització del paracetamol*

During all the ozonation experiments of solutions containing paracetamol, ozone was always continuously supplied into the treated solutions and it was therefore present in the solution during all the time of the experiment. The oxidation efficiency of ozone, which is related to its concentration in solution, is likely to be influenced by the ozone flow rate supplied into the treated solution.

The overall reaction of paracetamol mineralization with ozone can be written as



From this equation, the stoichiometric amount of ozone needed to efficiently oxidize solutions with a TOC content of 100 mg C L^{-1} (equivalent to $157 \text{ mg paracetamol L}^{-1}$) was calculated to be 0.045 g O_3 .

A series of ozonation experiments was carried out at different ozone flow values on paracetamol solutions containing 157 mg L^{-1} of the drug at $25.0 \text{ }^\circ\text{C}$ and $\text{pH } 3.0$. The mineralization extent at each time was evaluated through the TOC (Total Organic Carbon) measurement in the treated solution at different times.

Ozone flow values comprised between 0.5 and $1.0 \text{ g O}_3 \text{ h}^{-1}$ were tested on two different treatments: direct ozonation without catalysis (O_3 method) and ozonation catalyzed with 1 mM Fe^{2+} and 0.25 mM Cu^{2+} , with addition of $22 \text{ mM H}_2\text{O}_2$ and assisted by UV radiation ($\text{O}_3/\text{Fe}^{2+}, \text{Cu}^{2+}/\text{H}_2\text{O}_2/\text{UVA}$ method). The studied range of ozone flow comprises values which supply an amount of ozone situated far above the needed stoichiometric amount of O_3 to transform all 157 mg L^{-1} paracetamol in the 0.1 L cell into CO_2 in 4 hours of treatment.

For the O_3 treatment (i.e. ozone without catalysis), ozone supplied flows of 0.7 and $1.0 \text{ g O}_3 \text{ h}^{-1}$ were tested. The experimental curves obtained from these experiments, displayed in Figure 6.1, practically coincide. The variations of the ozone flow supplied for the direct ozonation treatment did not seem to produce a significant effect on the mineralization rate of the treated paracetamol solutions, since no differences were observed for the abatement curves at these two tested ozone flows.

A better efficiency was expected for the more oxidative $\text{O}_3/\text{Fe}^{2+}, \text{Cu}^{2+}/\text{H}_2\text{O}_2/\text{UVA}$ treatment. This strongly catalyzed treatment leads to a faster mineralization of the drug paracetamol, as shown in the corresponding abatement curves. The sharp descent of its curves could favour the observation of differences between treatments applied at different supplied flow values of ozone. For this treatment, ozone flow values of 0.5 and 1.0 g h^{-1} were applied. The results of these experiments, displayed in Figure 6.1, show a slightly enhanced mineralization behaviour at 1.0 g h^{-1} during the first 60 minutes of the process. However, this effect disappears completely after one hour of experiment. After the first hour of treatment, completely identical mineralization curves are obtained until the finalization of the 4-hour long experiments.

These results lead to the conclusion that an increase of the ozone flow lead to a faster mineralization rate only for highly oxidative ozonation treatments (those catalyzed by metal ions, assisted by radiation, and enhanced by the presence of other oxidants such as H_2O_2).

Even for these treatments, such enhancement is only observed during the first hour of treatment.

The low solubility of ozone in water (109 mg L^{-1} at $25 \text{ }^\circ\text{C}$), which prevents it from accumulating in the solution medium and reaching a higher concentration, and the process of ozone dissolution in water, which is kinetically limited by the low ozone mass transfer into water, explain why the ozone flow does not play a significant role on the paracetamol mineralization rate.

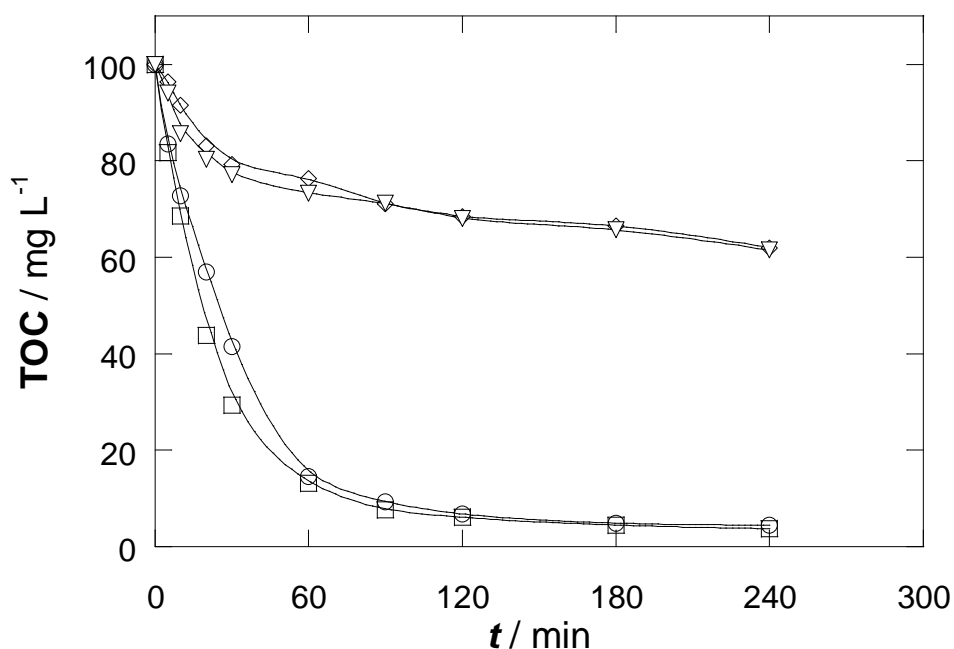


Figure 6.1. TOC decay with time for the mineralization of 100 mL of a 157 mg L^{-1} paracetamol solution of pH 3.0 and $25.0 \text{ }^\circ\text{C}$ under the O_3 and $\text{O}_3/\text{Fe}^{2+}, \text{Cu}^{2+}/\text{H}_2\text{O}_2/\text{UVA}$ methods at different ozone flow values. For the direct O_3 method: (\diamond) $0.7 \text{ g O}_3 \text{ h}^{-1}$, (∇) $1.0 \text{ g O}_3 \text{ h}^{-1}$. For the $\text{O}_3/\text{Fe}^{2+}, \text{Cu}^{2+}/\text{H}_2\text{O}_2/\text{UVA}$ method: (\circ) $0.5 \text{ g O}_3 \text{ h}^{-1}$, (\square) $1.0 \text{ g O}_3 \text{ h}^{-1}$. For the $\text{O}_3/\text{Fe}^{2+}, \text{Cu}^{2+}/\text{H}_2\text{O}_2/\text{UVA}$ method 1.0 mM Fe^{2+} , 0.25 mM Cu^{2+} and $22 \text{ mM H}_2\text{O}_2$ are present. The UV irradiation was supplied by a UV lamp situated 7 cm above the cell.

An ozone flow of 1 g h^{-1} was selected as default for the next experiments. This value was selected against lower flow values because the ozonator showed a better flow stability at 1 g h^{-1} .

The intensity of irradiation was another parameter to be studied as in many experiments UVA light from a fluorescent tube was supplied. Since this parameter depends on the position of the fluorescent tube with respect to the cell, two different distances were tested before setting one of them as default for the next experiments.

The gap distance between the lower part of the UV fluorescent tube and the rim of the treatment cell was selected as the d variable related to the irradiance on the solution (Fig. 6.2).

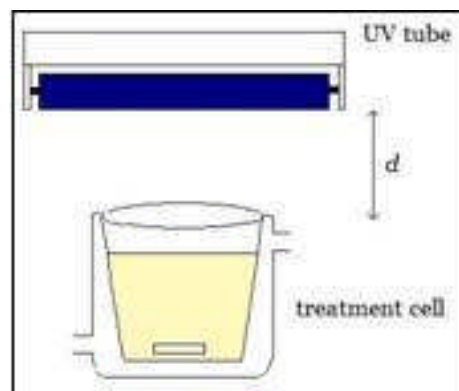


Figure 6.2. Scheme showing the d gap as a parameter related to the irradiance.

The gap distance can be an important parameter since for big values the radiation density supplied to the treated solution is smaller. In addition, the radiation scattering caused by the laboratory clamp which holds the tube and ozone difuser is higher at longer d distances, thus causing a more important loss of irradiation.

Gap distances of 7 cm and 14 cm were tested in two powerful treatments: $O_3/Fe^{2+}/UVA$ and $O_3/Fe^{2+},Cu^{2+}/UVA$. Since a synergistic effect between the UVA radiation and the catalytic activity of the metal cations is thought to be the cause of the highly mineralizing ability of these treatments, a different TOC abatement profile under these treatments at different irradiation intensities was expected.

The results obtained from these experiments, plotted in Figure 6.3, show that for both $O_3/Fe^{2+}/UVA$ and $O_3/Fe^{2+},Cu^{2+}/UVA$ treatments a smaller gap distance between the UVA radiation source and the treatment cell (which implies a higher irradiation intensity) leads to sharper mineralization profiles. The gap value $d = 7$ cm implied a stronger irradiation intensity than $d = 14$ cm, the processes related to the UVA light, such as the production of oxidant species like the $\bullet OH$ radical, and/or the regeneration of the Fe^{2+} catalyst, being more intense. Therefore, the default d value was set at 7 cm for the following experiments.

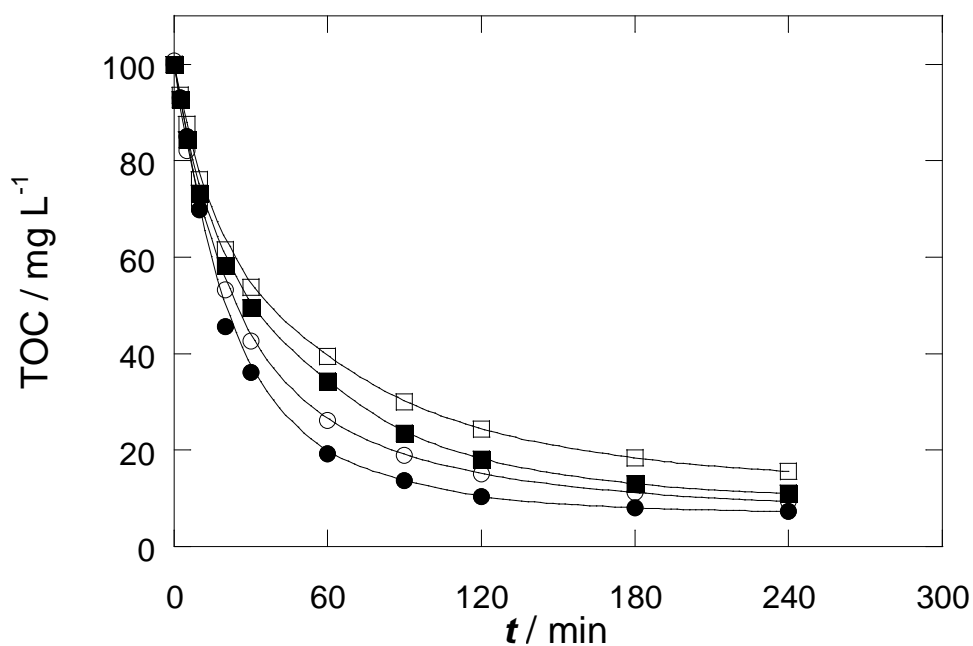


Figure 6.3. TOC abatement during the mineralization of 100 mL of a 157 mg L⁻¹ paracetamol solution at 25.0 °C, pH 3.0 and an ozone flow of 1.0 g h⁻¹. The experiments are carried out at two different distances between the UVA source and the cell containing the solution. $d = 14$ cm: (□) O₃ + 1.0 mM Fe²⁺ + UVA and (■) O₃ + 1.0 mM Fe²⁺ + 0.25 mM Cu²⁺ + UVA. $d = 7$ cm: (○) O₃ + 1.0 mM Fe²⁺ + UVA and (●) O₃ + 1.0 mM Fe²⁺ + 0.25 mM Cu²⁺ + UVA.

- Influence of temperature on paracetamol mineralization / *Influència de la temperatura a la mineralització del paracetamol*

The temperature could play an important role on the paracetamol mineralization rate. On one side, changes of temperature could alter the values of the rate constants of the several oxidation processes taking place during the mineralization of the drug. Besides, the temperature has an influence on the degree of solubility of ozone in water and, more importantly, on the mass transfer kinetics of the process of ozone dissolution, meaning that it would be able to modify the dissolution rate of ozone into water and consequently, the accumulated concentration of ozone in solution.

Solutions containing 157 mg L^{-1} of paracetamol, 1.0 mM Fe^{2+} , 0.25 mM Cu^{2+} and $22 \text{ mM H}_2\text{O}_2$ at pH 3.0 were ozonated and irradiated with a UVA lamp at $25.0 \text{ }^\circ\text{C}$ and $35.0 \text{ }^\circ\text{C}$ in order to observe if a $10 \text{ }^\circ\text{C}$ difference in temperature would be able to produce visible differences in the TOC abatement rate for the paracetamol solutions treated by these ozone-based AOPs.

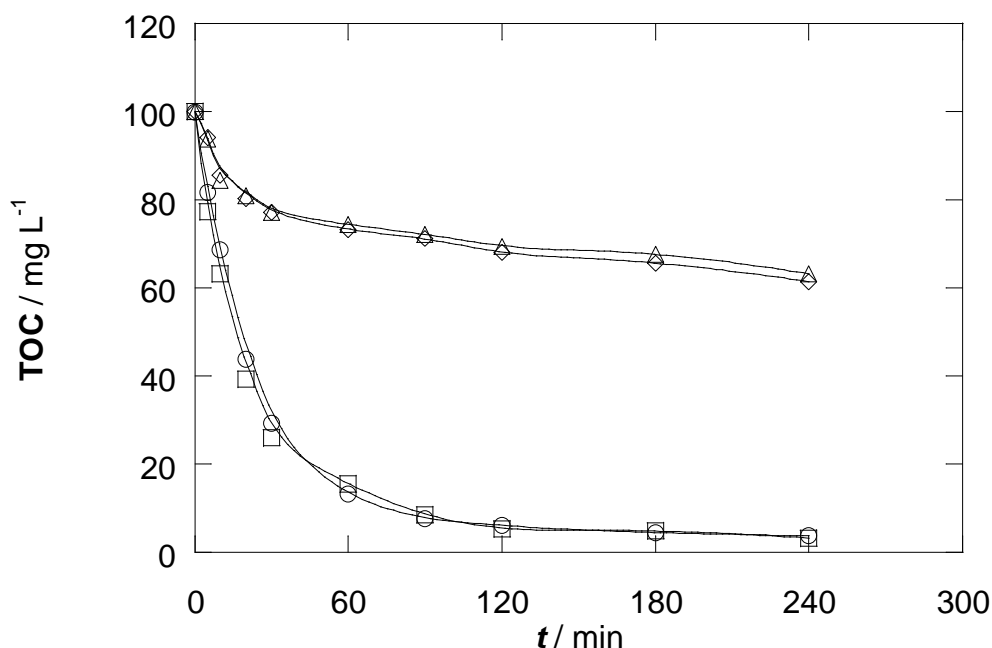


Figure 6.4. TOC removal with time in 100 mL of a 157 mg L^{-1} paracetamol solution at pH 3.0 under O_3 and $\text{O}_3/\text{Fe}^{2+}, \text{Cu}^{2+}/\text{H}_2\text{O}_2/\text{UVA}$ treatments at $25.0 \text{ }^\circ\text{C}$ and $35.0 \text{ }^\circ\text{C}$. $25.0 \text{ }^\circ\text{C}$: (○) $\text{O}_3 + 1.0 \text{ mM Fe}^{2+} + 0.25 \text{ mM Cu}^{2+} + 22 \text{ mM H}_2\text{O}_2 + \text{UVA}$, (◇) O_3 . $35.0 \text{ }^\circ\text{C}$: (□) $\text{O}_3 + 1.0 \text{ mM Fe}^{2+} + 0.25 \text{ mM Cu}^{2+} + 22 \text{ mM H}_2\text{O}_2 + \text{UVA}$, (△) O_3 . Ozone flow: 1.0 g h^{-1} , UVA lamp situated 7 cm above the treatment cell.

The curves in Figure 6.4 show no appreciable differences in the TOC mineralization rate of the two experiments despite the 10 °C increase in temperature, even for the powerful $O_3/Fe^{2+}, Cu^{2+}/H_2O_2/UVA$ treatment. As the mineralization of organic compounds by means of ozonation is a process in which $\bullet OH$ radicals are involved, the lack of temperature effect is not a surprise bearing in mind that temperature does not usually play an important role in the kinetics of radicalary processes.

- Influence of pH on the mineralization rate of paracetamol / *Influència del pH a la velocitat de mineralització del paracetamol*

The influence of pH was investigated for two different treatments to determine whether pH can influence the mineralization rate of paracetamol solutions under advanced oxidation processes based on ozonation.

Two different pH values, one in the acidic region (pH 3.0) and another in the basic region (pH 9.0), were tested for the O_3/UVA treatment, in which the solution is treated with O_3 and it is also irradiated. Results obtained are displayed in Figure 6.5.

At basic pH a significantly higher mineralization rate was observed at the beginning of the experiment. At high pH values, the phenol group of paracetamol dissociates to a major extent and yields a major proportion of its phenolate form. This phenolate group contributes to a faster reactivity of paracetamol with ozone since it gives the molecule a higher electron density. The observed acceleration of the initial mineralization rate at basic pH is then consistent with the reported increase in the rate constant of several phenolic compounds with O_3 when rising pH [143]. However, as more aliphatic carboxylic acids, such as oxalic and acetic acid, which are refractory to its oxidation with ozone [143], are accumulated in the medium, the abatement of paracetamol slows down and after the first 120 minutes of trial it does not further advance significantly.

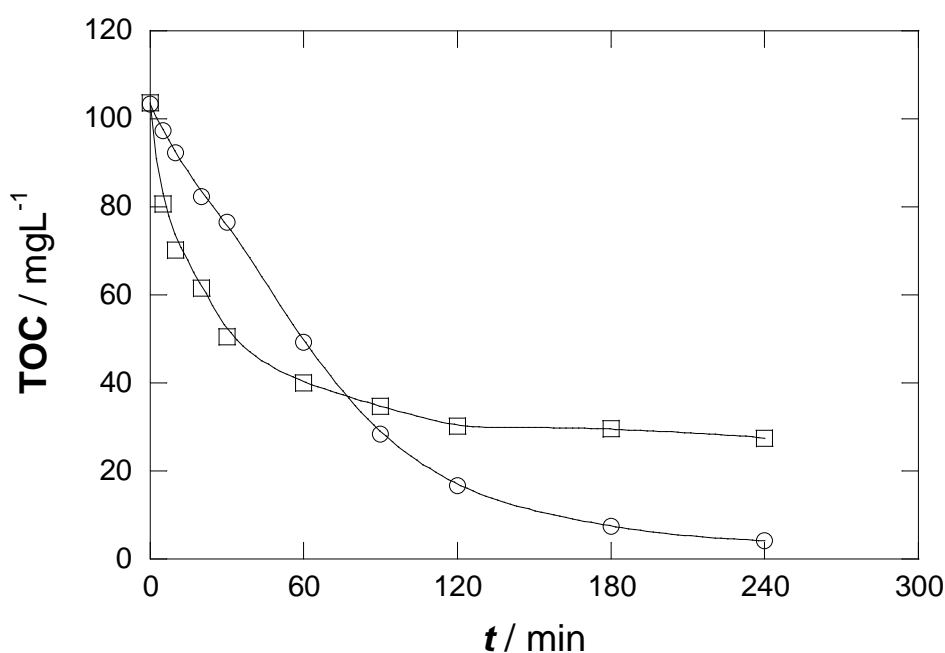
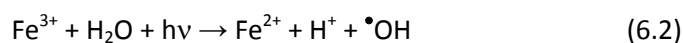


Figure 6.5. TOC abatement with time of a 157 mg L⁻¹ paracetamol solution under O₃/UVA treatment at two different pH values. Ozone flow : 1.0 g O₃ h⁻¹. (○) pH 3.0, (□) pH 9.0. Temperature: 25.0 °C, UVA irradiation: UV lamp situated at $d = 7$ cm above the cell.

At pH 3.0, the acidic medium does not promote the generation of the phenolate form of paracetamol, which as mentioned above, is much more reactive with ozone than its neutral phenol form counterpart. The resulting low degradation rate of paracetamol with ozone leads to a slower initial TOC abatement rate as seen in Figure 6.5. However, the acidic environment prevents the formation of species such as HCO₃⁻, which can act as •OH scavengers [93, 144]. The absence of these scavengers would account for the much more efficient mineralization attained at the end of the trial at acidic pH 3.0.

The influence of pH was tested on the O₃/Fe²⁺/UVA treatment as well, as displayed in Figure 6.6. The TOC abatement curve corresponding to the degradation experiment carried out at pH 6.0 shows the slowest mineralization profile. At this pH, Fe³⁺ can form insoluble hydroxides, this will make the regeneration of Fe²⁺ more difficult. As a consequence of that, a significant amount of solubilized iron catalyst is lost and a smaller amount of hydroxyl radical •OH is formed, since they are produced by several reactions involving the Fe²⁺ ion, mainly Fenton and photo-Fenton processes (reactions (1.3) and (6.2)).



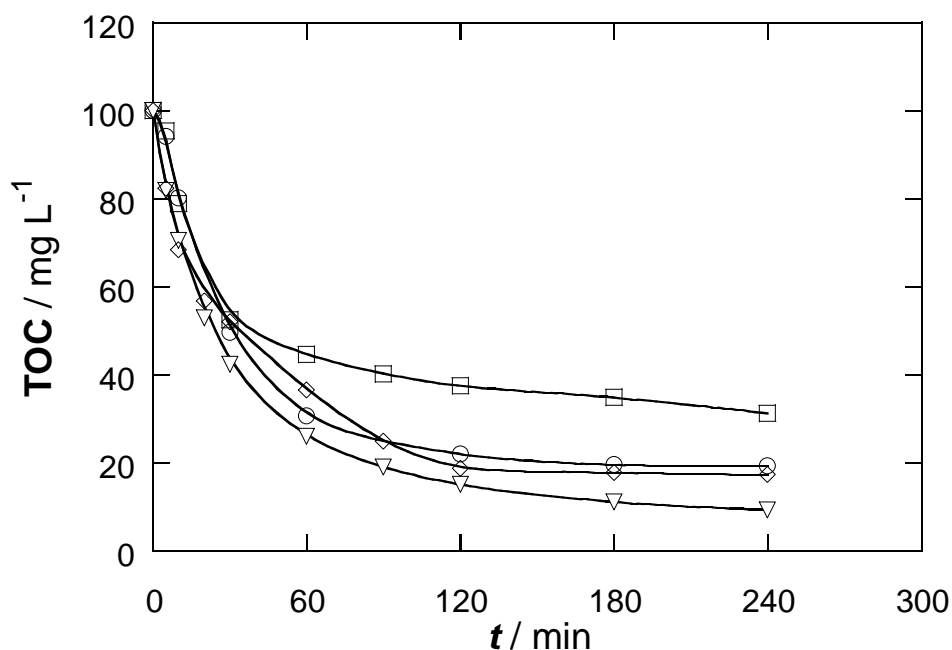


Figure 6.6. TOC evolution with time for 100 mL of a 157 mg L⁻¹ paracetamol solution containing 1.0 mM Fe²⁺ under the O₃/Fe²⁺/UVA treatment at 25.0 °C. Solution pH: (○) 2.0, (▽) 3.0, (◇) 4.0, (□) 6.0.

Apart from the loss of active solubilized catalyst, the formation of colloidal and non-catalytically active Fe³⁺ species causes the solution to become turbid. The dispersion caused by the formed colloids reduce the amount of irradiation reaching the solution from the UV lamp and consequently the drug mineralization rate slows down.

Far better results are obtained when pH is adjusted to more acidic values such as 2.0, 3.0 or 4.0. At these pH values all of the iron species are solubilized and no precipitation of Fe³⁺ in the form of hydroxides takes place. From the pH values ranging between 2.0 and 4.0, pH 3.0 seems clearly to be the one offering the most efficient mineralization for paracetamol. These results are consistent with other studies which conclude that the optimal pH for the Fenton reaction, which accounts for an important part of produced oxidant •OH radicals in the solution, lies between 2.7 – 2.8, very near to the optimal pH 3.0 found here [145].

Testing of several mineralization treatments / *Tests de diversos tractaments de mineralització*

After having established the default working conditions as

- ozone flow: 1 g h^{-1}
- selected temperature: $25.0 \text{ }^\circ\text{C}$
- pH 3.0

a group of several and varied mineralization treatments was selected in order to study the optimal conditions to attain a faster TOC abatement and more efficient mineralization of paracetamol. For this purpose, different treatment combinations were studied, always with an initial paracetamol concentration of 157 mg L^{-1} , which corresponds to a TOC in solution of 100 mg L^{-1} :

O_3	ozonation with no catalysis
$\text{O}_3/\text{Fe}^{2+}$	ozonation catalyzed by 1 mM Fe^{2+}
$\text{O}_3/\text{Cu}^{2+}$	ozonation catalyzed by 0.25 mM Cu^{2+}
O_3/UVA	photoassisted ozonation
$\text{O}_3/\text{Fe}^{2+}/\text{UVA}$	photoassisted ozonation catalyzed by 1 mM Fe^{2+}
$\text{O}_3/\text{Cu}^{2+}/\text{UVA}$	photoassisted ozonation catalyzed by 0.25 mM Cu^{2+}
$\text{O}_3/\text{Fe}^{2+}, \text{Cu}^{2+}/\text{UVA}$	photoassisted ozonation catalyzed by 1 mM Fe^{2+} and 0.25 mM Cu^{2+}
$\text{O}_3/\text{Fe}^{2+}, \text{Cu}^{2+}/\text{H}_2\text{O}_2/\text{UVA}$	photoassisted ozonation catalyzed by 1 mM Fe^{2+} , 0.25 mM Cu^{2+} and with presence of $22 \text{ mM H}_2\text{O}_2$.

The curves resulting from these experiments are depicted in Figure 6.7. O_3 and O_3/UVA treatments show very similar initial mineralization rates ($67 \text{ mg TOC L}^{-1} \text{ h}^{-1}$ for O_3 and $72 \text{ mg TOC L}^{-1} \text{ h}^{-1}$ for O_3/UVA). However, the paracetamol mineralization profile under the O_3 system, flattens out soon, showing that the mineralization nearly stops reaching only a poor 39%

mineralization extent. The O₃/UVA system, on the contrary, allows the mineralization of paracetamol getting on steadily up to a 96% of mineralization at the end of the 4-hour trial.

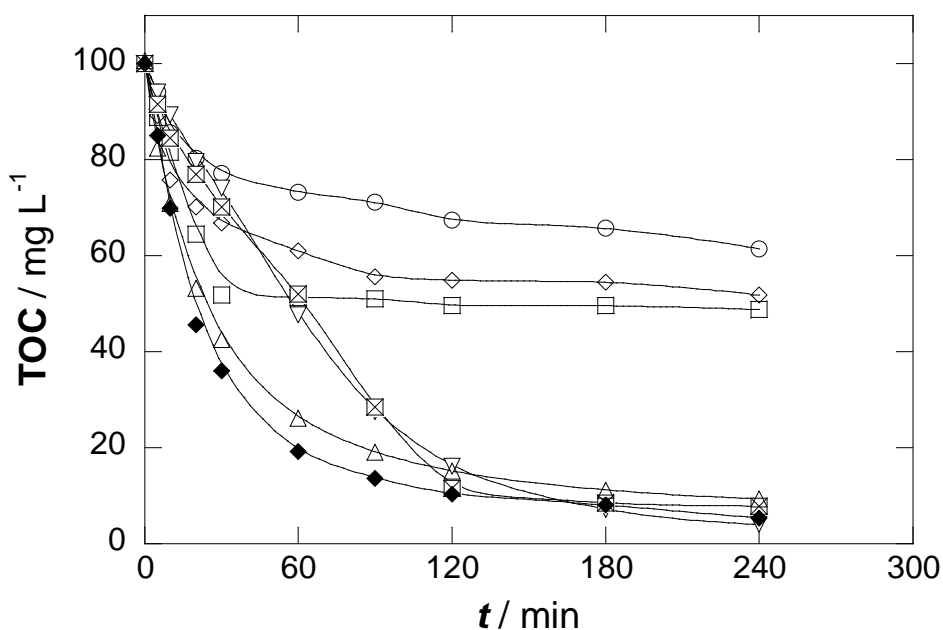


Figure 6.7. TOC abatement with time during the mineralization of 100 mL of a 157 mg L⁻¹ paracetamol solution at 25.0 °C, pH 3.0 under several ozone-based mineralization treatments: (○) O₃; (□) O₃ + 1.0 mM Fe²⁺; (◇) O₃ + 0.25 mM Cu²⁺; (▽) O₃/UVA; (⊠) O₃/H₂O₂/UVA; (△) O₃ + 1.0 mM Fe²⁺ + UVA; (◆) O₃ + 1.0 mM Fe²⁺ + 0.25 mM Cu²⁺ + UVA.

For many of these trials the H₂O₂ concentration was monitored as displayed in Figure 6.8. Under the O₃ system a steady H₂O₂ concentration of 0.16 mM from 15 minutes after the experiment start-up can be observed. This H₂O₂ concentration is formed as a consequence of the reaction of ozone with olefinic compounds, which are formed from the degradation from the paracetamol aromatic rings [146]. This steady concentration of H₂O₂, always lingering in the solution, shows that under non-catalyzed O₃ treatment, the formed concentration of H₂O₂ alone does not significantly degrade paracetamol. An experiment consisting of treating a paracetamol solution at pH 3.0 and 25.0 °C with 22 mM H₂O₂ was carried out. No degradation of paracetamol was found, confirming the fact that this oxidant alone is not effective to destroy this drug.

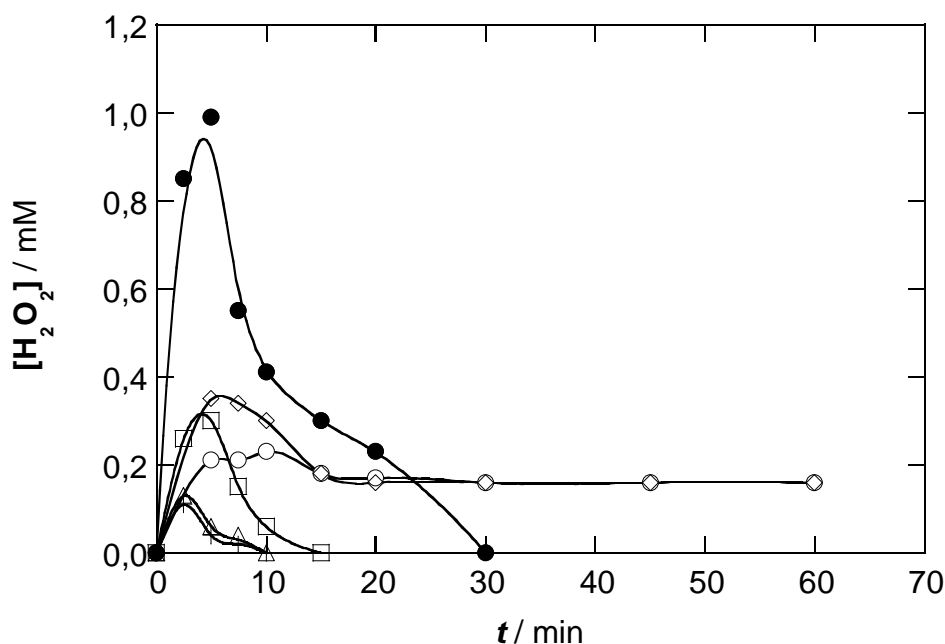
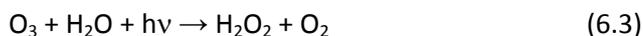


Figure 6.8. H_2O_2 concentration during several ozone-based mineralization treatments on a 157 mg L^{-1} paracetamol solution under the same experimental conditions described for Figure 6.5. (\circ) O_3 , (\square) $\text{O}_3/\text{Fe}^{2+}$, (\diamond) $\text{O}_3/\text{Cu}^{2+}$, (\bullet) O_3/UVA , (\triangle) $\text{O}_3/\text{UVA}/\text{Fe}^{2+}$, (+) $\text{O}_3/\text{UVA}/\text{Fe}^{2+}, \text{Cu}^{2+}$. UVA irradiation (6 W UV lamp situated 7 cm above the cell).

The evolution of H_2O_2 concentration under the O_3/UVA treatment, however, followed a very different pattern. A peak concentration reaching near 1 mM H_2O_2 was attained after few minutes. This species, however, disappeared 30 minutes after the experiment start-up. The formation of H_2O_2 from the photolysis of ozone with UVA radiation yielding hydrogen peroxide as



accounts for this high peak of reached H_2O_2 concentration. The used ultraviolet lamp had a maximum wavelength emission of $\lambda_{\text{max}} = 360 \text{ nm}$ and emitted within a spectrum between 300 – 420 nm. The existing absorption band-tail of ozone between 300 – 320 nm [147] allows its photodecomposition to H_2O_2 . This way the UVA irradiance accounts for this increment in the accumulated amount of formed H_2O_2 . The quick disappearance of H_2O_2 for the O_3/UVA treatment, however, cannot be ascribed to its homolytic cleavage

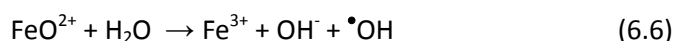


as it would then yield hydroxyl radicals, whose strong oxidant activity would lead to a sharp TOC decay, which does not occur. In addition, the initial TOC decay profile under the O₃/UVA treatment reflects a slow abatement, very similar to that under the O₃ method, far from suggesting the formation of any extra amount of •OH. A possible explanation for the better mineralization performance of the O₃/UVA treatment lies in the fact that the continuously supplied UVA radiation during the application of this mineralization method may induce the activation of the organics present in the treated solution (paracetamol and their intermediates including both aromatics and carboxylic aliphatic acids) thus making them more easy to react with O₃.

When 1.0 mM Fe²⁺ was added to the paracetamol solution (O₃/Fe²⁺ treatment), a significant rise of the initial mineralization rate was observed in comparison with the non catalyzed O₃ method with an initial mineralization rate rising from only 69 mg TOC L⁻¹ h⁻¹ for O₃ up to 109 mg TOC L⁻¹ h⁻¹ for the O₃/Fe²⁺ treatment. This result is explained by the oxidation of Fe²⁺ by O₃ yielding the oxidant iron (IV) species ferryl cation

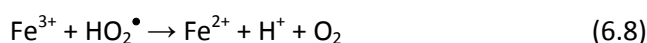


which consequently undergoes hydrolysis yielding Fe³⁺, hydroxide, and the very oxidant hydroxyl radical [148, 149].



The formation of this last species would account for the rising of the initial mineralization rate on the O₃/Fe²⁺ system in comparison to O₃, where no addition of catalysts was done.

For the O₃/Fe²⁺ treatment H₂O₂ disappears at only 15 minutes after the start-up (Figure 6.8). H₂O₂, which has been generated from the ozone attack to olefinic compounds arisen from the destruction of aromatic rings, is quickly destroyed through its reaction with Fe²⁺ to yield hydroxyl radicals in the Fenton process (reaction (1.3)) [145]. The Fe²⁺ consumed in the Fenton reaction can be regenerated through reduction of Fe³⁺ with H₂O₂ and hydroperoxyl radical HO₂• [145]:



The regeneration of Fe^{2+} (reactions (6.7) and (6.8)) leads to an even bigger production of oxidant $\bullet\text{OH}$ radicals through the Fenton reaction, thus explaining the higher TOC decay under the $\text{O}_3/\text{Fe}^{2+}$ treatment in comparison with that of the O_3 treatment.

But although the $\text{O}_3/\text{Fe}^{2+}$ treatment has a significantly higher initial mineralization rate than O_3 , its paracetamol mineralization profile also ends up becoming flat and, like under the O_3 treatment, the mineralization eventually stops. The reason for that is the formation of carboxylic acids, which are not easily degraded under these treatment conditions.

The assistance with UVA light in the $\text{O}_3/\text{Fe}^{2+}/\text{UVA}$ treatment raises its initial mineralization rate again, this time from $109 \text{ mg TOC L}^{-1} \text{ h}^{-1}$ for $\text{O}_3/\text{Fe}^{2+}$ up to $174 \text{ mg TOC L}^{-1} \text{ h}^{-1}$ for the $\text{O}_3/\text{Fe}^{2+}/\text{UVA}$ treatment. Apart from that, the radiation assistance causes an important increase of the final mineralization percentage from a 51% attained with $\text{O}_3/\text{Fe}^{2+}$ to a 91% of TOC removal at the end of the trial. One of the causes for this significant and important improvement lies on the synergic effect between the presence of Fe^{2+} catalyst and the UVA irradiation. In the presence of Fe^{2+} , several complexes consisting of Fe^{3+} and carboxylic acids, mainly oxalic acid, are formed. When no UV radiation is supplied, these Fe^{3+} – oxalato complexes can resist the O_3 attack without undergoing significant destruction, but the addition of UV radiation leads to their photolysis [150]. The UV irradiation stimulates an electronic transference from oxalate into Fe(III) reducing it back to Fe(II) on the account of the oxalato ligand. The resulting oxalate radical can be very easily oxidized into CO_2 by O_2 molecules present in the medium. This effect has already been observed [147, 151 – 154] and is represented in Figure 6.9.

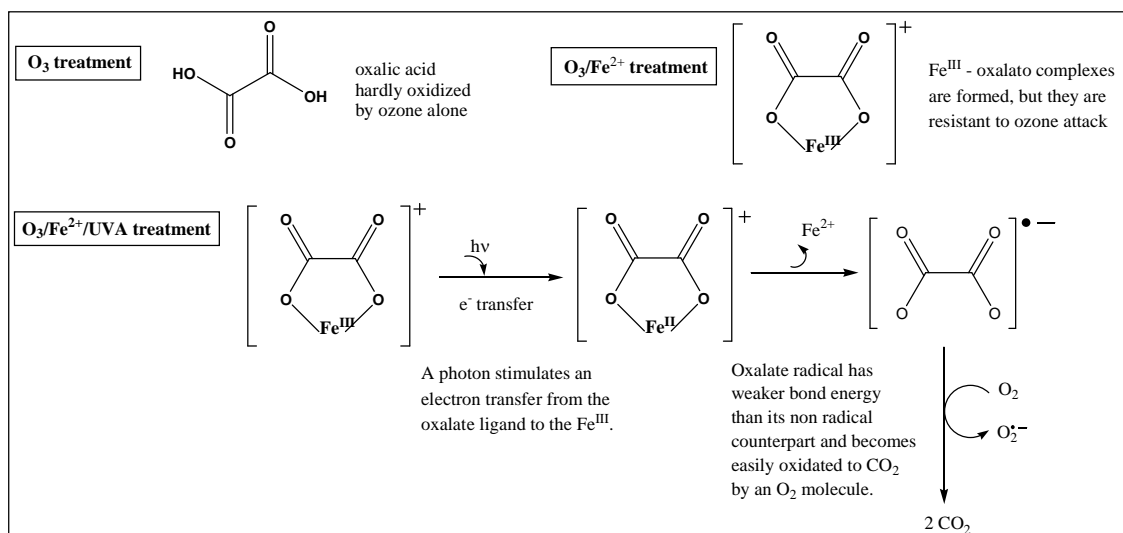
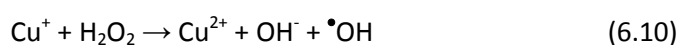


Figure 6.9. Photolytically induced oxidation of Fe(III)-oxalato complexes arisen from the degradation of paracetamol solutions.

A second cause accounting for the important increase in the mineralization rate of O₃/Fe²⁺/UVA method lies on the regeneration of Fe²⁺ with the simultaneous release of hydroxyl radicals in the photo-Fenton process (reaction (6.2)) [155]. Not surprisingly a much faster depletion of the H₂O₂ concentration for the O₃/Fe²⁺/UVA treatment can be observed if compared to that for the O₃/Fe²⁺ treatment (Figure 6.8). Although the UVA light assistance is also responsible for the formation of H₂O₂ via the photodegradation of ozone (reaction (6.4)), the extra amount of regenerated Fe²⁺ will lead to a major extent of the Fenton reaction, which leads to a more significant consumption of H₂O₂ overcoming the little excedent produced by reaction (6.4) and thus causing a fast depletion of the H₂O₂ concentration.

Still a bigger amount of produced oxidant hydroxyl radical could be expected when adding Cu²⁺ on the basis of the O₃/Fe²⁺/UVA method. This is expected from the reported behavior of copper cations when reacting with hydroperoxyl and oxygen peroxide similarly as in the Fenton reaction:



The so-called *Fenton-like* process (reaction (6.10)) [156] was, however, not observed in our trials, as the addition of 0.25 mM Cu^{2+} did not lead to any significant improvements of the mineralization rate. Indeed, the $\text{O}_3/\text{Fe}^{2+}, \text{Cu}^{2+}/\text{UVA}$ treatment does not show any significantly higher initial mineralization rate in comparison to that under the $\text{O}_3/\text{Fe}^{2+}/\text{UVA}$ method. The addition of Cu^{2+} causes only a small 6 mg TOC $\text{L}^{-1} \text{h}^{-1}$ increase of the initial mineralization rate. Moreover, a very similar H_2O_2 concentration profile was observed for both treatments: H_2O_2 did not disappear faster than under the $\text{O}_3/\text{Fe}^{2+}/\text{UVA}$ treatment, 10 minutes after the start of the trial.

The addition of Cu^{2+} is neither significant regarding the final mineralization extent obtained. The addition of Cu^{2+} only raised the TOC removal a 3% from 91% for the $\text{O}_3/\text{Fe}^{2+}/\text{UVA}$ method to 94% under the $\text{O}_3/\text{Fe}^{2+}, \text{Cu}^{2+}/\text{UVA}$ oxidation method. The $\bullet\text{OH}$ generated from reactions (6.9) and (6.10) would lead to a much bigger increase of the TOC removal and would cause a faster depletion of the H_2O_2 concentration profile with time, which does not take place. These results state only a very feeble effect of the possible Fenton-like process, thus indicating that these Fenton-like processes take place at a very small extent.

Another reason to prove that practically no Fenton-like reaction took place and no $\bullet\text{OH}$ radicals were formed at significant amounts by the action of Cu^{2+} ions can be found comparing the H_2O_2 time-concentration profiles of O_3 and $\text{O}_3/\text{Cu}^{2+}$ treatments. The H_2O_2 concentration with time for the $\text{O}_3/\text{Cu}^{2+}$ treatment shows a steady concentration of about 0.16 mM H_2O_2 , just the same as that for the O_3 treatment. This shows that there is a practically negligible participation of the reaction (6.10), which would have led to a significant depletion of the hydrogen peroxide concentration.

The more important TOC abatement of paracetamol solutions under $\text{O}_3/\text{Cu}^{2+}$ treatment (48%) than that attained under the O_3 one (only 39%) then cannot be accounted to the generation of $\bullet\text{OH}$ through Fenton-like reaction, but only to the major oxidability of carboxylic acids when forming complexes with Cu^{2+} .

The differences concerning $\bullet\text{OH}$ concentration on the systems involving participation of metal ion catalysts were studied by comparing the degradation of a 20 mg L^{-1} oxamic acid solution using the different oxidation methods. As oxamic acid is one of the last intermediate compounds of paracetamol present in the solution, its degradation was studied in the presence and in the absence of *tert*-butanol (t-BuOH). The concentration evolution of this acid

was monitored by ion-exclusion chromatography and the results obtained are shown in Figure 6.10.

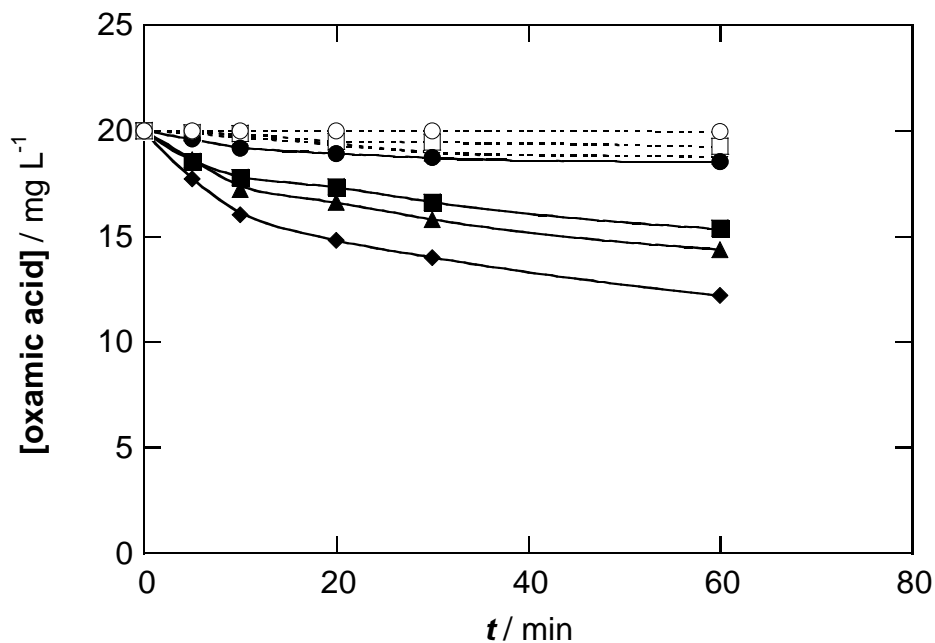


Figure 6.10. Oxamic acid concentration evolution in Fe²⁺ catalyzed ozonation treatments. A 20 mg L⁻¹ oxamic acid solution at pH = 3.0 was used for several treatments: (○, ●) O₃/Fe²⁺; (□, ■) O₃/Fe²⁺/UVA; (Δ, ▲) O₃/Fe²⁺/Cu²⁺; (◇, ◆) O₃/Fe²⁺, Cu²⁺/UVA. In (○, □, Δ, ◇) 30 mM t-butanol was added to the initial solution. Ozone flow rate 1.0 g h⁻¹, 25 °C. FeSO₄ and CuSO₄: 1.0 mM and 0.25 mM when present. The UV irradiation source was a 6 W UV lamp situated 7 cm above the cell.

As t-BuOH is a hydroxyl radical scavenger, the comparison in Figure 6.10 between the couples of curves corresponding to t-BuOH presence and t-BuOH absence would correspond to couples of curves implying •OH-less and •OH-assisted treatments, respectively. These comparison curves provide an idea of the amount of •OH radical generated within each tested system.

Among all tested systems, O₃/Fe²⁺, Cu²⁺/UVA is that one in which a bigger difference between the oxamic degradation curves involving and excluding t-BuOH can be observed. This means that O₃/Fe²⁺, Cu²⁺/UVA is, among the tested treatments, the only one in which the activity of •OH radicals is more important and easy to see. The fact that the O₃/Fe²⁺, Cu²⁺/UVA treatment is more affected by the removal of its •OH radical activity with the addition of t-BuOH proves a bigger production of •OH when this treatment is used in comparison with the

amount of generated $\bullet\text{OH}$ under $\text{O}_3/\text{Fe}^{2+}/\text{UVA}$ or $\text{O}_3/\text{Fe}^{2+}$ treatments. For the $\text{O}_3/\text{Fe}^{2+}$ method only a very small difference was observed in the degradation profile of oxamic acid after the addition of t-BuOH suggesting that a much smaller amount of oxidant hydroxyl radicals are produced during this treatment in comparison to the other systems tested.

- Influence of the cation ratio and concentration on the mineralization rate / *Influència de la proporció en cations i la seva concentració a la velocitat de mineralització*

After having shown that Fe^{2+} and Cu^{2+} do play a significant role as catalysts in the mineralization of paracetamol solutions by ozone-based AOPs, a more in-depth study of the effect of both Fe^{2+} and Cu^{2+} was necessary to be carried out.

Several combinations of Fe^{2+} and Cu^{2+} concentrations were tested on the basis of the O_3 treatment, with no UV radiation involved, in order to study the catalytic influence of these ions. For this purpose, a set of experiments was carried out and the curves obtained are depicted in Figure 6.11.

The $\text{O}_3/\text{Fe}^{2+}$ treatment shows a significantly better mineralization efficiency than the O_3 treatment, which as stated before is explained by an additional $\bullet\text{OH}$ radical production from reactions (6.5 – 6.8). The better mineralization results obtained under the $\text{O}_3/\text{Cu}^{2+}$ treatment seem surprising as equivalent reactions with copper ion instead of iron (reactions (6.9), (6.10)) did not seem to take place. This mineralization enhancement can be explained by the presence of oxamic acid, which (along with oxamic acid) is one of the most persistent formed intermediates when oxidating dissolutions of paracetamol. Independent experiments treating solutions of oxamic acid with ozone with Cu^{2+} present in solution allowed a much faster mineralization than that attained in experiments in which no Cu^{2+} was present. This suggested that the Cu^{2+} - oxamate complexes could be more easily ozonated than uncomplexed oxamate anions. These results explain the better results in paracetamol mineralization in the presence of Cu^{2+} as the destruction of oxamate, as an intermediate of paracetamol will lead to a TOC decay.

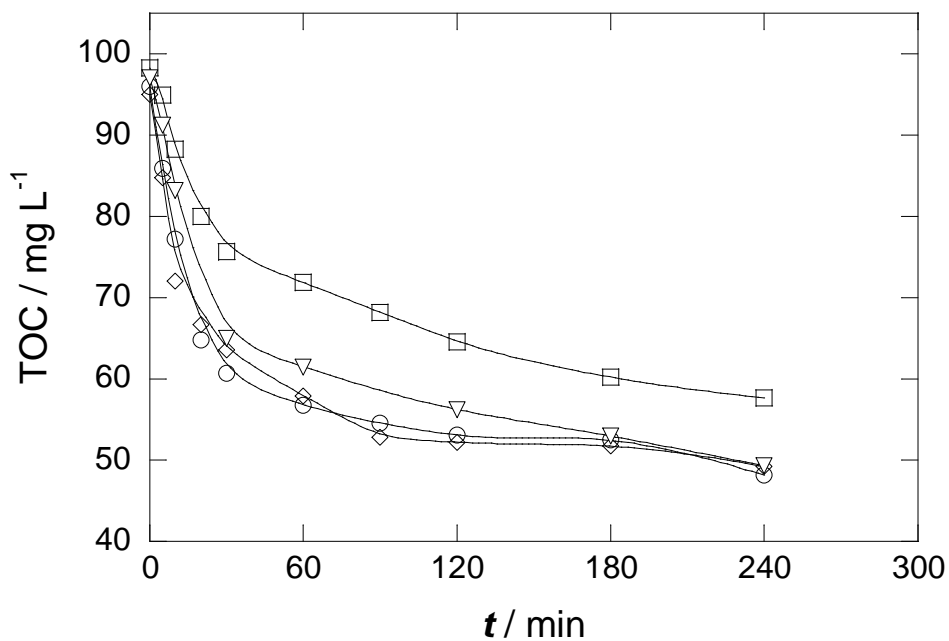


Figure 6.11. TOC abatement profiles for 100 mL of a 157 mg L⁻¹ paracetamol solution treated by O₃-based systems at different added concentrations of Fe²⁺ and Cu²⁺ at pH 3.0 and 25.0 °C. (□) with no addition of catalysts, (○) 1 mM Fe²⁺, (◇) 0,25 mM Cu²⁺, (▽) 1 mM Fe²⁺ + 0,25 mM Cu²⁺.

Finally, the participation of both Fe²⁺ and Cu²⁺ together did not lead to any synergistic effects, as the obtained mineralization profile of O₃/Fe²⁺,Cu²⁺ treatment was almost identical to that of the O₃/Cu²⁺ treatment.

For a further study of the influence of Fe^{2+} and Cu^{2+} catalysts on the mineralization efficiency of paracetamol a set of experiments based on $\text{O}_3/\text{H}_2\text{O}_2/\text{UVA}$ was carried out.

Figure 6.12 shows that the $\text{O}_3/\text{H}_2\text{O}_2/\text{UVA}$ treatment can attain a very high mineralization extent after 4 hours of treatment (92% mineralization). This is probably caused by an activation of paracetamol by the UVA radiation, which would help the O_3 and H_2O_2 to oxidize the drug. This treatment, however, also displays a rather slow mineralization rate during the first 2 hours, before stopping. When 1 mM Fe^{2+} was present ($\text{O}_3/\text{Fe}^{2+}/\text{H}_2\text{O}_2/\text{UVA}$ treatment) a much sharper initial TOC-decay was obtained. The improvement of this initial mineralization rate is mainly explained by:

- The formation of important amounts of $\bullet\text{OH}$ radical through reactions involving the participation of Fe^{2+} cations, especially through the Fenton and photoFenton reactions which account for most of produced $\bullet\text{OH}$ and for the regeneration of Fe^{2+} from Fe^{3+} cations.
- The photodecarboxylation of oxalic acid, one of most persistent intermediates formed from the degradation of paracetamol, which only complexed with iron ions and irradiated with UVA radiation can be significantly oxidized to CO_2 .

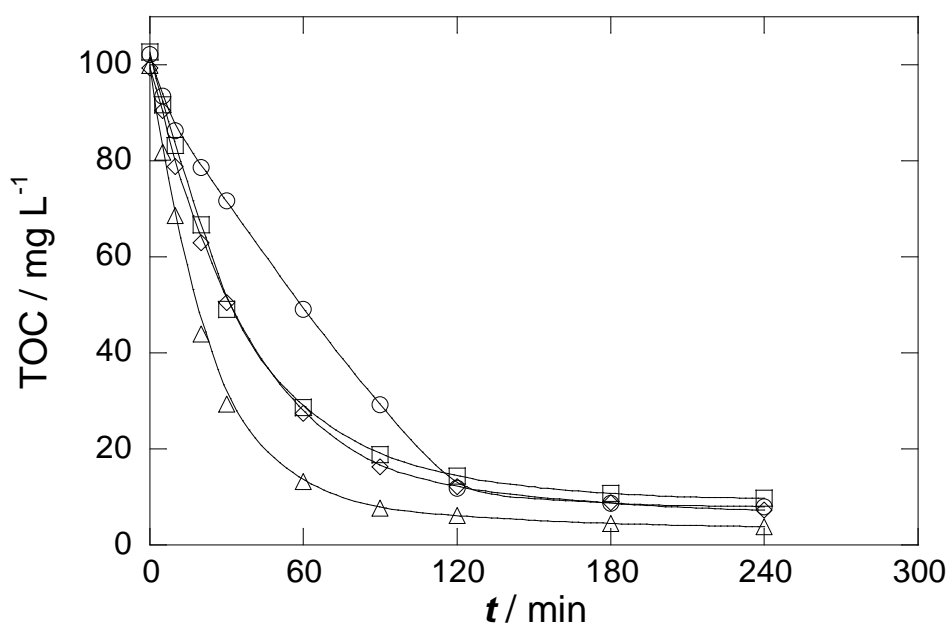


Figure 6.12. Mineralization decay profile for 100 mL of a 157 mg L^{-1} paracetamol solution at $25.0 \text{ }^\circ\text{C}$ and $\text{pH } 3.0$ under different treatments based on $\text{O}_3/\text{H}_2\text{O}_2/\text{UVA}$: (O) $\text{O}_3 + 22 \text{ mM H}_2\text{O}_2 + \text{UVA}$, (□) $\text{O}_3 + 1.0 \text{ mM Fe}^{2+} + 22 \text{ mM H}_2\text{O}_2 + \text{UVA}$, (◇) $\text{O}_3 + 0.25 \text{ mM Cu}^{2+} + 22 \text{ mM H}_2\text{O}_2 + \text{UVA}$, (△) $\text{O}_3 + 1.0 \text{ mM Fe}^{2+} + 0.25 \text{ mM Cu}^{2+} + 22 \text{ mM H}_2\text{O}_2 + \text{UVA}$.

When instead of Fe^{2+} , Cu^{2+} is added ($\text{O}_3/\text{Cu}^{2+}/\text{UVA}$ method) a very similar mineralization profile is obtained to that under the $\text{O}_3/\text{Fe}^{2+}/\text{UVA}$ treatment. Under the presence of Cu^{2+} , Fenton-like processes generating $\bullet\text{OH}$ radicals do not take place at significant extent, but the formation of more easily oxidable Cu^{2+} - oxamate complexes allows the destruction of oxamate anions, the most persistent paracetamol intermediates, which are still detected in the solution at the end of most of applied treatments.

A significant synergistic effect is observed when both ion catalysts Fe^{2+} and Cu^{2+} are present in a treatment based on ozonation assisted by H_2O_2 and UVA ($\text{O}_3/\text{H}_2\text{O}_2/\text{UVA}$). A remarkable acceleration of the initial mineralization rate is easily observed in Figure 6.12. The combination of the increase in concentration of $\bullet\text{OH}$ radicals, the photodecarboxylation of oxalate caused by the presence of Fe^{2+} (as the photocarboxylation takes place in Fe^{3+} - oxalate complexes) and the elimination of the very persistent oxamate anion catalyzed by Cu^{2+} result in an additive effect of these processes.

Different experiments were carried out with different tested concentrations of Fe^{2+} and Cu^{2+} , as well as with different ratios between them, in order to observe if some of such combinations lead to a significantly higher mineralization speed.

Curves *a* and *b* (Figure 6.13) show that treatments with increasing concentrations of Cu^{2+} from 0.25 mM to 1.0 mM display an improvement on its mineralization rate which can be accounted on a higher amount of easily oxidable Cu^{2+} - complexes, especially Cu^{2+} - oxamate complexes.

Catalysis with 0.25 mM Fe^{2+} (Figure 6.13, curve *c*) proved to be insufficient to attain a quantitative mineralization of paracetamol, indicating that a higher concentration of Fe^{2+} is necessary to produce significative improvements in its mineralization. The combination of 0.25 mM Fe^{2+} + 1.0 mM Cu^{2+} (curve *d*) produced a significant increase in the initial mineralization rate of the drug, caused by the good efficiency of ozone in eliminating several Cu^{2+} - complexes, but after 2 hours of treatment the mineralization stagnated at only 77% mineralization of the total amount.

An increase in the Fe^{2+} concentration to 1.0 mM causes a very significant mineralization boost, as many processes yielding $\bullet\text{OH}$, such as mainly Fenton and photo-

Fenton reactions take place in a higher extent and also a higher amount of photolyzable Fe^{3+} - complexes (especially Fe^{3+} - oxalate) is formed.

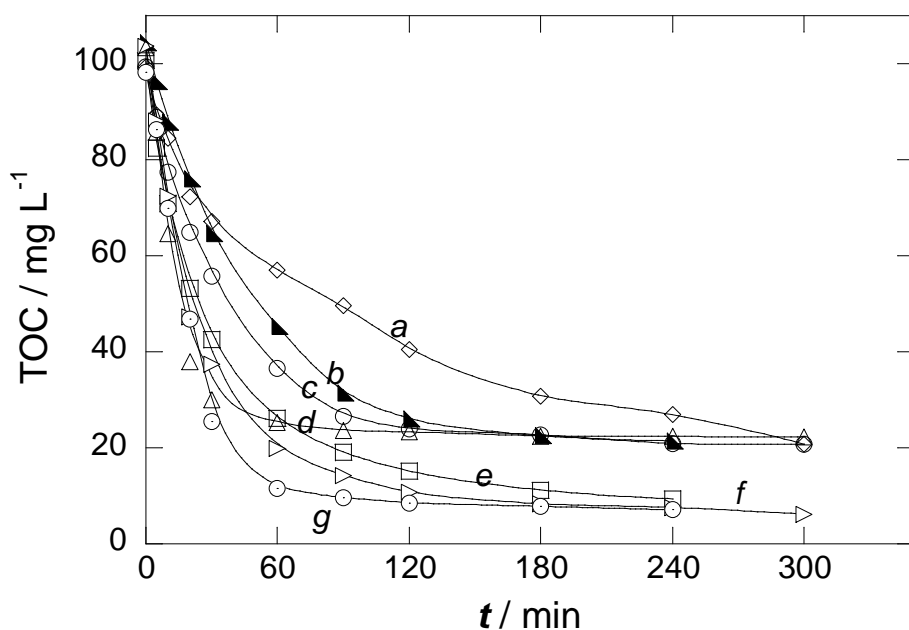


Figure 6.13. TOC abatement of 100 mL of a 157 mg L^{-1} paracetamol solution treated by several O_3/UVA -based methods with different added concentrations of Fe^{2+} and Cu^{2+} . (a, \diamond) 0.25 mM Cu^{2+} , (b, \blacktriangle) 1 mM Cu^{2+} , (c, \circ) 0.25 mM Fe^{2+} , (d, \triangle) $0.25 \text{ mM Fe}^{2+} + 1 \text{ mM Cu}^{2+}$, (e, \square) 1 mM Fe^{2+} , (f, \triangleright) $1 \text{ mM Fe}^{2+} + 0.25 \text{ mM Cu}^{2+}$, (g, \odot) $0.5 \text{ mM Fe}^{2+} + 0.5 \text{ mM Cu}^{2+}$.

When 0.25 mM Cu^{2+} is added to 1.0 mM Fe^{2+} a synergistic effect is observed. This effect leads to a faster initial mineralization rate and it also improves the attained mineralization extent. The presence of Cu^{2+} causes the formation of more easily oxidable by ozone Cu^{2+} - oxamate complexes. This effect of copper is added to the $\bullet\text{OH}$ radical generation and oxalate photodecarboxilation catalyzed by the Fe^{2+} catalyst. The optimal ratio found for Fe^{2+} and Cu^{2+} ions was though $0.5 \text{ mM} / 0.5 \text{ mM}$, which led to the fastest initial mineralization rate ($143 \text{ mg TOC h}^{-1}$) and to a final 93% mineralization.

- Influence of initial concentration of paracetamol on its mineralization rate / *Influència de la concentració inicial del paracetamol sobre la seva velocitat de mineralització*

O_3/UVA , $O_3/Fe^{2+}/UVA$, $O_3/Fe^{2+},Cu^{2+}/UVA$ and $O_3/Fe^{2+},Cu^{2+}/H_2O_2/UVA$ proved to be the most oxidantly stronger treatments for 157 mg L⁻¹ paracetamol solutions. Different tests on these treatments applied to paracetamol solutions within a wide range of initial paracetamol concentrations were also carried out. The purpose of these experiments is to survey the possible effect of the initial concentration on the attained mineralization percentage and also to see to what extent these different treatments are limited by the concentration of treated paracetamol.

The results of mineralization percentage and initial mineralization rate obtained from these experiments are gathered on Table 6.1. Their decay curves are shown on Figure 6.14 (a, b, c and d).

All treatments are capable of mineralizing over 82% of dissolved paracetamol in all cases. These results show that O_3/UVA , $O_3/Fe^{2+}/UVA$, $O_3/Fe^{2+},Cu^{2+}/UVA$ and $O_3/Fe^{2+},Cu^{2+}/H_2O_2/UVA$ treatments are very efficient to remove high amounts of paracetamol dissolved in water.

The oxidative capacity of these methods, directly related to their ability of producing the strongly oxidant hydroxyl radicals appears to increase in the order $O_3/UVA < O_3/Fe^{2+}/UVA < O_3/Fe^{2+},Cu^{2+}/UVA < O_3/Fe^{2+},Cu^{2+}/H_2O_2/UVA$, which agrees with the results shown previously (Figures 6.12, 6.13) where these different treatments exhibit a mineralization efficiency in the same order.

Table 6.1. Percentage of TOC removal after 2 and 4 hours of treatment of 100 mL of different paracetamol solutions at pH 3.0 and 25.0 °C by catalyzed ozonation processes.

O ₃ /UVA		
C ₀ / mg L ⁻¹	% mineralized after 2h	% mineralized after 4h
157	84	96
315	61	88
629	63	87
O ₃ /Fe ²⁺ /UVA		
78	80	86
157	85	91
315	82	86
629	73	90
943	73	92
O ₃ / Fe ²⁺ ,Cu ²⁺ /UVA		
78	82	87
157	90	93
315	83	92
629	88	93
943	79	93
O ₃ / Fe ²⁺ ,Cu ²⁺ /UVA/H ₂ O ₂		
78	87	90
157	94	96
315	94	98
629	93	96

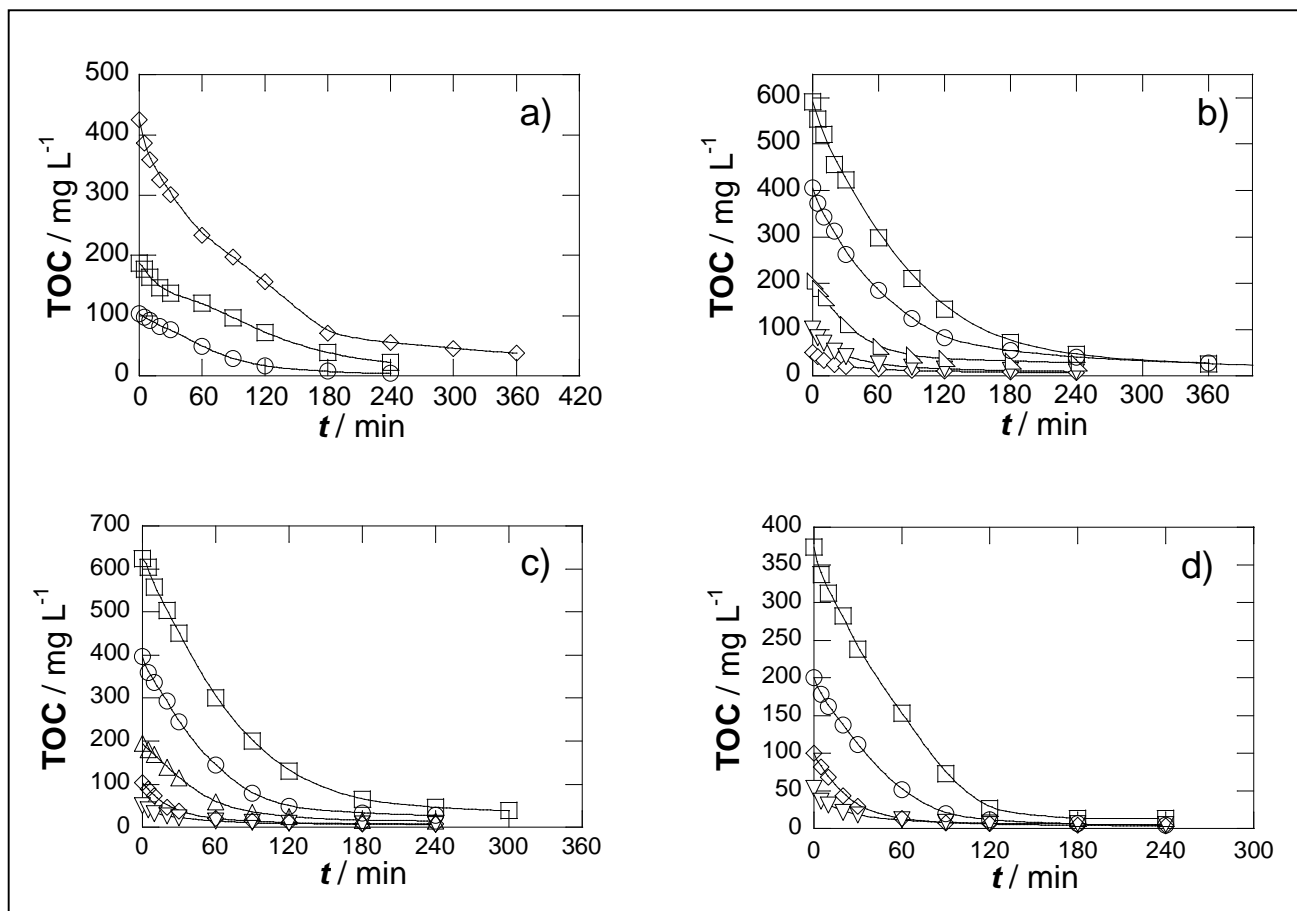


Figure 6.14. TOC decay curves for solutions of 100 mL of paracetamol solutions at 25.0 °C and pH 3.0 at several initial concentrations of drug. The solutions were mineralized under: a) O₃/UVA; b) O₃/Fe²⁺/UVA; c) O₃/Fe²⁺, Cu²⁺/UVA and d) O₃/Fe²⁺, Cu²⁺/UVA/H₂O₂ treatment.

6.1.2 Study of paracetamol and its degradation intermediates time-course / *Estudi de l'evolució del paracetamol i dels seus intermedis de degradació*

Several intermediates were identified for the different mineralization treatments of paracetamol. Different analytical techniques were applied to identify them and later to monitor their concentrations during such treatments.

The aromatic intermediates *p*-benzoquinone, hydroquinone and 2-hydroxy-4-(*N*-acetyl)aminophenol were identified by gas chromatography coupled to mass spectrometry (GC-MS). Reversed-phase chromatography was used to monitor the concentration of *p*-benzoquinone and hydroquinone. 2-Hydroxy-4-(*N*-acetyl)aminophenol could not be observed by reversed-phase chromatography.

The aliphatic carboxylic intermediates oxalic, oxamic, ketomalonic, maleic, glyoxylic, glycolic and tartronic acid were identified comparing their retention times to those of standards using ion exclusion chromatography. The ion exclusion chromatography enabled at the same time the determination of their concentrations during the treatment and thus their monitoring during the experiments.

Ions such as ammonium, nitrate and nitrite were identified by their retention time using ion exchange chromatography, which also enabled the determination of their concentrations along with time during the treatments.

- Study of paracetamol degradation kinetics / *Estudi de la cinètica de la degradació del paracetamol*

The paracetamol concentration was monitored by reversed-phase HPLC during the application of the oxidative treatments O_3 , O_3/UVA , $O_3/Fe^{2+}/UVA$ and $O_3/Fe^{2+},Cu^{2+}/UVA$. The paracetamol molecule exhibited a peak at $t_R = 2.76$ minutes. The time-evolution curves corresponding to these treatments are depicted in Figure 6.15.

The Figure 6.15 shows that paracetamol is quickly eliminated by all treatments in less than 6 minutes and there are only very slight differences on the paracetamol concentration abatement among the direct ozonation treatment (O_3) and the catalyzed treatments (O_3/UVA ,

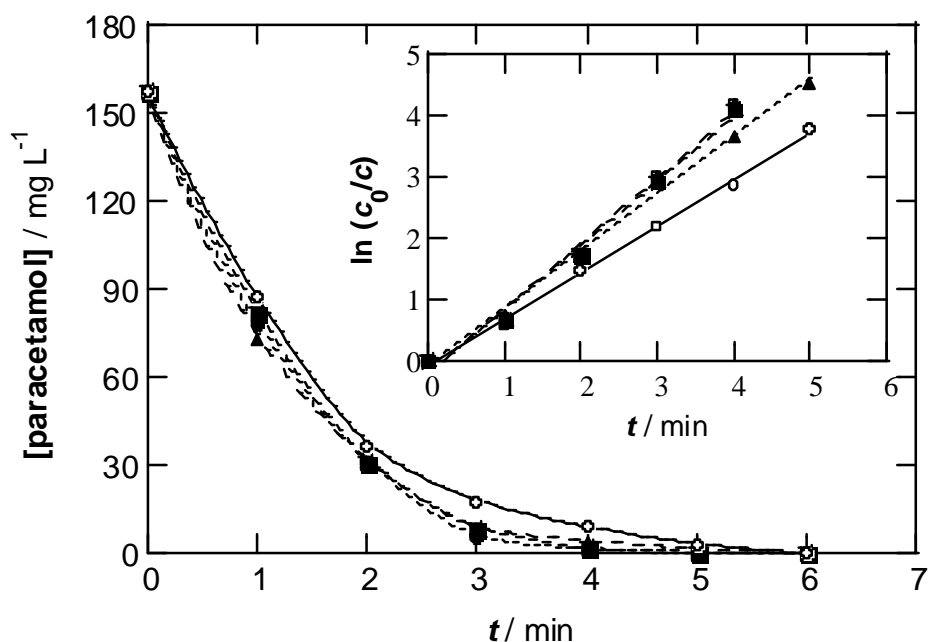


Figure 6.15. Paracetamol concentration abatement for 100 mL of a 157 mg L^{-1} solution at $25.0 \text{ }^\circ\text{C}$ and $\text{pH } 3.0$). Applied treatment: (O) O_3 ; (●) O_3/UVA ; (■) $O_3/UVA/Fe^{2+}$, (▲) $O_3/UVA/Fe^{2+}/Cu^{2+}$. The panel inset presents the corresponding kinetic analysis assuming a pseudo-first-order reaction for paracetamol.

$O_3/Fe^{2+}/UVA$ and $O_3/Fe^{2+},Cu^{2+}/UVA$), as also appreciated from the calculation of its rate constants, listed in Table 6.2. These results suggest that paracetamol is not photolyzed by UVA radiation. This was checked treating a 157 mg L^{-1} paracetamol solution under UVA radiation for 4 h. No decay was observed in the concentration of paracetamol, thus confirming this feature.

Table 6.2. Pseudo-first-order rate constants for the paracetamol degradation.

treatment	k / s^{-1}
O_3	$1.2 \cdot 10^{-2}$
O_3/UVA	$1.7 \cdot 10^{-2}$
$O_3/ Fe^{2+}/UVA$	$1.7 \cdot 10^{-2}$
$O_3/ Fe^{2+}, Cu^{2+}/UVA$	$1.6 \cdot 10^{-2}$

The paracetamol concentration was also monitored for the $O_3/Fe^{2+},Cu^{2+}/UVA$ treatment working at different initial concentrations of paracetamol. Its decay curves are represented in the Figure 6.16 and their pseudo-first-order rate constants are shown in Table 6.3.

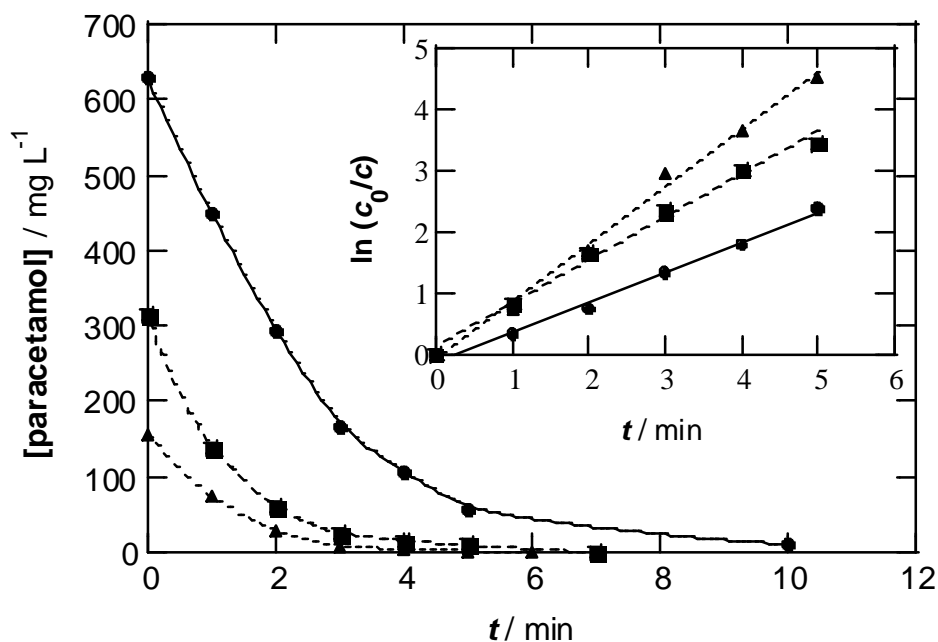


Figure 6.16. Paracetamol concentration decay for solutions at different initial concentrations of this drug, under the application of the $O_3 + 1.0$ mM $Fe^{2+} + 0.25$ mM $Cu^{2+} + UVA$ treatment at 25.0 °C and pH 3.0. Initial drug concentration: (▲) 157 mg L^{-1} ; (■) 315 mg L^{-1} ; (●) 628 mg L^{-1} . The panel inset presents the corresponding kinetic analysis assuming a pseudo-first-order reaction for paracetamol.

Table 6.3. Pseudo-first-order rate constants for the degradation of solutions of different initial concentration of paracetamol under the $O_3/Fe^{2+},Cu^{2+}/UVA$ treatment.

$C_0/mg L^{-1}$	k / s^{-1}
157	$1.6 \cdot 10^{-2}$
315	$1.1 \cdot 10^{-2}$
629	$8.0 \cdot 10^{-3}$

Lower rate constants have been observed for higher initial concentrations of paracetamol solutions. At high concentrations of paracetamol, most of O_3 is consumed in its direct reaction with paracetamol and the formation of hydroxyl radicals from O_3 takes place in a smaller extent. This leads to a lower concentration of hydroxyl radicals in the solution, which accounts for their smaller kinetic constants.

- Monitoring of aromatic intermediates of paracetamol / *Seguiment d'intermedis aromàtics del paracetamol*

Hydroquinone, *p*-benzoquinone and 2-hydroxy-4-(N-acetyl)aminophenol were detected as aromatic intermediates formed during the degradation of paracetamol. Hydroquinone and *p*-benzoquinone were monitored by reversed-phase chromatography during times lower than 10 minutes.

The evolution of these aromatic intermediates is shown in Figures 6.17 and 6.18. For the several applied treatments hydroquinone and *p*-benzoquinone are quickly formed and also quickly eliminated. They do not remain in the solution longer than 7 minutes in any case.

Figure 6.17 shows the time-course evolution of hydroquinone, which was detected by reversed-phase HPLC at a retention time of $t_R = 3.60$ minutes. The formed hydroquinone decreases much faster under catalyzed treatments in the order $O_3/Fe^{2+}, Cu^{2+}/UVA = O_3/Fe^{2+}/UVA > O_3/UVA > O_3$. The more oxidative the treatment, the faster hydroquinone disappears from the solution. This is consistent with the fact that under treatments capable of generating a higher amount of oxidant $\bullet OH$ species, such as $O_3/Fe^{2+}, Cu^{2+}/UVA$ the intermediates formed from the oxidation of paracetamol can be quickly destroyed in comparison with other treatments which produce smaller amounts of $\bullet OH$. This smaller production of $\bullet OH$ radicals when treatments O_3 and O_3/UVA are applied also accounts for the significantly bigger accumulation of hydroquinone (up to near 6 mg L^{-1} and 8 mg L^{-1} for O_3/UVA and O_3 , respectively) when no Fe^{2+} or Cu^{2+} catalysts are used.

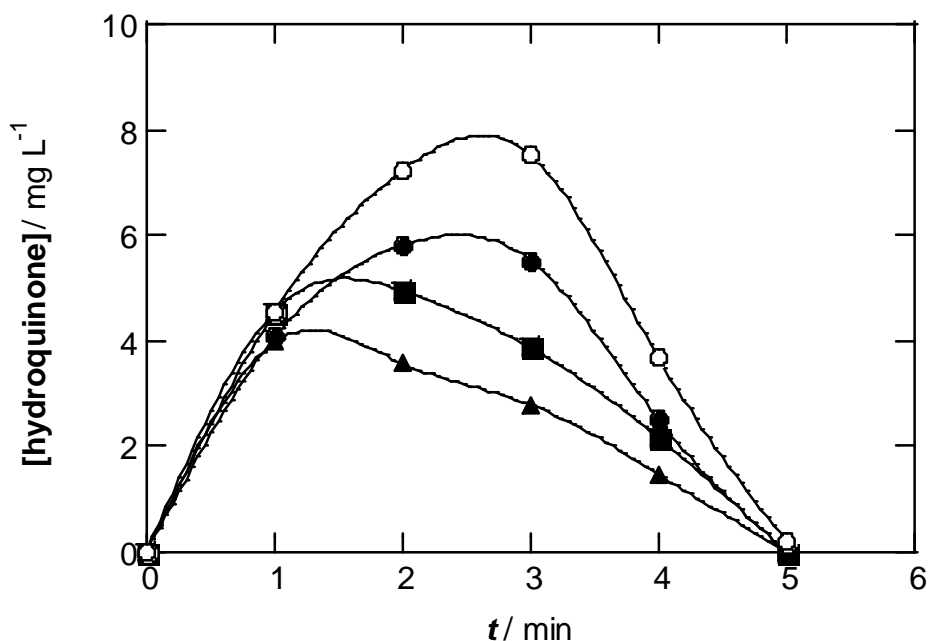


Figure 6.17. Time-course of the concentration of hydroquinone during the treatment of a 157 mg L^{-1} paracetamol solution of pH 3.0 at $25 \text{ }^\circ\text{C}$ by the treatment: (O) O_3 , (●) O_3/UVA , (■) $\text{O}_3 + 1.0 \text{ mM Fe}^{2+} + \text{UVA}$, (▲) $\text{O}_3 + 1.0 \text{ mM Fe}^{2+} + 0.25 \text{ mM Cu}^{2+} + \text{UVA}$.

The Figure 6.18 shows the evolution of the other paracetamol aromatic intermediate, *p*-benzoquinone, which was also detected by reversed-phase HPLC. The peak corresponding to this species eluted at $t_R = 3.31 \text{ min}$. This compound, unlike hydroquinone, reveals a more significant accumulation of this intermediate under the more $\bullet\text{OH}$ radical-yielding treatments $\text{O}_3/\text{Fe}^{2+}/\text{UVA}$ and $\text{O}_3/\text{Fe}^{2+}, \text{Cu}^{2+}/\text{UVA}$ (up to 8 mg L^{-1} and 10 mg L^{-1} accumulated, respectively, whereas values of only 4 and 5 mg L^{-1} are attained under O_3/UVA and O_3 treatments, respectively). The quicker elimination of hydroquinone under treatments $\text{O}_3/\text{Fe}^{2+}/\text{UVA}$ and $\text{O}_3/\text{Fe}^{2+}, \text{Cu}^{2+}/\text{UVA}$ leads to a faster formation of the intermediate *p*-benzoquinone, which is the product of the direct oxidation of hydroquinone. Thus, from the slower oxidation of hydroquinone under O_3 and O_3/UVA treatments only a smaller amount of its oxidation product *p*-benzoquinone can arise and it will only attain a lower maximal concentration than that reached under the more catalyzed oxidation treatments.

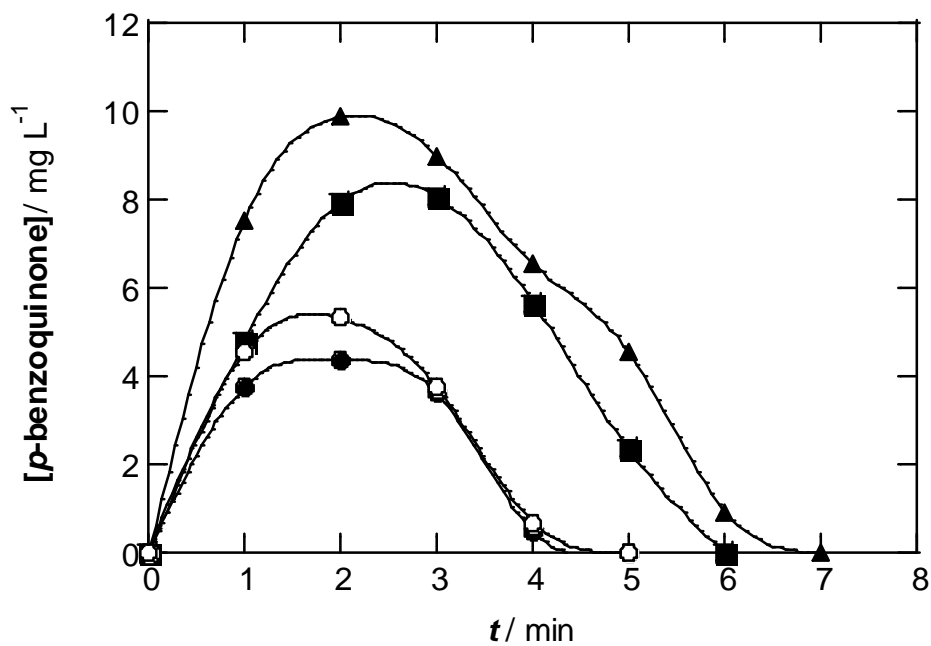


Figure 6.18. Time-course of the concentration of *p*-benzoquinone during the treatment of a 157 mg L⁻¹ paracetamol solution of pH 3.0 at 25 °C by the treatment: (O) O₃, (●) O₃/UVA, (■) O₃ + 1.0 mM Fe²⁺ + UVA, (▲) O₃ + 1.0 mM Fe²⁺ + 0.25 mM Cu²⁺ + UVA.

- Monitoring of aliphatic carboxylic acid intermediates / *Suiviement d'intermédies acides carboxyliques alifatiques*

Several aliphatic carboxylic acid intermediates were detected by ion-exclusion liquid chromatography during the different applied treatments to mineralize paracetamol solutions. Glycolic, tartronic, maleic, glyoxylic, ketomalonic, oxalic and oxamic acid were detected. Most of them were detected only during the first minutes of treatment, whereas oxalic and oxamic acids stayed in the treated solutions during several hours. It was for oxalic and oxamic acids that a study of their evolution with time was carried out.

The evolution of oxalic acid in treated solutions of paracetamol is displayed in Figure 6.19. When the weaker O_3 treatment is used, oxalic acid reaches a steady concentration of about 200 mg L^{-1} after 1 hour of mineralization treatment without undergoing any significant abatement for the next 3 hours of treatment. The O_3 molecule is capable of destroying the

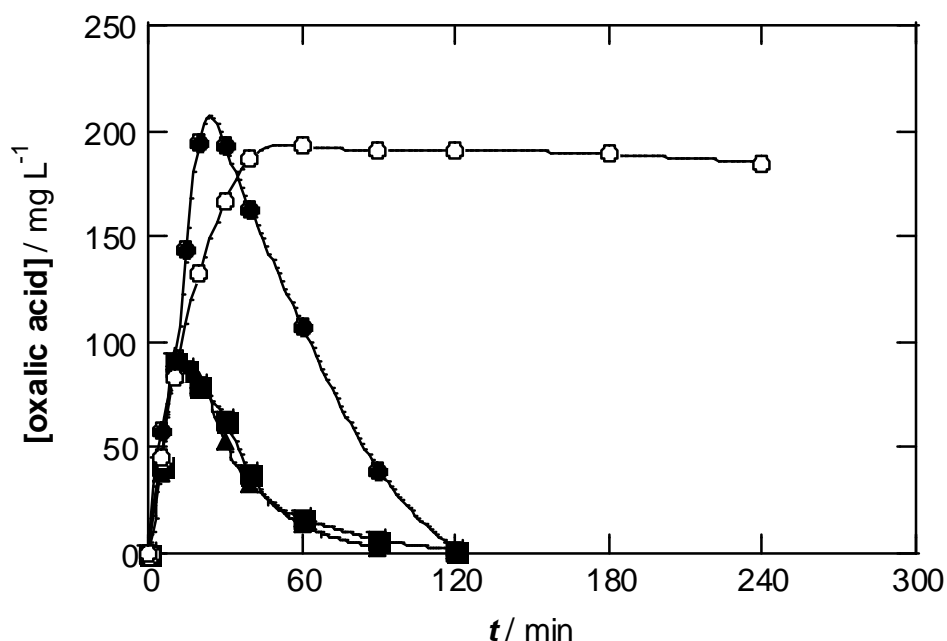


Figure 6.19. Time-course of the concentration of oxalic acid during the treatment of a 157 mg L^{-1} paracetamol solution of pH 3.0 at $25.0 \text{ }^\circ\text{C}$ by the treatment: (O) O_3 , (●) O_3 /UVA, (■) $O_3 + 1.0 \text{ mM Fe}^{2+} + \text{UVA}$, (▲) $O_3 + 1.0 \text{ mM Fe}^{2+} + 0.25 \text{ mM Cu}^{2+} + \text{UVA}$.

aromatic rings of paracetamol and the other aromatic intermediates hydroquinone and *p*-benzoquinone, as well as many aliphatic carboxylic acids, but it is not capable of destroying oxalic acid, which accumulates as the oxidation product of most of paracetamol intermediates.

When UV radiation is applied along with ozone, oxalic acid reaches its maximal concentration, again up to about 200 mg L^{-1} , in only half an hour. The higher concentration of generated $\bullet\text{OH}$ radicals under this treatment promotes the acceleration of the oxidation paths for the several formed intermediates, most of them leading to the formation of oxalic acid. But the presence of UV radiation and the same $\bullet\text{OH}$ radicals also cause the oxidation of this acid, making it disappear after 2 hours of treatment.

When the $\text{O}_3/\text{Fe}^{2+}/\text{UVA}$ and $\text{O}_3/\text{Fe}^{2+},\text{Cu}^{2+}/\text{UVA}$ treatments are applied only a maximal concentration below 100 mg L^{-1} is reached and oxalic acid disappears after 2 hours of treatment. As explained above (see Figure 6.9), under these treatments Fe(III) – oxalato complexes are formed. These complexes undergo a photolysis with the supplied UV radiation which leads to the decarboxylation of oxalic acid. The higher concentration of $\bullet\text{OH}$ radicals when using these treatments also accounts for the faster removal of this acid from the medium.

Another aliphatic carboxylic acid whose evolution with time could be well studied is oxamic acid. Figure 6.20 shows its time-course under the several applied ozone-based AOPs.

Under the weaker O_3 treatment, oxamic acid shows a slow, but steady increase in its concentration. The low concentration of $\bullet\text{OH}$ radicals causes a slow increasing of the concentration of oxamic acid, as the oxidation reactions which yield this intermediate product are also slow. When UVA radiation is applied (O_3/UVA treatment), a maximal concentration over 40 mg L^{-1} oxamic acid is attained after 90 minutes as a result of the increase of the oxidation reactions which lead to the formation of oxamic acid. After this point, this paracetamol degradation intermediate also undergoes oxidation and its concentration falls to 10 mg L^{-1} after 4 hours of treatment.

When the most oxidative $\text{O}_3/\text{Fe}^{2+}/\text{UVA}$ and $\text{O}_3/\text{Fe}^{2+},\text{Cu}^{2+}/\text{UVA}$ treatments are applied, significantly lower maximum concentrations of oxamic acid are attained (only 16 mg L^{-1} and 12 mg L^{-1} , respectively) before this acid undergoes a steady decay to attain concentrations of 10 and 5 mg L^{-1} , respectively. Again, the higher concentration of $\bullet\text{OH}$ radical accounts for the smaller maximal concentration attained for this intermediate. In the case of the $\text{O}_3/\text{Fe}^{2+},\text{Cu}^{2+}/\text{UVA}$ treatment, the formation of more easily oxidizable copper-oxamato complexes could play a significant role explaining the remarkably low accumulation and final concentration of this intermediate after the end of the treatment in the presence of Cu^{2+} catalyst ($\text{O}_3/\text{Fe}^{2+},\text{Cu}^{2+}/\text{UVA}$ treatment).

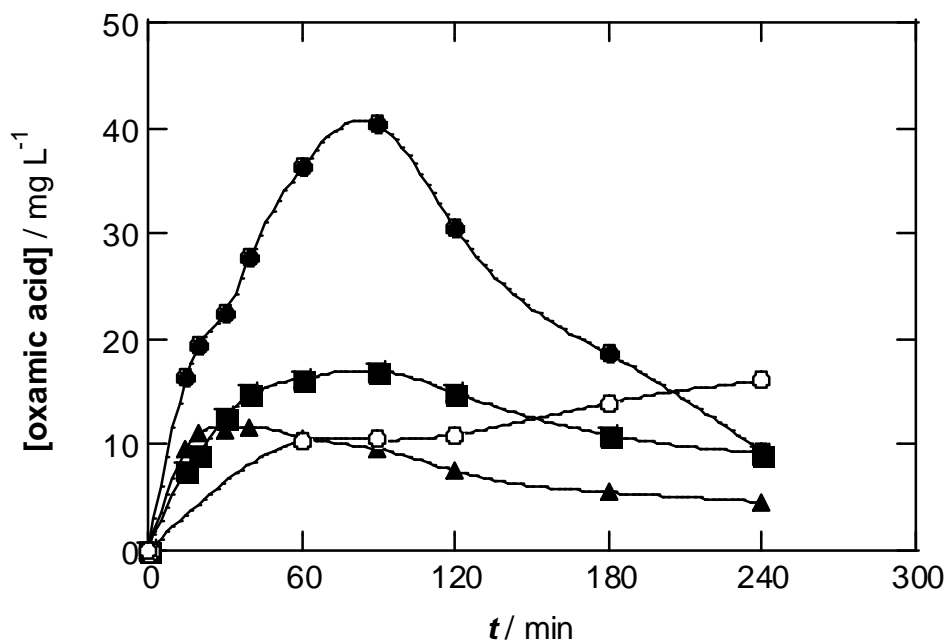


Figure 6.20. Time-course of the concentration of oxamic acid during the treatment of a 157 mg L⁻¹ paracetamol solution of pH 3.0 at 25.0 °C by the treatment: (○) O₃, (●) O₃/UVA, (■) O₃ + 1.0 mM Fe²⁺ + UVA, (▲) O₃ + 1.0 mM Fe²⁺ + 0.25 mM Cu²⁺ + UVA.

- Monitoring of ions / *Seuiment d'ions*

The formation of several ions which originate from the nitrogen atom of paracetamol was also studied for the ozone-AOPs applied on paracetamol solutions. Ammonium and nitrate ions were monitored with time for the several oxidation treatments by ion-exchange liquid chromatography. No significant amounts of nitrite anions were detected.

The evolution with time of ammonium cations arising from paracetamol degradation is represented on Figure 6.21. Under all of the treatments, except the O_3 one, the concentration of ammonium cation undergoes a steady increase along the mineralization process. One of the most important nitrogen sources for the formation of NH_4^+ cation is oxamic acid. These trends are consistent in the case of O_3/UVA , $O_3/Fe^{2+}/UVA$ and $O_3/Fe^{2+},Cu^{2+}/UVA$ treatments, with the constant decrease of oxamic acid with time after reaching its maximal concentration. Under the O_3 treatment, the concentration of oxamic acid only grows, suggesting that this intermediate only accumulates in the medium without undergoing significant degradation.

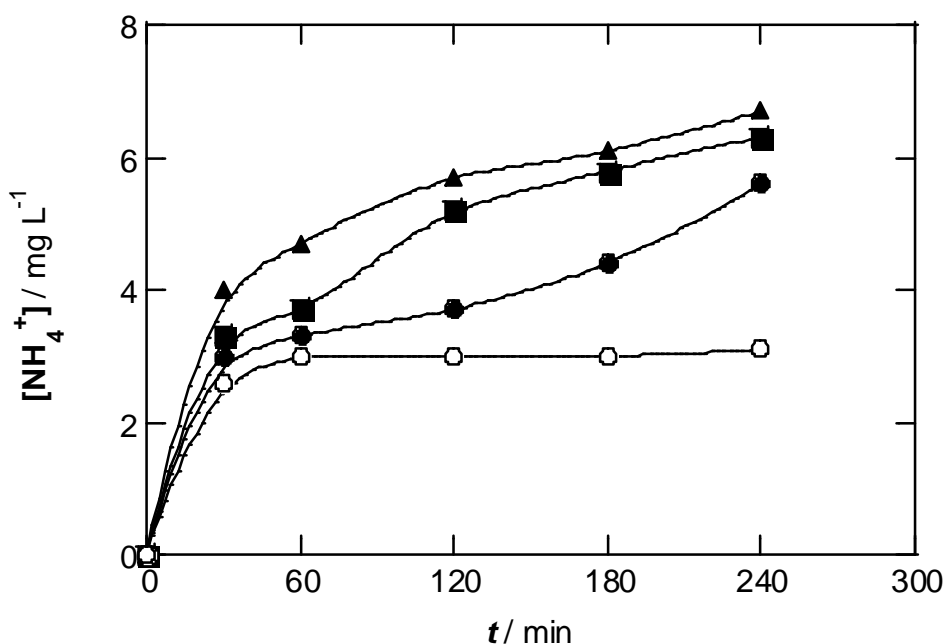


Figure 6.21. Time-course of the concentration of ammonium ion during the treatment of a 157 mg L^{-1} paracetamol solution of pH 3.0 at $25.0 \text{ }^\circ\text{C}$ by the treatment: (O) O_3 , (●) O_3/UVA , (■) $O_3 + 1.0 \text{ mM Fe}^{2+} + UVA$, (▲) $O_3 + 1.0 \text{ mM Fe}^{2+} + 0.25 \text{ mM Cu}^{2+} + UVA$.

This lack of degradation of oxamic acid explains the stop in the increase of the concentration of NH_4^+ cation, as this cation arises from the destruction of oxamic acid. The most powerful

the applied treatment, the higher the final concentration of formed ammonium: both aspects go in the order: $O_3 < O_3/UVA < O_3/Fe^{2+}/UVA < O_3/Fe^{2+},Cu^{2+}/UVA$. Powerful oxidation treatments capable of producing more oxidant $\bullet OH$ radicals and destroying a bigger amount of oxamic acid, will also produce a higher concentration of nitrogen-containing ions.

The evolution of the formed nitrate anion with time was also studied and is shown in Figure 6.22.

Similarly to the time-course profiles for the ammonium cation, the concentration of nitrate shows steady increases with time for the O_3/UVA , $O_3/Fe^{2+}/UVA$ and $O_3/Fe^{2+},Cu^{2+}/UVA$ treatments and only an almost insignificant formation under the O_3 method could be observed. This fact is again consistent with the possibility that oxamic acid is the main source of nitrogen and thus the main source of both ammonium and nitrate ions.

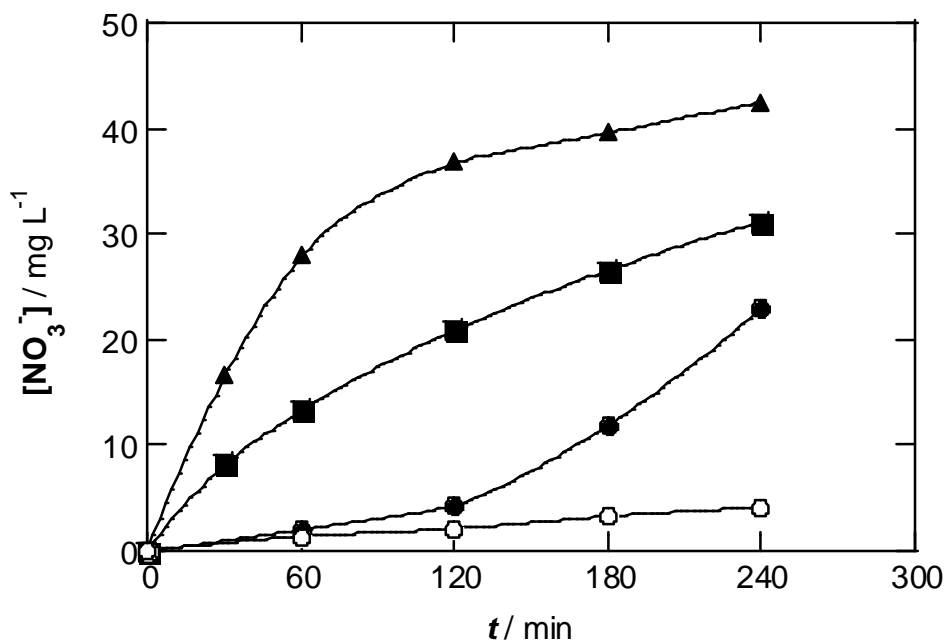


Figure 6.22. Time-course of the concentration of nitrate ion during the treatment of a 157 mg L^{-1} paracetamol solution of pH 3.0 at $25.0 \text{ }^\circ\text{C}$ by the treatment: (O) O_3 , (●) O_3/UVA , (■) $O_3 + 1.0 \text{ mM Fe}^{2+} + UVA$, (▲) $O_3 + 1.0 \text{ mM Fe}^{2+} + 0.25 \text{ mM Cu}^{2+} + UVA$.

6.1.3 Proposal of a degradation mechanism for paracetamol mineralization by ozone / *Proposta d'un mecanisme per a la mineralització del paracetamol amb ozó*

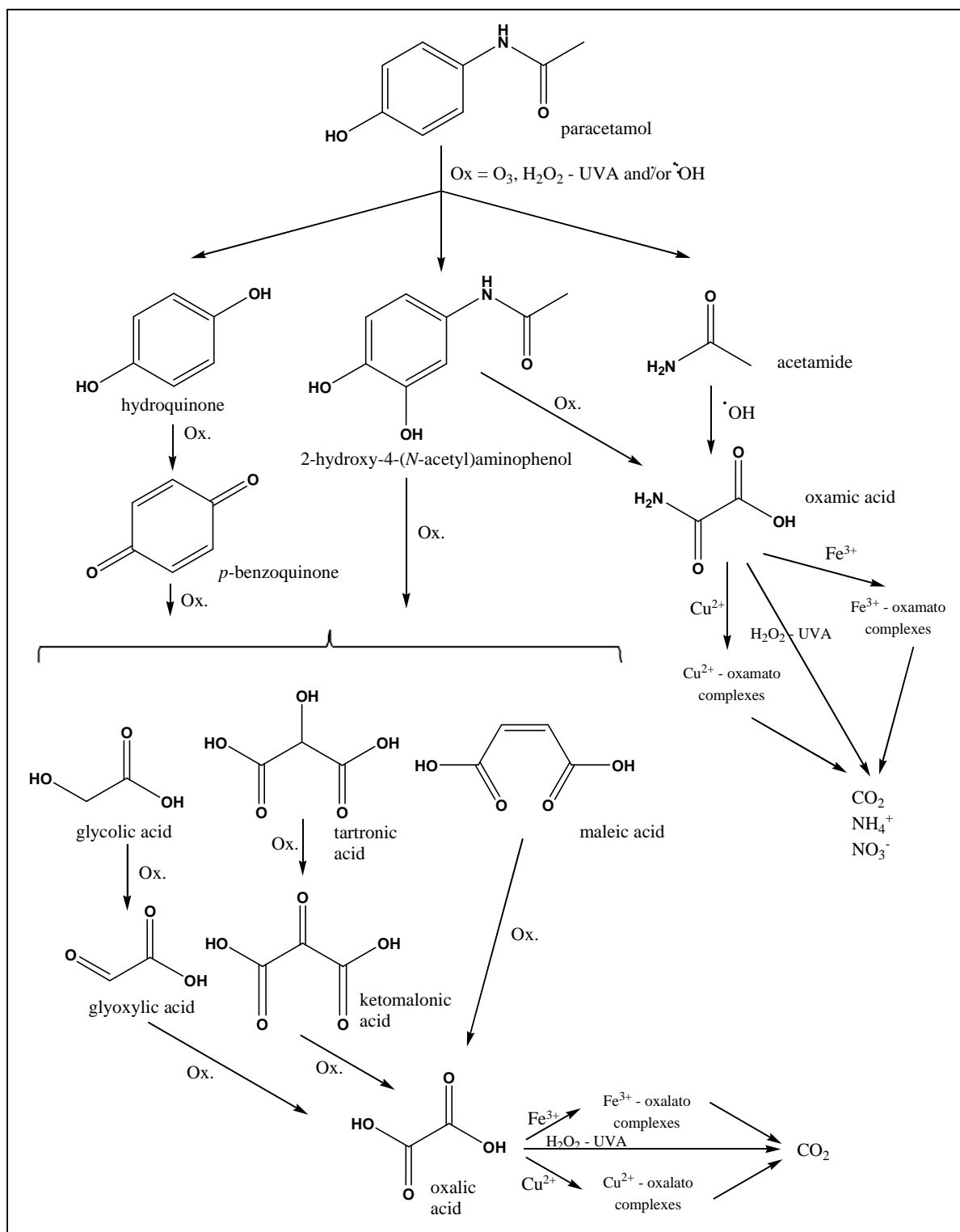


Figure 6.23. Degradation pathway proposed for the mineralization of paracetamol in acidic medium by O_3 and ozonation catalyzed with Fe^{2+} , Cu^{2+} and/or UVA light.

Figure 6.23 shows the proposed degradation pathway of paracetamol, in the different conditions studied, considering all the intermediates detected in this work, their chemical properties and the above discussion.

The paracetamol molecule undergoes an attack either directly by ozone molecules or by $\bullet\text{OH}$ radicals, which are formed from ozone photolysis or Fenton and photo-Fenton processes. This attack leads to the cleavage of the aryl C-N bond and the molecule splits into hydroquinone and acetamide.

Further oxidation of hydroquinone would yield *p*-benzoquinone. Direct attack by the hydroxyl radical species to paracetamol would also yield 2-hydroxy-4-(N-acetyl)aminophenol, which could be detected by GC/MS. The breakdown of the aromatic ring of *p*-benzoquinone leads to the formation of several carboxylic aliphatic acids, such as glycolic, tartronic and maleic acid. These acid intermediates can also arise from the breakdown of the aromatic ring of 2-hydroxy-4-(N-acetyl)aminophenol, which would also yield oxamic acid.

Further oxidation of glycolic acid would lead to the formation of glyoxylic acid, and ketomalonic acid would arise from the oxidation of tartronic acid. The further oxidation of glyoxylic, ketomalonic and maleic acids leads to the formation of oxalic acid. This acid reacts with dissolved Fe^{3+} to yield Fe^{3+} - oxalato complexes, which can be photolyzed into CO_2 .

Oxamic acid also forms complexes with Fe^{3+} yielding Fe^{3+} - oxamato complexes, which are not photolyzed by UV-light, but they are mineralized by $\bullet\text{OH}$ radicals into CO_2 , NH_4^+ and NO_3^- .

6.2 Study of chloroxylenol mineralization by means of electrochemical advanced oxidation processes / *Estudi de la mineralització del cloroxilenol mitjançant mètodes electroquímics d'oxidació avançada*

In this section, the mineralization of the antiseptic chloroxylenol is studied. Some preliminary results about the ozonation of chloroxylenol solutions are first shown and discussed, and then, the Electrochemical Advanced Oxidation Processes are introduced. The influence of several parameters on the mineralization efficiency of EAOPs, such as the nature of the electrodes, the applied current density and pH are also discussed. Finally, the concentration evolution of the antiseptic and the several arisen intermediates are shown and discussed for the several parameters.

6.2.1 Effect of experimental parameters on chloroxylenol mineralization / *Efecte de paràmetres experimentals en la mineralització del cloroxilenol*

In this section, the mineralization of chloroxylenol will be studied and discussed. The non-efficacy of ozone-based oxidation treatments on chloroxylenol will be shown first and the need of application of Electrochemical Advanced Oxidation Processes (EAOPs) is set out. The influence of several EAOP parameters on the mineralization rate of chloroxylenol solutions will be investigated.

Ozone-based AOPs applied to chloroxylenol mineralization / *AOPs basats en ozó aplicats a la mineralització del cloroxilenol*

After seeing that the Advanced Oxidation Processes based on ozone could show a good efficiency in the mineralization of paracetamol solutions, similar experiments were designed to carry out the mineralization of solutions containing the biocide chloroxylenol.

Three main ozone-based treatments were tested: O_3 , O_3/UVA and $O_3/Fe^{2+}/UVA$ in order to see to what extent the increasing of oxidative power of the treatment could lead to an increase in the mineralization rate and extent of chloroxylenol in aqueous solutions.

These different tests, whose resulting mineralization curves appear depicted in Figure 6.24, show that for chloroxylenol no quantitative mineralization was attained for the different ozone-based treatments, even when they were catalyzed to enhance a higher production of oxidant species. After 4 hours of trial, the direct ozonation (O_3 treatment) led only to a poor 28% mineralization as seen in Figure 6.24, curve *a*.

When under the same conditions UVA radiation was supplied (O_3 /UVA treatment represented in Figure 6.24, curve *b*), the mineralization extent grew to about 66%. A possible explanation to this enhancement of the mineralization process is the fact that UVA light can activate the present organic compounds making them more reactive not only with O_3 , but also with H_2O_2 , which can be formed in the solution from the photolysis of ozone (reaction (6.3)). The photolysis of ozone can take place with assisted UVA light of $\lambda > 300$ nm [147] as it is the case, since the used black light blue tube emitted in a wavelength range of 300 – 420 nm.

The addition of 1.0 mM Fe^{2+} does not appear to improve the mineralization rate of chloroxylenol, as observed from Figure 6.24, curve *c*, where only a 67% of mineralization was reached, very far from a quantitative mineralization. From these results it can be inferred that the increment of $\bullet OH$ radical concentration stimulated by UVA light through processes such as the photolysis of O_3 into H_2O_2 (reaction (6.3)), which can further react with Fe^{2+} to yield $\bullet OH$ reaction (6.2) or through the photo-Fenton reaction reaction (6.3), regenerating the Fe^{2+} and generating $\bullet OH$ at the same time, do not lead to any efficient mineralization results for the ozonation treatment of chloroxylenol solutions.

Ozone-based Advanced Oxidation Methods, which proved to be very efficient for the elimination of paracetamol, attaining quantitative mineralizations of paracetamol solutions, do not seem to be so effective for the mineralization of the biocide chloroxylenol, only attaining a 67% mineralization.

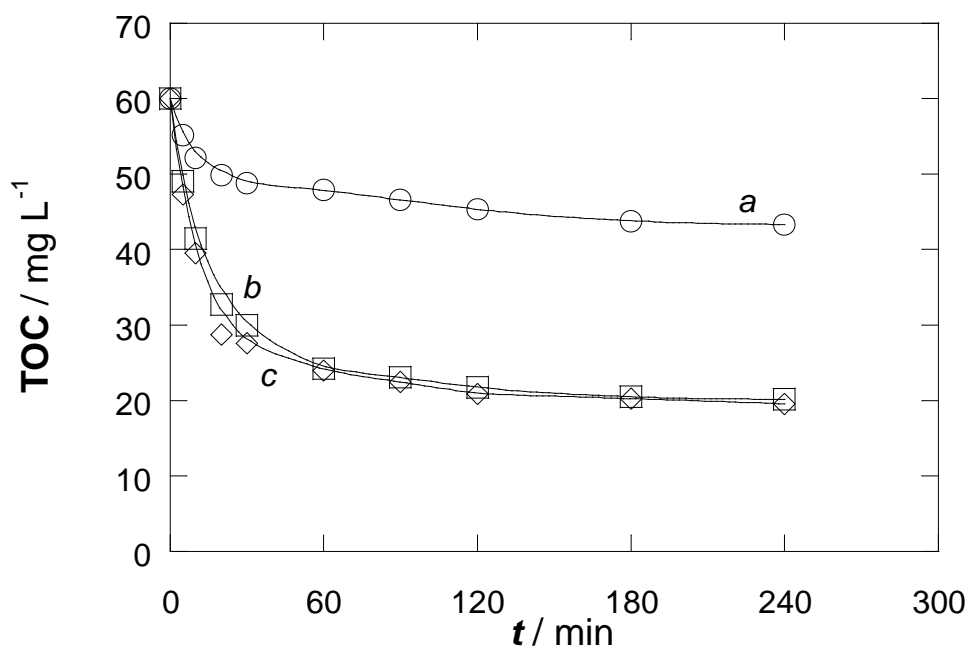


Figure 6.24. TOC decay profiles for 100 mL of a 100 mg L⁻¹ chloroxylenol solution at 25.0 °C and pH 3.0 under different ozone-based AOPs supplying 1 g O₃ h⁻¹. (a, O) O₃, (b, □) O₃/UVA, (c, ◇) O₃ + 1.0 mM Fe²⁺ + UVA. (For the two latter experiments a 6 W black light blue tube was situated 7 cm above the cell).

These unsatisfactory results rule out the ozone-based treatments as candidates for reaching an effective mineralization of chloroxylenol. From now on, Electrochemical Advanced Oxidation Processes (EAOPs), based on the electrochemical formation of the [•]OH radical will be implemented to try to reach the goal of quantitative mineralization.

- First trials on AEOPs: Pt and BDD anodes / *Primers tests amb AEOPs: Ànodes de platí i BDD.*

In the first trials on the Electrochemical Advanced Oxidation Processes, the oxidative power of the platinum and boron doped diamond (BDD) anodes was compared. Two experiments in which the main oxidative power comes from the formation of hydroxyl radicals at the surface of the anode were carried out. In these experiments a 3 cm² stainless steel (AISI 304) electrode was used as cathode, and 3 cm² platinum or BDD electrodes were used as anodes. These experiments were carried at 25.0 °C and pH 3.0.

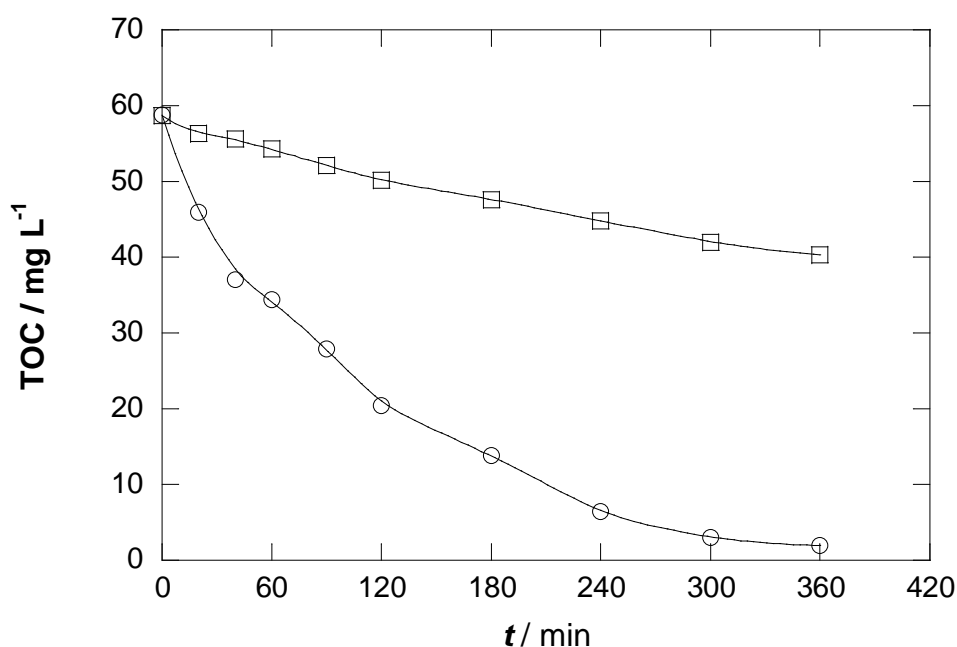


Figure 6.25. TOC decay for 100 mL of a solution containing 100 mg L⁻¹ chloroxylenol in 0.05 M Na₂SO₄ at 25.0 °C and pH 3.0 mineralized by anodic oxidation applying a current density of 100 mA cm⁻² using a stainless steel (AISI 304) cathode coupled with a: (□) platinum anode; (○) BDD anode.

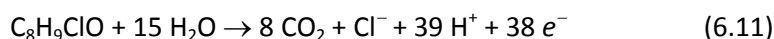
The curves in Figure 6.25 show a much faster mineralization rate when using a boron doped diamond anode (BDD), for which a 97% of the initial chloroxylenol concentration has been mineralized in 6 hours of time, whereas only a poor 31% mineralization has been reached at the same time when using a platinum anode.

As the main oxidation process taking place is the oxidation of organics with the hydroxyl radical $\bullet\text{OH}$ electrogenerated and adsorbed at the surface of the anode (reaction (1.1)), a higher reactivity of the hydroxyl radicals at the BDD surface than that of the same species adsorbed at the surface of the platinum anode can be inferred. Indeed, BDD has a high O_2 -overvoltage which favors the formation of bigger amounts of oxygen species with very positive reduction potentials such as $\bullet\text{OH}$ in comparison to other anodic materials [157 – 159]. $\bullet\text{OH}_{(\text{Pt})}$ are chemisorbed on the platinum surface whereas hydroxyl radicals, which are only physisorbed, are formed on the BDD surface [158], which allows them to oxidize the surrounding species much more freely.

The oxidation power of several EAOPs at different current densities for chloroxylenol mineralization was compared during the treatment of 100 mg L^{-1} chloroxylenol solutions at $25.0 \text{ }^\circ\text{C}$ and $\text{pH } 3.0$. Current density values comprised between 33 mA cm^{-2} and 150 mA cm^{-2} were tested for several treatments:

- a) BDD-AO: Anodic oxidation method using a 3 cm^2 BDD anode and a 3 cm^2 stainless steel (AISI 304) cathode.
- b) Pt-EF: Electro-Fenton method consisting of a 3 cm^2 platinum anode coupled to a 3 cm^2 oxygen diffusion cathode and 1.0 mM Fe^{2+} .
- c) BDD-PEF: Photoelectro-Fenton method consisting of a 3 cm^2 BDD anode coupled to a 3 cm^2 oxygen diffusion cathode and 1.0 mM Fe^{2+} and a supply of UVA irradiation from a black light blue tube.

Figure 6.26 shows that for the BDD-AO treatment, an increase in current density leads to bigger TOC removal as a greater supply of electrons should lead to the electrooxidation of more chloroxylenol molecules. This is in agreement with the equation for the mineralization of chloroxylenol:



For the BDD-AO method the enhancement in its oxidation power is easily appreciable when increasing the current density from 33 to 100 mA cm^{-2} (Figure 6.26), but not any more when the current density is increased from 100 to 150 mA cm^{-2} . From this result, a kinetic limitation by the quantity of reactive $\bullet\text{OH}_{(\text{BDD})}$ generated at about 100 mA cm^{-2} can be deduced.

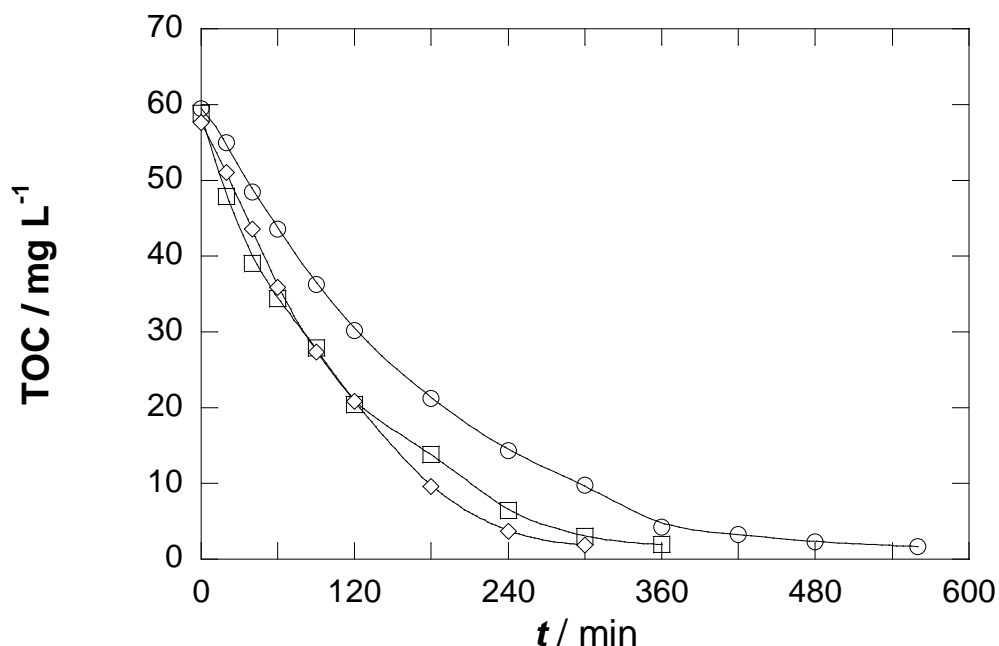
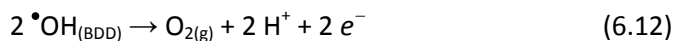
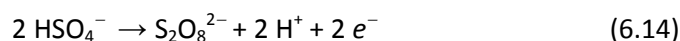


Figure 6.26. TOC abatement profiles for the degradation of 100 mL solution of a 100 mg L⁻¹ chloroxylenol solution in 0.05 M Na₂SO₄, at 25.0 °C and pH 3.0 using a BDD anode and a stainless steel cathode at different applied current densities. Applied current density: (○) 33 mA cm⁻²; (□) 100 mA cm⁻²; and (◇) 150 mA cm⁻².

Also, the current efficiency decreases when increasing values of current density j , as shown in Figure 6.27, where under the same values of applied charge, the methods operating at lower current densities cause a bigger decrease of TOC. This behavior suggests that although higher j values lead to the production of larger amounts of $\bullet\text{OH}_{(\text{BDD})}$, which favour the removal of organics, a larger specific charge has been consumed because the $\bullet\text{OH}$ are generated in less relative extent due to the quicker acceleration of its non-oxidative reactions such as its oxidation to O₂ and recombination into H₂O₂:



In addition, the production of $\bullet\text{OH}_{(\text{BDD})}$ related to the supplied current density can also be diminished as a consequence of the faster generation of weaker oxidants such as S₂O₈²⁻ according to the following reaction:



The little enhancement of TOC removal from 100 mA cm^{-2} to 150 mA cm^{-2} (Figure 6.26) can then be ascribed to the limitation of the degradation rate of organic pollutants by their mass transport to the anode giving rise to a quick loss of reactive $\bullet\text{OH}_{(\text{BDD})}$ by acceleration of reactions (6.11) – (6.13) and the formation of ozone as

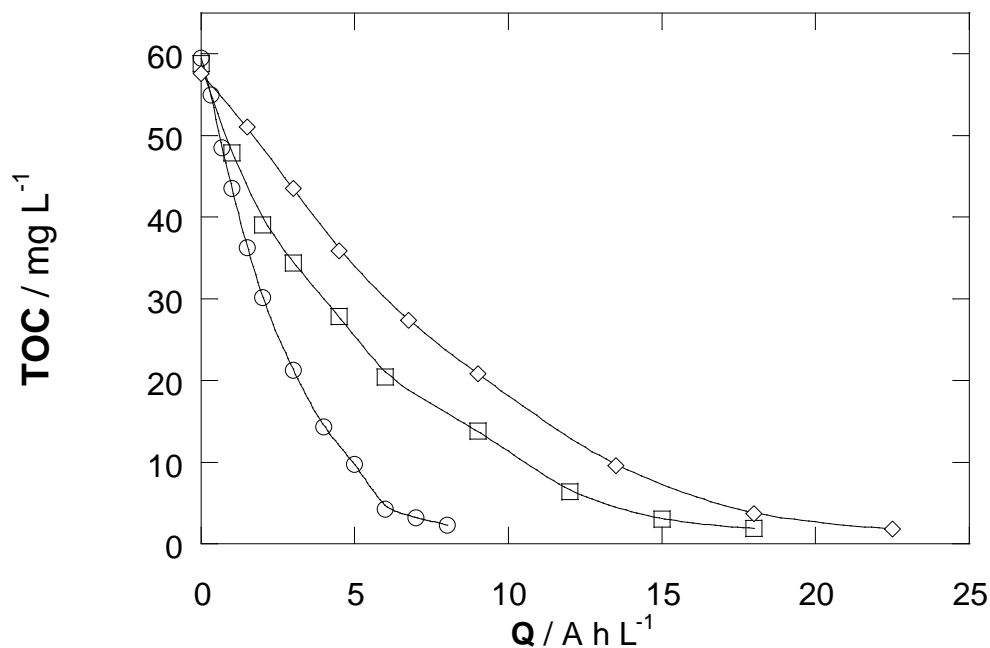
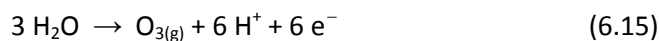


Figure 6.27. TOC decay versus applied specific charge for the degradation of 100 mL of a 100 mg L^{-1} chloroxylenol solution in $0.05 \text{ M Na}_2\text{SO}_4$, at $25.0 \text{ }^\circ\text{C}$ and $\text{pH } 3.0$ using a BDD anode and a stainless steel cathode at different applied current densities. Applied current density: (○) 33 mA cm^{-2} ; (□) 100 mA cm^{-2} ; and (◇) 150 mA cm^{-2} .

Experiments at the same current densities were carried out for the Pt-EF and BDD-PEF methods and similar results were obtained. Figures 6.28 and 6.29 show the curves of TOC removal versus the applied specific charge at different applied current densities. The most efficient treatment is again that carried out at 33 mA cm^{-2} .

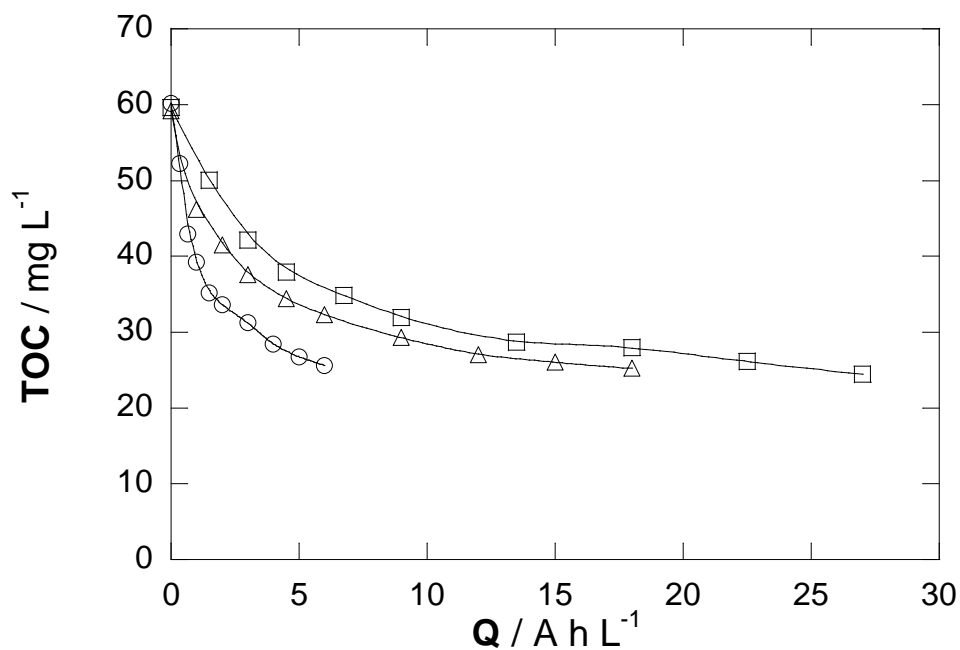


Figure 6.28. TOC decay versus applied specific charge for the degradation of 100 mL of a 100 mg L⁻¹ chloroxylenol solution in 0.05 M Na₂SO₄, at 25.0 °C and pH 3.0 using a Pt anode and an oxygen diffusion cathode at different applied current densities. Applied current density: (○) 33 mA cm⁻²; (□) 100 mA cm⁻²; and (◇) 150 mA cm⁻².

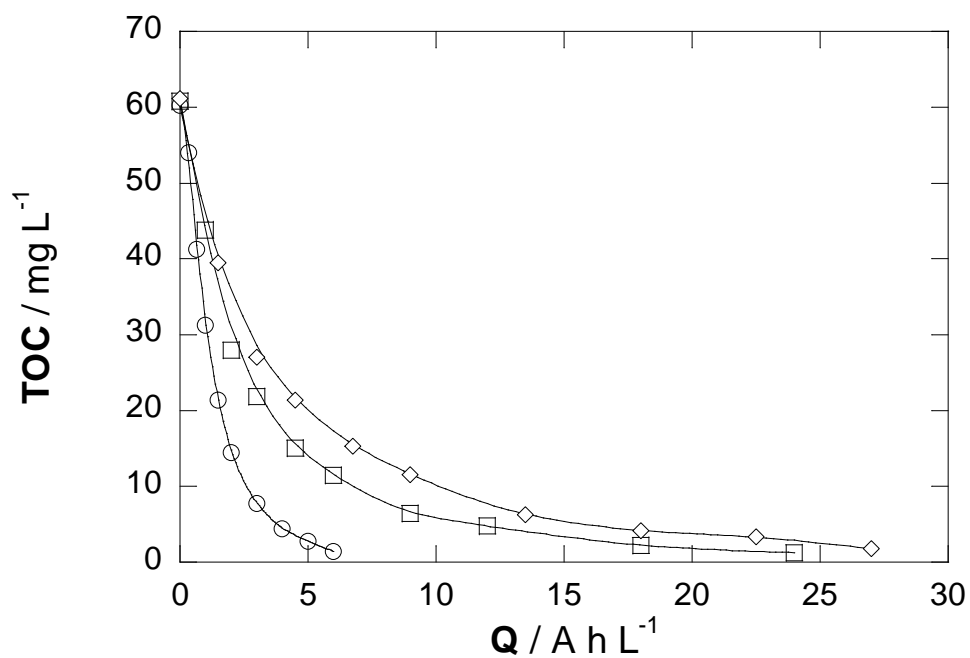


Figure 6.29. TOC decay versus applied specific charge for the degradation of 100 mL of 100 mg L⁻¹ chloroxylenol solutions in 0.05 M Na₂SO₄, at 25.0 °C and pH 3.0 using a BDD anode and an oxygen diffusion cathode at different current densities. Applied current density: (○) 33 mA cm⁻²; (□) 100 mA cm⁻²; and (◇) 150 mA cm⁻².

After seeing that no significant improvements are attained when increasing the applied current density from 33 mA cm^{-2} and the fact that this increase leads to a loss of current efficiency, the different EAOPs will be tested at a default current density of 33 mA cm^{-2} .

A set of different EAOPs was carried out to evaluate which of these treatments showed the most efficient performance at mineralizing the biocide chloroxylenol. The tested EAOPs included:

- Pt-AO: Anodic oxidation using a 3 cm^2 platinum anode coupled to a 3 cm^2 stainless steel cathode.
- BDD-AO: Anodic oxidation consisting of a 3 cm^2 BDD anode coupled to a 3 cm^2 stainless steel cathode.
- Pt-EF: Platinum-electro-Fenton method, which consists of a 3 cm^2 platinum anode and an oxygen diffusion cathode which has 3 cm^2 area of carbon black – PTFE cloth. The treated solution contains 1.0 mM Fe^{2+} .
- BDD-EF: BDD-electro-Fenton method, which consists of a 3 cm^2 BDD anode coupled to an oxygen diffusion cathode with a 3 cm^2 area of carbon black – PTFE cloth, both immersed in a solution containing 1.0 mM Fe^{2+} .
- Platinum-photoelectro-Fenton (Pt-PEF) and BDD-photoelectro-Fenton (BDD-PEF) methods are just the same as Pt-EF and BDD-EF with the extra supply of UVA radiation between $300 - 420 \text{ nm}$, with a maximum at $\lambda_{\text{max}} = 360 \text{ nm}$ from a 6 W black light blue tube.

The mineralization curves resulting from the described EAOPs are shown in Figure 6.30 below.

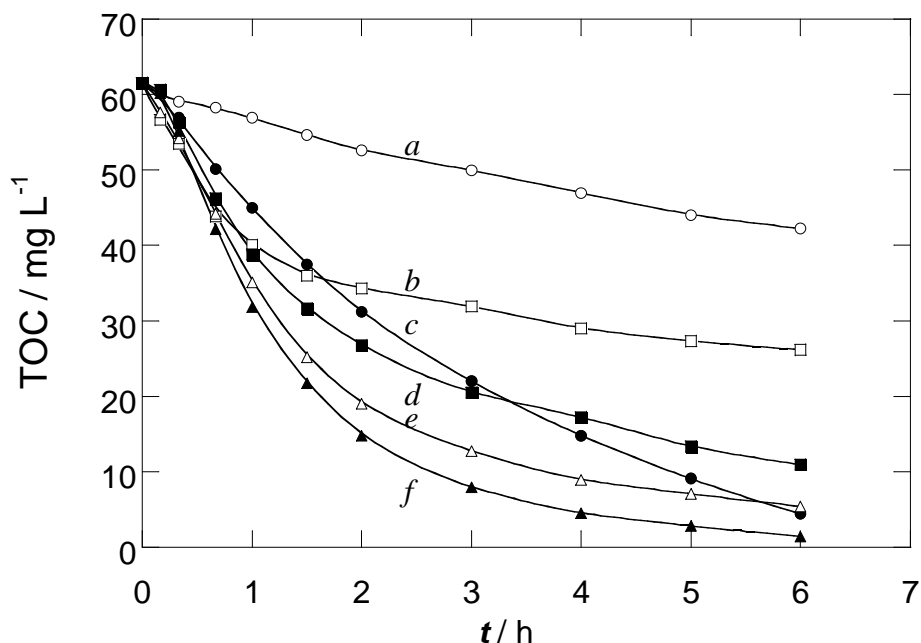


Figure 6.30. TOC decay vs time for the degradation of 100 mL of a 100 mg L⁻¹ chloroxylenol solution in 0.05 M Na₂SO₄ at 25.0 °C and pH 3.0 at 33 mA cm⁻². Method: (a,○) Pt-AO; (b,□) Pt-EF; (c,●) BDD-AO; (d,■) BDD-EF; (e,△) Pt-PEF; and (f,▲) BDD-PEF.

The Pt-AO treatment (Figure 6.30, curve *a*) is by far the less efficient method. It only reaches a 31% mineralization of the biocide after 6 hours of trial. When an oxygen diffusion cathode is coupled with the platinum anode replacing the stainless-steel cathode in the Pt-EF treatment (Figure 6.30, curve *b*) the extent of mineralization is increased to 57% in the same time. The improvement of the mineralization efficiency is due to the additional supply of $\bullet\text{OH}$ radicals. Hydrogen peroxide formed in the oxygen diffusion cathode from the reduction of oxygen at the surface of the carbon black –PTFE cloth (reaction (1.2)) reacts easily with dissolved Fe²⁺ (reaction (6.3)), thus generating $\bullet\text{OH}$ radicals in the bulk of the solution. This leads to the presence of such a highly oxidant species everywhere in the treated solution, and not only on the anode surface, as it happens in anodic oxidation. When UVA light is supplied to this latter method (Pt-PEF, Figure 6.30, curve *e*), the mineralization efficiency is considerably increased up to attain about 91%. The UVA radiation enables the photo-Fenton reaction, which accounts for an extra production of $\bullet\text{OH}$ together with the regeneration of Fe²⁺ by reducing Fe³⁺ back to Fe²⁺ (reaction (6.2)), which further stimulates the Fenton process (reaction (1.3)).

Along with the increase of the $\bullet\text{OH}$ radical concentration in the medium, the presence of Fe^{2+} together with UV radiation enables the photodecarboxylation of iron – oxalato complexes. Oxalic acid is one of the most persistent degradation intermediates from the mineralization of chloroxylenol and complexes with Fe^{3+} and undergoes a photolysis followed by a decarboxylation yielding CO_2 . The destruction of this intermediate is reflected in a larger TOC decay.

Under a BDD-AO treatment (Figure 6.30, curve *c*) chloroxylenol undergoes a slow, but steady destruction, up to reach a 93% mineralization. The initial mineralization rate for the BDD-AO treatment is lower than that for the treatments based on the oxygen diffusion cathode as no $\bullet\text{OH}$ radical is produced in the bulk solution from Fenton and Photo-Fenton processes. Still, the good ability of the BDD material to generate weakly adsorbed and highly reactive $\bullet\text{OH}$ radicals on its surface (reaction (1.1)) enables the BDD-AO method to attain an almost complete mineralization after 6 hours of treatment.

When the powerful BDD anode is coupled with an oxygen diffusion cathode (BDD-EF treatment, Figure 6.30, curve *d*) a faster initial mineralization rate is observed, but a lower mineralization grade (82%) is reached at the end of the trial when compared with the 93% attained using the stainless steel cathode. The implementation of the oxygen diffusion cathode with the presence of Fe^{2+} salt in the medium involves an additional $\bullet\text{OH}$ formation, which explains the faster initial mineralization rate of the BDD-EF treatment than that of the BDD-AO. However, oxalate complexes with Fe^{3+} are difficultly destroyed by the $\bullet\text{OH}_{(\text{BDD})}$ and the $\bullet\text{OH}$ in the bulk solution, thus leading to 22% of organic carbon still remaining in the solution after 6 hours of treatment.

This problem is nonetheless solved when UVA radiation is applied in a treatment using the BDD anode coupled with the oxygen diffusion cathode (BDD-PEF method, Figure 6.30, curve *f*). A 98% mineralization is reached. The Photo-Fenton reaction not only involves an additional supply of $\bullet\text{OH}$ radical to the system, but also the reduction of Fe^{3+} ions back to Fe^{2+} , which boosts the Fenton process. More importantly, the photodecarboxylation of iron – oxalate complexes to CO_2 accounts for most of the sharper TOC abatement of this mineralization method (from 22% without using a UV lamp in BDD-EF to the 98% mineralization with the use of the UV lamp).

6.2.2 Study of chloroxylenol and its degradation intermediates time-course / Estudi de l'evolució del cloroxilenol i dels seus intermedis de degradació

The concentration of chloroxylenol was monitored by reverse phase HPLC to study its evolution with time under the main applied mineralization treatments. The chloroxylenol molecule exhibited a well defined peak at a retention time of $t_R = 2.25$ min at $\lambda = 220$ nm.

It was first studied under the application of EAOPs based on the anodic oxidation, i.e. using a stainless steel cathode and a platinum or BDD anode. Figure 6.31 shows the evolution of chloroxylenol concentration with time comparing the performance of platinum and BDD anodes and, for the treatments based on the BDD anode, the effect of different applied current densities.

The anodic oxidation involving a platinum anode and a stainless steel cathode (Pt-AO) takes over 11 hours before the parent compound disappears from solution when working at a current density of 33 mA cm^{-2} . When the platinum anode is replaced by a BDD one, the time required for a total removal of this drug goes down to 7 hours. The results in Figure 6.31 show that the higher ability of BDD to generate $\bullet\text{OH}$ radicals causes also a faster elimination of chloroxylenol itself.

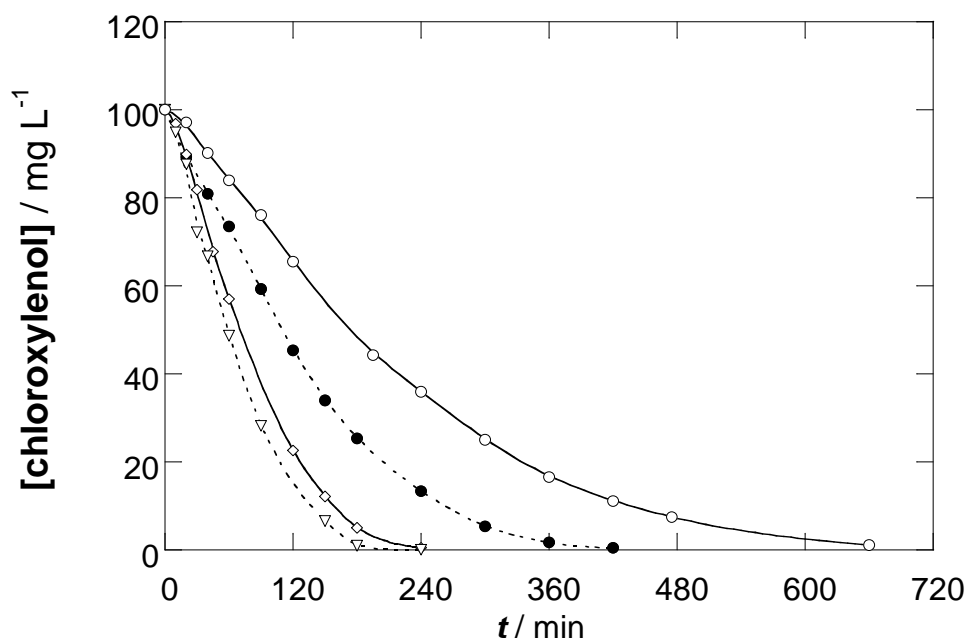


Figure 6.31. Chloroxylenol concentration decay with electrolysis time during the treatment of 100 mL of a 100 mg L^{-1} biocide solution in $0.05 \text{ M Na}_2\text{SO}_4$ at $25.0 \text{ }^\circ\text{C}$ and $\text{pH } 3.0$. (\circ) Pt-AO at 33 mA cm^{-2} ; BDD-AO at (\bullet) 33 mA cm^{-2} ; (\diamond) 100 mA cm^{-2} ; and (∇) 150 mA cm^{-2} .

After seeing the better performance of the BDD anode in removing the biocide chloroxylenol from the solution, different current intensity values were applied for the anodic oxidation treatments coupling the BDD anode with the stainless steel cathode (BDD-AO treatment) in order to study whether the current density played a significant role on the removal rate of chloroxylenol.

Figure 6.31 depicts the decay curves of chloroxylenol treated by the BDD-AO method at 33 mA cm^{-2} , 100 mA cm^{-2} and 150 mA cm^{-2} . A big difference is noticeable when increasing the applied current density from 33 mA cm^{-2} to 100 mA cm^{-2} , since the biocidal drug is destroyed before in the latter conditions (3h). The higher current density causes a raise in the amount of generated $\bullet\text{OH}$ radicals at the surface of the BDD anode, thus accounting for the important improvement in the elimination of the drug. However, a much more modest improvement is observed when the applied current density is raised from 100 mA cm^{-2} to 150 mA cm^{-2} . Although a further increase from 100 mA cm^{-2} produces $\bullet\text{OH}$ radicals at a higher rate, other side reactions may undergo an acceleration at these high current densities, such as the formation of oxygen from adsorbed $\bullet\text{OH}$ species (reaction (6.12)), the dimerization of $\bullet\text{OH}$ radicals to yield hydrogen peroxide (reaction (6.13)), and the loss of $\bullet\text{OH}$ by reaction with H_2O_2



or with Fe^{2+} [160].



All of these waste processes involve the loss of $\bullet\text{OH}$ radicals. This explains the fact that the increase of current density does not lead to a proportional growth of the $\bullet\text{OH}$ generation and thus to the amount of eliminated molecules of chloroxylenol.

The several oxidation processes taking place during the mineralization of chloroxylenol by anodic oxidation treatments appear to be very complex as the kinetic analysis of the several concentration decays of chloroxylenol did not reveal a definite kinetic order for this drug.

The concentration of chloroxylenol was also monitored for the mineralization treatments based on the oxygen diffusion cathode. The Figure 6.32 shows a much faster elimination of this biocide under electro-Fenton and photoelectro-Fenton oxidation treatments, which cause the total removal of chloroxylenol in only 15 minutes. Since under these treatments the concentration of $\bullet\text{OH}$ in the bulk solution undergoes a significant

increase, these results show that the $\bullet\text{OH}_{\text{bulk}}$ is by far the main oxidant species of chloroxylenol, much more important than $\bullet\text{OH}_{(\text{BDD})}$ or $\bullet\text{OH}_{(\text{Pt})}$, for which the complete elimination of the parent compound only is reached after several hours.

A kinetic analysis from these results was carried out considering a pseudo-first-order reaction for chloroxylenol (see inset in Figure 6.32). The values obtained for the kinetic constants, displayed in Table 6.4, show increasing values following the order Pt-EF < BDD-EF < Pt-PEF < BDD-PEF, which is consistent with the nature of the more reactive $\bullet\text{OH}_{(\text{BDD})}$ than $\bullet\text{OH}_{(\text{Pt})}$ and the boosting effect of the UVA radiation stimulating the further generation of bulk $\bullet\text{OH}$.

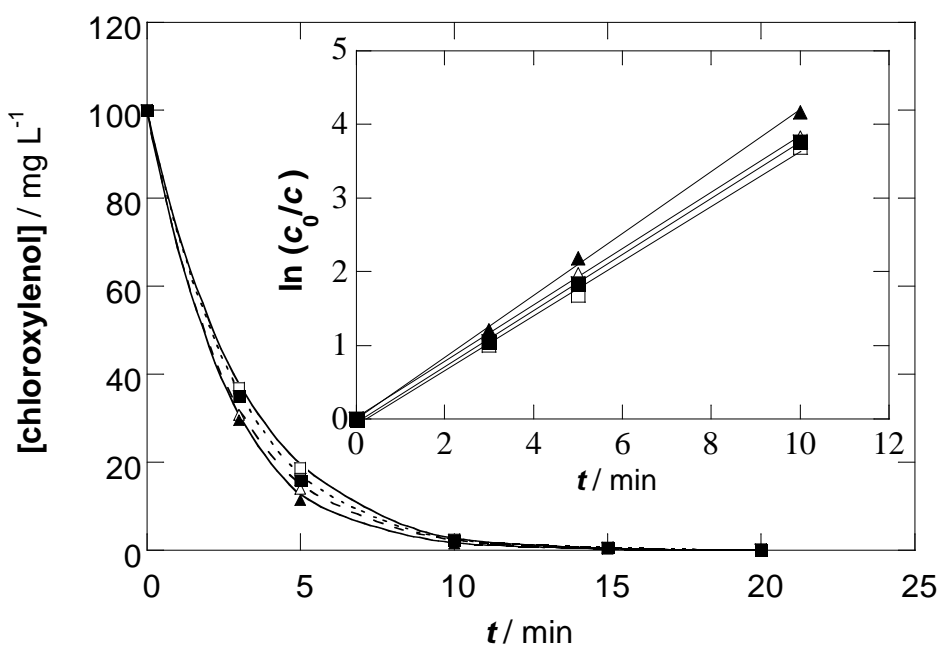


Figure 6.32. Chloroxylenol concentration decay with electrolysis time during the degradation of 100 mL of a 100 mg L^{-1} chloroxylenol solution in $0.05 \text{ M Na}_2\text{SO}_4$ and 1.0 mM Fe^{2+} at $25.0 \text{ }^\circ\text{C}$ and $\text{pH } 3.0$ at 33 mA cm^{-2} . (\square) Pt-EF; (\blacksquare) BDD-EF; (\triangle) Pt-PEF; and (\blacktriangle) BDD-PEF. The inset panel gives the kinetic analysis considering a pseudo-first-order reaction for chloroxylenol.

Table 6.4. Kinetic constants obtained for the electro-Fenton and photoelectro-Fenton oxidation treatments considering a pseudo-first order for chloroxylenol for its degradation.

treatment	k / s^{-1}
Pt-EF	$6.2 \cdot 10^{-3}$
BDD-EF	$6.3 \cdot 10^{-3}$
Pt-PEF	$6.4 \cdot 10^{-3}$
BDD-PEF	$6.9 \cdot 10^{-3}$

- Evolution of chloroxylenol intermediates / *Evolució dels intermedis del cloroxilenol*

Several intermediates were identified during the mineralization of chloroxylenol solutions. These species included the aromatic 2,6-dimethyl-*p*-benzoquinone and several aliphatic carboxylic acids such as acetic, pyruvic, and oxalic. The concentration of chloride arising from the releasing of the chlorine atom from the chloroxylenol molecule was also monitored.

- *Aromatic intermediates / Intermedis aromàtics*

The intermediate 2,6-dimethyl-*p*-benzoquinone was detected from all of the applied mineralization treatments and its concentration with time was measured by reversed-phase HPLC, for which it exhibited a well defined peak at a retention time of $t_R = 1.43$ min at $\lambda = 254$ nm.

The evolution with time of 2,6-dimethyl-*p*-benzoquinone under the Pt-AO and BDD-AO treatments is depicted in Figure 6.33. Under the anodic oxidation treatment based on the platinum anode and stainless steel cathode, this aromatic intermediate undergoes an important accumulation up to 37 mg L^{-1} whereas its maximal concentration when applying an anodic oxidation coupling BDD and stainless steel electrodes (BDD-AO) scarcely attains a maximal concentration of 3 mg L^{-1} . After 15 hours of Pt-AO treatment, still significant concentrations of this intermediate were present in the solution (over 5 mg L^{-1}), whereas the anodic oxidation based on the BDD anode had already eliminated it completely after 8 hours.

This intermediate is formed from the hydrolysis of the chloro-group of chloroxylenol to yield the short-live intermediate 2,6-dimethylhydroquinone, followed by the oxidation of 2,6-dimethylhydroquinone. After its formation, 2,6-dimethyl-*p*-benzoquinone is sequentially attacked by the adsorbed $\bullet\text{OH}$ radicals. Bearing that in mind, these results show that the $\bullet\text{OH}$ radicals adsorbed on the platinum surface area able to oxidize the hydroquinone derivative to its *p*-benzoquinone equivalent, but the concentration of $\bullet\text{OH}$ on the platinum surface seems insufficient to destroy the much more stable 2,6-dimethyl-*p*-benzoquinone. The BDD-AO treatment, on the contrary, shows a good ability to destroy this benzoquinone form, not letting it accumulate over 3 mg L^{-1} .

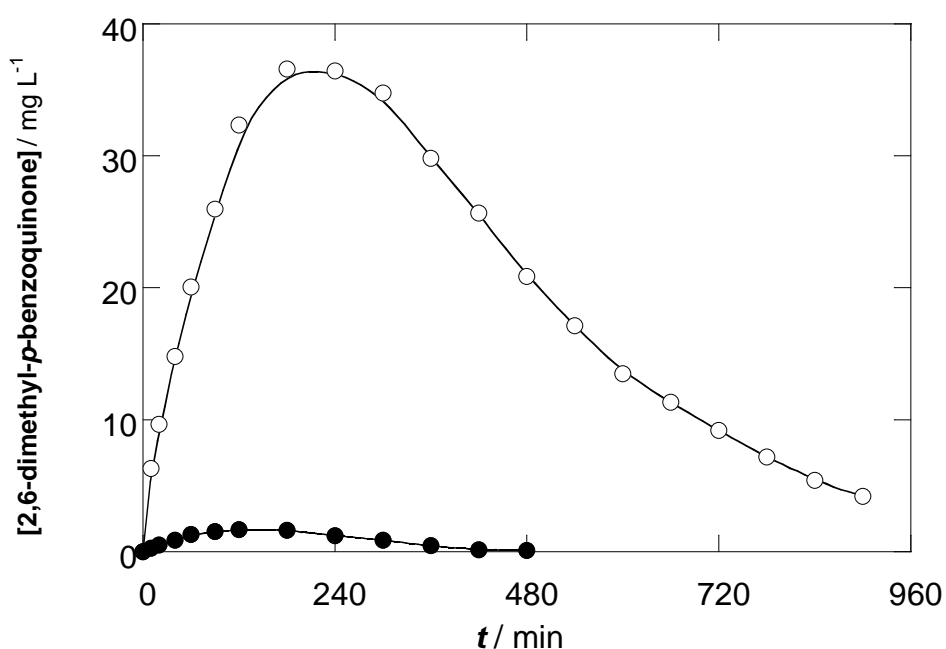


Figure 6.33. Time-course of 2,6-dimethyl-*p*-benzoquinone concentration formed as by-product during the degradation of 100 mL of a 100 mg L^{-1} chloroxylenol solution at $25.0 \text{ }^\circ\text{C}$ and pH 3.0 by anodic oxidation based EAOPs at an applied intensity of 33 mA cm^{-2} . Treatments: (○) Pt-AO; and (●) BDD-AO.

The evolution study of 2,6-dimethyl-*p*-benzoquinone under Pt-EF, Pt-PEF, BDD-EF and BDD-PEF methods, displayed in Figure 6.34, shows very similar curves regardless of the nature of the anode (platinum or BDD) and the existence of UVA radiation supply. For all of these treatments 2,6-dimethyl-*p*-benzoquinone attains a maximum peak of about 8 mg L^{-1} after 4 minutes. Under Pt-EF and Pt-PEF treatments, this maximal concentration is slightly higher than

that reached under the other two methods based on BDD anodes. After 20 minutes this intermediate has disappeared completely from the solution for all of these four treatments.

The higher maximal accumulation of this intermediate (around 8 mg L^{-1}) in comparison with that accumulated with the anodic oxidation treatment coupling a stainless steel cathode with a BDD anode (BDD-AO treatment) can be explained by the fact that the presence of $\bullet\text{OH}$ radicals in the bulk solution under (photo)electro-Fenton methods causes an acceleration of the oxidation of the intermediate 2,6-dimethylhydroquinone, a reaction which has the intermediate 2,6-dimethyl-*p*-benzoquinone as a product. This same $(\bullet\text{OH})_{\text{bulk}}$ radicals account for the fast elimination of this intermediate from the solution, since before half an hour of treatment this intermediate has been completely eliminated from the solution.

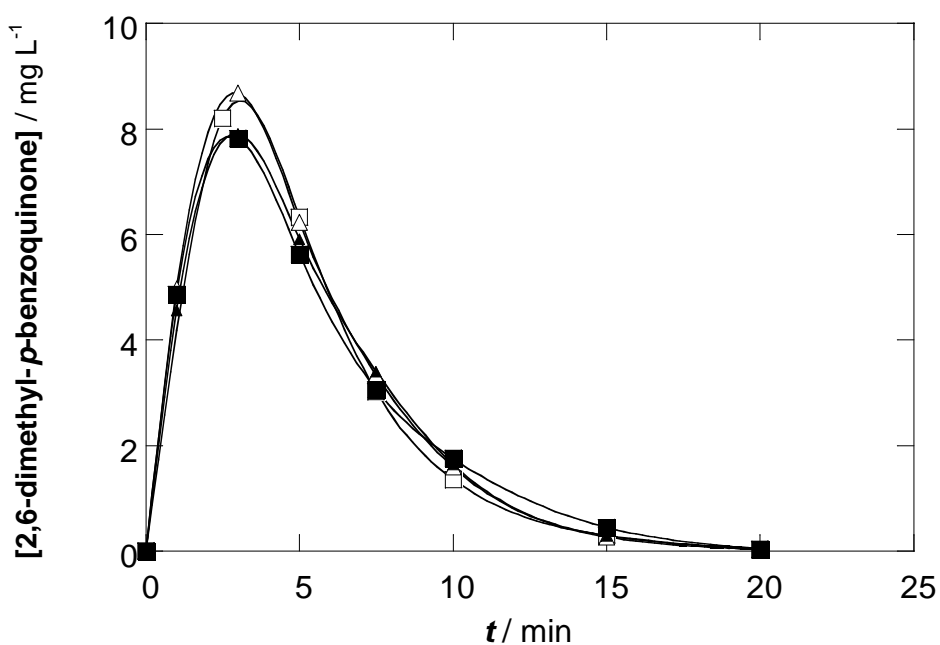


Figure 6.34. Time-course of 2,6-dimethyl-*p*-benzoquinone concentration formed as by-product during the degradation of 100 mL of a 100 mg L^{-1} chloroxylenol solution in $0.05 \text{ M Na}_2\text{SO}_4$, 1.0 mM Fe^{2+} at $25.0 \text{ }^\circ\text{C}$ and $\text{pH } 3.0$ by EAOPs. Treatments: (\square) Pt-EF; (\blacksquare) BDD-EF; (\triangle) Pt-PEF; and (\blacktriangle) BDD-PEF.

- Evolution of aliphatic carboxylic intermediates of chloroxylenol / *Evolució d'intermedis alifàtics carboxílics del cloroxilenol*

Several aliphatic carboxylic acid intermediates were detected by ion-exclusion liquid chromatography during the several applied treatments to mineralize chloroxylenol solutions. Pyruvic, oxalic, acetic, maleic and ketomalonic acids were found in these treated solutions. Most of them were detected only during the first minutes of treatment, whereas others, such as oxalic and acetic acids stayed in the treated solutions for several hours. For pyruvic, oxalic and acetic acids a study of their evolution with time was carried out.

Pyruvic acid is formed as a result of the break of the aromatic ring of chloroxylenol and its intermediates. This aliphatic carboxylic acid was detected for the degradation of the biocide with the treatments based on the oxygen diffusion cathode during the first hour of experiment.

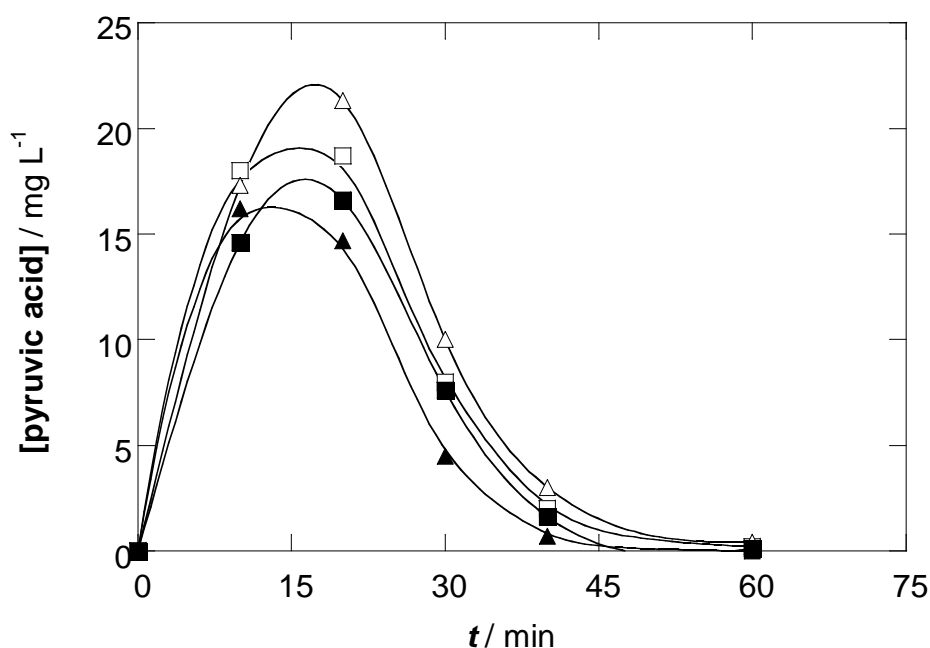


Figure 6.35. Evolution of the concentration of pyruvic acid detected when 100 mL of a 100 mg L⁻¹ chloroxylenol solution in 0.05 M Na₂SO₄, 1,0 mM Fe²⁺ at 25.0 °C and pH 3.0 are electrolyzed at 33 mA cm⁻² by: (□) Pt-EF; (■) BDD-EF; (△) Pt-PEF; and (▲) BDD-PEF method.

Pyruvic acid was not detected for treatments based on anodic oxidation (Pt-AO and BDD-AO). Figure 6.35 shows a bigger accumulation of this intermediate for methods using the platinum anode (pyruvic acid accumulates up to 18.3 and 21.7 mg L⁻¹ for Pt-EF and Pt-PEF

methods, respectively), whereas under BDD-EF and BDD-PEF, this acid reaches lower concentrations (16.2 and 16.6 mg L⁻¹, respectively).

The much slower degradation of chloroxylenol and its aromatic intermediates under the treatments based on the anodic oxidation (Pt-AO and BDD-AO) leads to a very slow formation of pyruvic and other aliphatic carboxylic acids, which are formed after the breakdown of the aromatic rings. This fact explains that pyruvic acid was not detected under these treatments.

Although both the $\bullet\text{OH}$ from the bulk solution ($\bullet\text{OH}_{(\text{bulk})}$) and the $\bullet\text{OH}$ adsorbed on the anode surface ($\bullet\text{OH}_{(\text{BDD})}$ or $\bullet\text{OH}_{(\text{Pt})}$) take part in the oxidation of pyruvic acid, the action of the latter is reflected in the fact that pyruvic acid accumulates more with platinum-based treatments than in treatments where BDD is used as anode. This can only be explained by the better oxidation performance of the $\bullet\text{OH}_{(\text{BDD})}$ species, indicating that unlike what happens with aromatic intermediates, which are mainly destroyed by the $\bullet\text{OH}$ present in the bulk solution, $\bullet\text{OH}_{(\text{bulk})}$, the $\bullet\text{OH}$ on the anode surface play an important role in the oxidation of pyruvic acid.

Acetic acid, which is formed from the oxidation of pyruvic acid, was also only detected for the electro-Fenton and photoelectro-Fenton oxidation treatments applied to chloroxylenol. The curves showing the evolution of acetic acid under these treatments are displayed on Figure 6.36.

Under the Pt-EF method, acetic acid reaches a maximum concentration of 31.4 mg L⁻¹ at 60 minutes before undergoing a slow abatement until it reaches a concentration of 20.2 mg L⁻¹ after 6 hours of experiment.

Under the other three treatments, Pt-PEF, BDD-EF and BDD-PEF, acetic acid attains similar maximum concentration values (between 28 – 30 mg L⁻¹), but after this point, it undergoes a practically complete destruction after 6, 5 and 4 hours of electrolysis, respectively. The additional amount of $\bullet\text{OH}$ radicals generated in the bulk solution by the photo-Fenton reaction, as well as the regeneration of Fe²⁺ through the reduction of Fe³⁺ back to Fe²⁺ in this same reaction would explain the more effective performance of Pt-PEF treatment than that of Pt-EF for acetic acid oxidation.

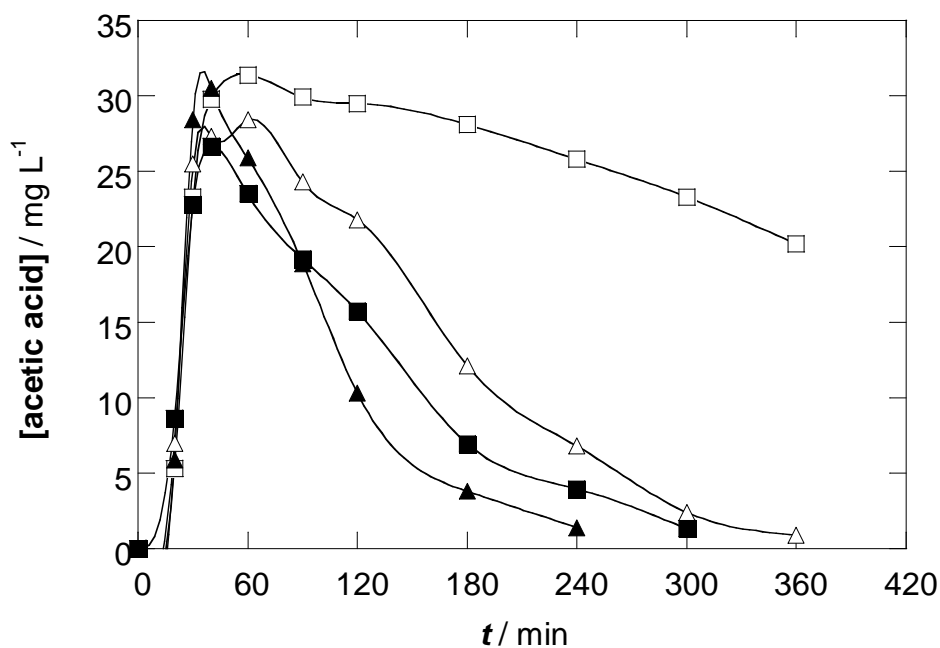


Figure 6.36. Evolution of the concentration of acetic acid detected when 100 mL of a 100 mg L⁻¹ chloroxylenol solution with 0.05 M Na₂SO₄ and 1.0 mM Fe²⁺ at 25.0 °C and pH 3.0 was electrolyzed at 33 mA cm⁻² by: (■) BDD-EF; (△) Pt-PEF; (□) Pt-EF and (▲) BDD-PEF method.

Again, the participation of the $\bullet\text{OH}$ radicals adsorbed on the anode surface proves to be significant as the only explanation for the complete elimination attained under the BDD-EF method can be the good ability of the BDD anode to generate weakly adsorbed and highly reactive $\bullet\text{OH}$, which is not the case in the platinum anode. The BDD-PEF method, which combines both the electrocatalytic ability of the boron doped diamond material to generate the more reactive $\bullet\text{OH}_{(\text{BDD})}$ radicals and the boosting effect of the UVA radiation on the Photo-Fenton reaction, thus increasing the concentration of $\bullet\text{OH}$ in the bulk of the solution, is the treatment which faster eliminates acetic acid, after only 4 hours of electrolysis.

Oxalic acid is the ultimately formed intermediate when chloroxylenol is mineralized. This species is the final oxidation product of most aliphatic carboxylic acids previously formed. Due to this reason, it is in the majority of cases accumulated in the medium before being oxidized. Likewise pyruvic and acetic acids, it could be monitored only for electro-Fenton and photoelectro-Fenton based treatments.

Figure 6.37 shows the evolution of oxalic acid with time under Pt-EF, Pt-PEF, BDD-EF and BDD-PEF treatments. The curve corresponding to the Pt-EF treatment shows a quick growth of the oxalic acid concentration which eventually slows down, but the trend is not reversed. After the end of the trial, 36.7 mg L⁻¹ oxalic acid are accumulated. Oxalic acid is mainly formed and accumulated and its destruction is not observed. When the platinum anode is replaced by the BDD one (BDD-EF treatment), the concentration of oxalic acid reaches a maximum of 30.1 mg L⁻¹ after 2 hours of treatment before starting to decline until it attains a concentration of 24.5 mg L⁻¹ at the end of the trial. These results show again the lack of ability of the Pt anode to destroy significant amounts of oxalic acid and the better performance of the BDD anode to produce more reactive [•]OH radicals able to destroy this acid.

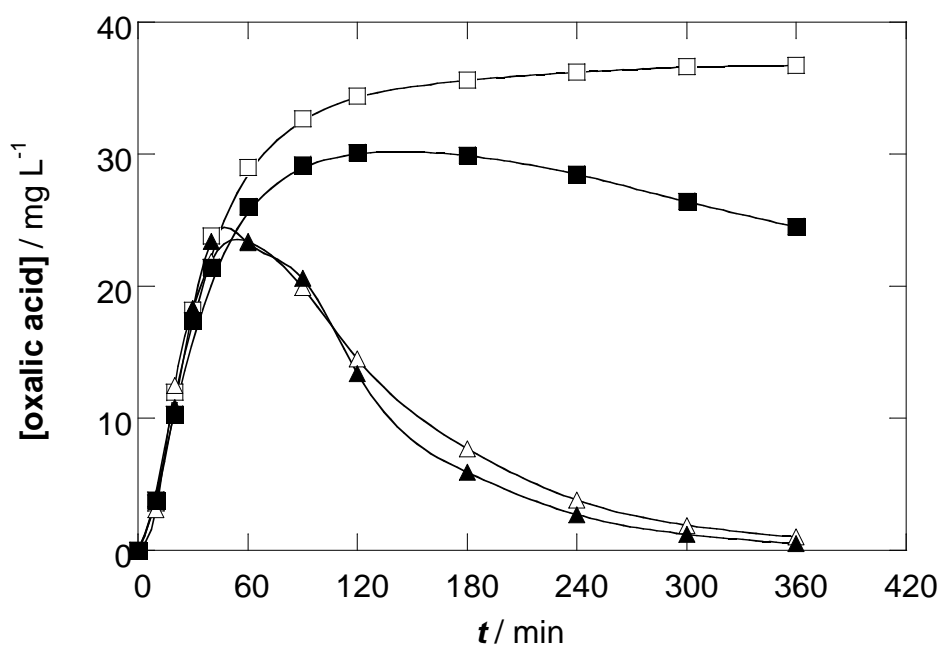


Fig. 6.37. Evolution of the concentration of oxalic acid detected during the electrolysis at 33 mA cm⁻² of 100 mL of a 100 mg L⁻¹ chloroxylenol solution in 0.05 M Na₂SO₄ and 1.0 mM Fe²⁺ under the treatment: (□) Pt-EF; (■) BDD-EF; (△) Pt-PEF; and (▲) BDD-PEF.

Figure 6.37 also shows the performance of platinum-photoelectro-Fenton (Pt-PEF) and BDD-photoelectro-Fenton (BDD-PEF) treatments. Both treatments show a similar profile for the evolution of oxalic acid, reaching a maximum concentration just above 23 mg L⁻¹ after 60 minutes of treatment and attaining its complete removal after 5 hours (for Pt-PEF) and 6 hours (for BDD-PEF). The most important effects taking place in these UV-assisted treatments are again:

- a) The formation of an additional amount of $\bullet\text{OH}$ in the bulk solution, formed by the photoelectro-Fenton process (reaction (6.2))
 - b) The regeneration of Fe^{2+} in the same photoelectro-Fenton process, which stimulates the Fenton reaction to produce further $\bullet\text{OH}$ radicals (reaction (1.3))
 - c) The photodecarboxylation of Fe^{3+} - oxalato complexes, which enables the oxidation of oxalic acid to CO_2 .
- Evolution of chloride anion concentration / *Evolució de la concentració d'anió clorur*

During the application of the several mineralization treatments of chloroxylenol solutions the concentration of chloride was followed with time by means of ion exchange chromatography and a conductivity detector. Chloride anion displayed a peak at $t_R = 3.45$ min.

In order to obtain information about the transformation of the chloro group present in the chloroxylenol molecule along the degradation of this biocide, the chloride concentration was measured during these several mineralization treatments: anodic oxidation (Pt-AO and BDD-AO), and the several treatments based on the oxygen diffusion cathode: Pt-EF, Pt-PEF, BDD-EF and BDD-PEF. The results are shown in Figure 6.38.

Under the Pt-AO method, the concentration of Cl^- goes through a slow but steady increase until it attains a final value of 21.4 mg L^{-1} , which corresponds to almost 100% conversion of the chlorine from the chloroxylenol molecule. When the platinum anode is replaced by a BDD anode (BDD-AO) only very low concentrations of chloride (never surpassing 4 mg L^{-1}) are reached. As no perchlorate or chlorate anions were detected in the solution, this suggests that the Cl^- anion formed from the destruction of chloroxylenol on the BDD surface may be further oxidized to Cl_2 .

Pt-EF and Pt-PEF treatments have very similar Cl^- -evolution profiles. Under these treatments the chloride concentration reaches a value around 22.6 mg L^{-1} after only 1 hour of treatment. After this point, the concentration of chloride stays constant with time during the remaining 5 hours until the end of the experiment.

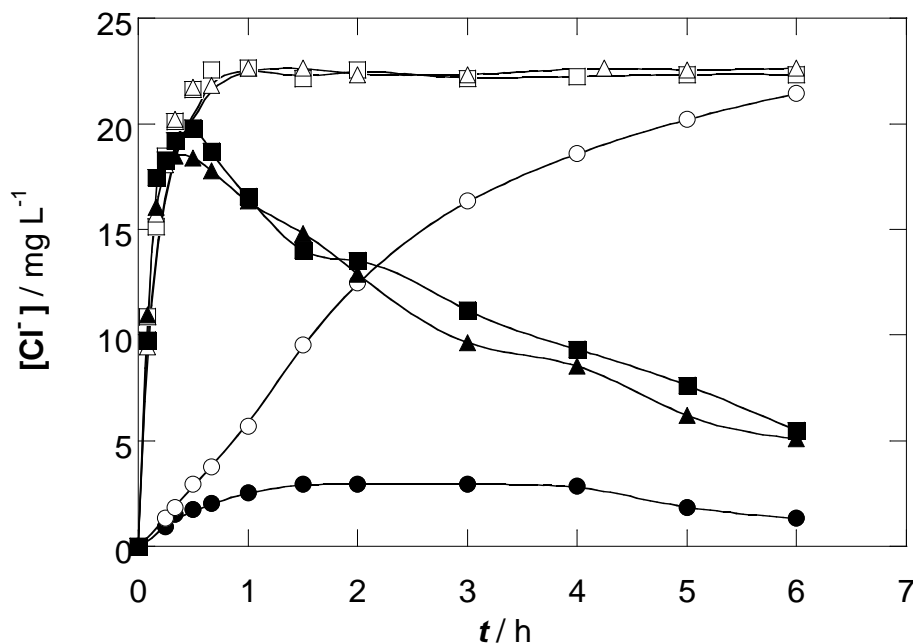


Figure 6.38. Concentration of chloride ion released vs. time for the degradation of 100 mL of a 100 mg L⁻¹ chloroxylenol solution in 0.05 M Na₂SO₄ of pH 3.0 at 33 mA cm⁻² and 25.0 °C. The solution contains 1.0 mM Fe²⁺ for methods *b*, *d*, *e* and *f*. Applied treatment: (*a*, ○) Pt-AO; (*b*, □) Pt-EF; (*c*, ●) BDD-AO; (*d*, ■) BDD-EF; (*e*, △) Pt-PEF; and (*f*, ▲) BDD-PEF.

The quick formation of chloride under these treatments (the 100% conversion of the chlorine of chloroxylenol to chloride is attained after just 1 hour of electrolysis) is explained by the presence of $\bullet\text{OH}$ radicals in the bulk of the solution. As seen in Figure 6.32, chloroxylenol is rapidly destroyed with the electro-Fenton and photoelectro-Fenton methods, which implies that the Cl^- ion will be also quickly released from the molecule. At the same time, the inability of the platinum anode to oxidize Cl^- to Cl_2 explains the lack of evolution of the Cl^- concentration in Pt-EF and Pt-PEF methods after the attainment of its maximum concentration.

A different behaviour is observed in the treatments in which the oxygen diffusion cathode is coupled to a BDD anode (BDD-EF and BDD-PEF treatments). Under these treatments, chloride is also quickly generated but it reaches a lower maximal concentration (just below 20 mg L⁻¹) at 30 – 40 minutes after the trial start. After this point, the concentration of chloride starts declining until reaching concentrations around 5 mg L⁻¹ after 6 hours of treatment. The increasing trend of the chloride concentration, which is produced by its quick formation

because of the presence of $\bullet\text{OH}$ in the bulk solution, which destroys chloroxylenol molecules releasing the chloride is braked and eventually reversed as BDD is also capable of oxidating the released chloride anions to Cl_2 .

6.2.3. Proposal of a degradation pathway for chloroxylenol mineralization by EAOPs / Proposta d'una ruta de degradació per a la mineralització del cloroxilenol mitjançant EAOPs

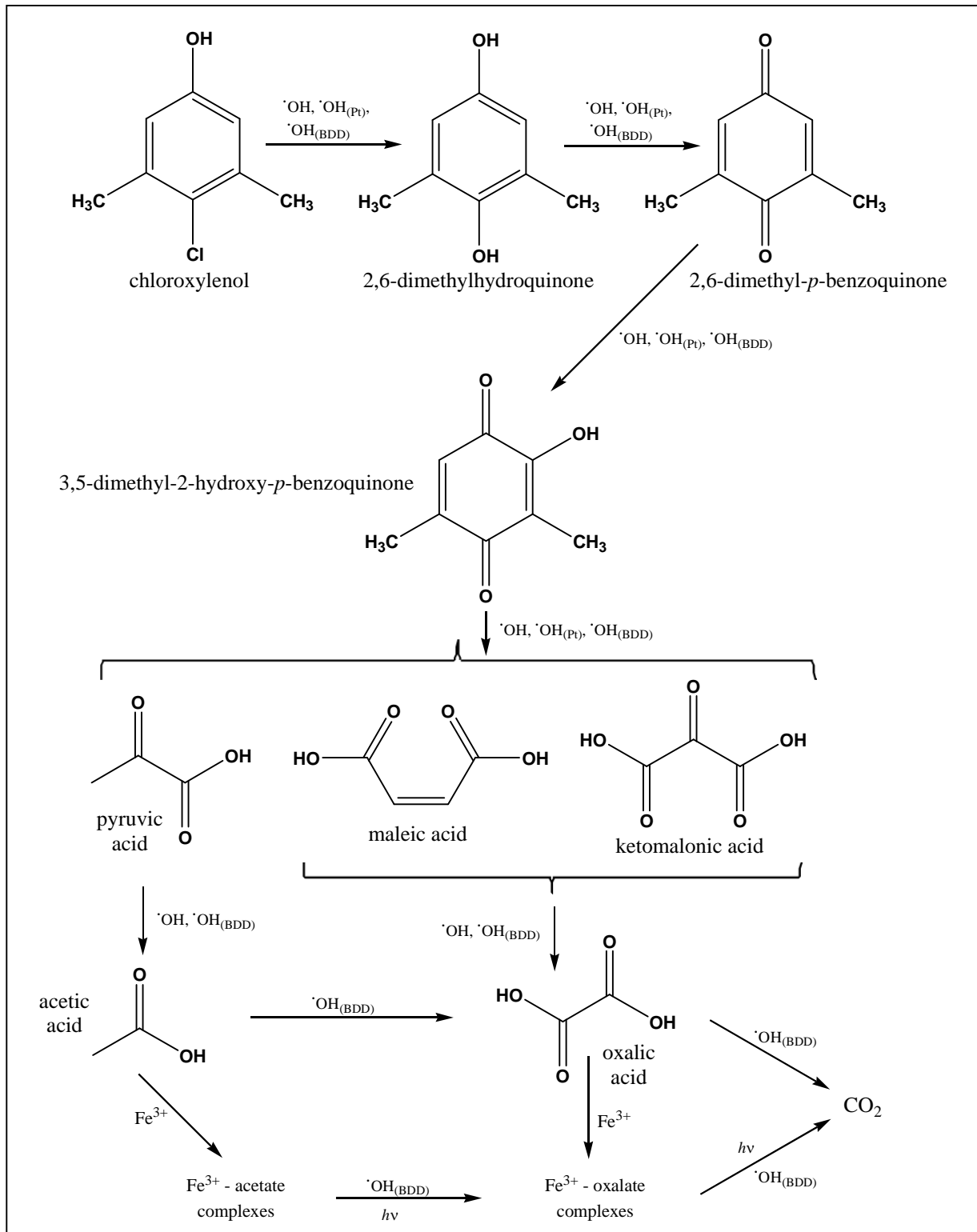


Figure 6.39. Proposed degradation pathway for the mineralization of chloroxylenol in acidic medium by EAOPs.

The chloroxylenol molecule undergoes hydrolysis of its chloro group by the action of $\bullet\text{OH}$ radicals either adsorbed on platinum or BDD electrodes or in the bulk solution, and the aromatic intermediate 2,6-dimethylhydroquinone is formed. 2,6-Dimethylhydroquinone, which must undergo a very fast oxidation as it was not detected by HPLC techniques, transforms into 2,6-dimethyl-*p*-benzoquinone, a stable intermediate, which is further hydroxylated by the $\bullet\text{OH}$ radicals yielding 3,5-dimethyl-2-hydroxy-*p*-benzoquinone.

Further degradation of 3,5-dimethyl-2-hydroxy-*p*-benzoquinone would lead to the breakdown of its aromatic ring and yields pyruvic, maleic and ketomalonic acid.

Pyruvic acid undergoes further oxidation by $\bullet\text{OH}$ radicals from the bulk solution or those adsorbed at the BDD anode yielding acetic acid, which would form a complex with dissolved Fe^{3+} . These Fe^{3+} – acetate complexes can further oxidize to Fe^{3+} – oxalato complexes. Maleic and malonic acids can be oxidized by $\bullet\text{OH}_{\text{bulk}}$ from bulk solution or $\bullet\text{OH}_{(\text{BDD})}$ to oxalic acid, thus leading to additional Fe^{3+} – oxalato complexes. Both oxalic acid and oxalato complexes can be mineralized to yield CO_2 due to their oxidation by $\bullet\text{OH}$ radicals or UV-photolysis.

6.3 Study of ibuprofen mineralization by means of electrochemical advanced oxidation processes / *Estudi de la mineralització de l'ibuprofè mitjançant mètodes electroquímics d'oxidació avançada*

In this section, the mineralization of ibuprofen is studied first. The influence of several parameters on the mineralization efficiency of EAOPs, such as the nature of the electrodes, the applied current density, the effect of pH and the concentration of Fe^{2+} are first discussed. Finally, the concentration evolution of this antiinflammatory drug and its several arisen intermediates are shown and discussed.

6.3.1 Effect of experimental parameters on ibuprofen mineralization / *Efecte de paràmetres experimentals en la mineralització de l'ibuprofè*

The mineralization of ibuprofen by means of several EAOPs is studied by the monitoring of its TOC evolution. First, oxidation treatments based on the combination of platinum and BDD anodes with stainless steel cathodes (anodic oxidation) will be tested. Afterwards, oxidation methods involving an oxygen diffusion cathode and the addition of catalytic amounts of Fe^{2+} in the solution will be tested.

Two experiments were carried out in order to compare the ability of platinum and the boron doped diamond to mineralize ibuprofen solutions. For this purpose, platinum and BDD anodes were coupled to a stainless steel cathode to electrolyze a solution containing 41 mg L^{-1} ibuprofen and $0.05 \text{ M Na}_2\text{SO}_4$ at 33 mA cm^{-2} , pH 3.0 and $25.0 \text{ }^\circ\text{C}$. Figure 6.40 shows that during the first hours of electrolysis, both treatments, Pt-AO and BDD-AO have a similar effect on the mineralization of ibuprofen. However, the mineralization by the Pt-AO treatment stops at only 81% after 6 hours of treatment, whereas under the BDD-AO treatment it goes further until attaining a final 96% mineralization. This can be explained by the higher reactivity of the hydroxyl radical generated at the BDD anode ($\bullet\text{OH}_{(\text{BDD})}$). This species is only weakly physisorbed on the surface of BDD and this enables it to react more easily, whereas $\bullet\text{OH}$ radicals generated at the platinum anode ($\bullet\text{OH}_{(\text{Pt})}$) are strongly chemisorbed on its surface. Whereas the first hydroxyl radicals would be able to oxidize the different arising intermediates, the latter would not be so reactive as to destroy them, causing their accumulation in the solution.

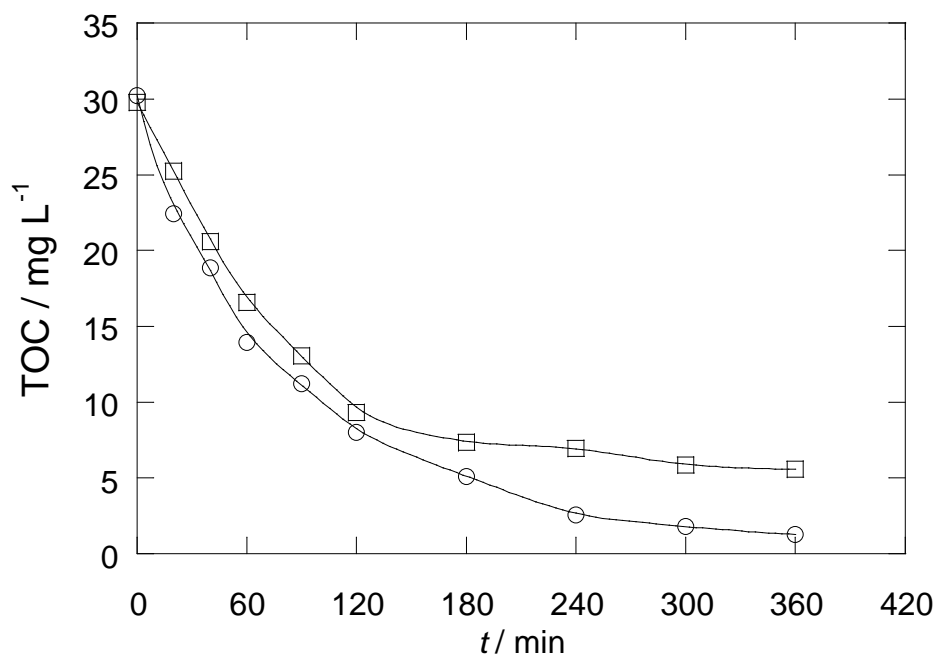


Figure 6.40. TOC abatement for of solutions containing 41 mg L⁻¹ ibuprofen in 0.05 M Na₂SO₄ at 25.0 °C and pH 3.0, electrolyzed at 33 mA cm⁻² by methods based on coupling a stainless steel cathode with a: (□) platinum anode, (○) BDD anode.

These results show again that treatments based on anodic oxidation using platinum as anode have a low efficiency. The irradiation with UV light from a 6 W black light blue fluorescent lamp and the addition of small amounts of Fe²⁺ only could increase the low mineralization extent of Pt-AO method by less than 5%. After that, several BDD-AO treatments were carried out to set up the optimal conditions to attain the biggest mineralization extent. These results are shown in Figure 6.41.

Although the TOC removal in ibuprofen solutions by anodic oxidation using a BDD anode is much faster than using the platinum anode, it still takes over 6 hours of electrolysis to attain a quantitative mineralization of the drug. The irradiation with UVA does not seem to have any significant catalytic effect on its mineralization rate, as well as the combined addition of 1 mM Fe²⁺ with the UVA irradiation. Raising the pH only causes the mineralization rate for the drug to slow down.

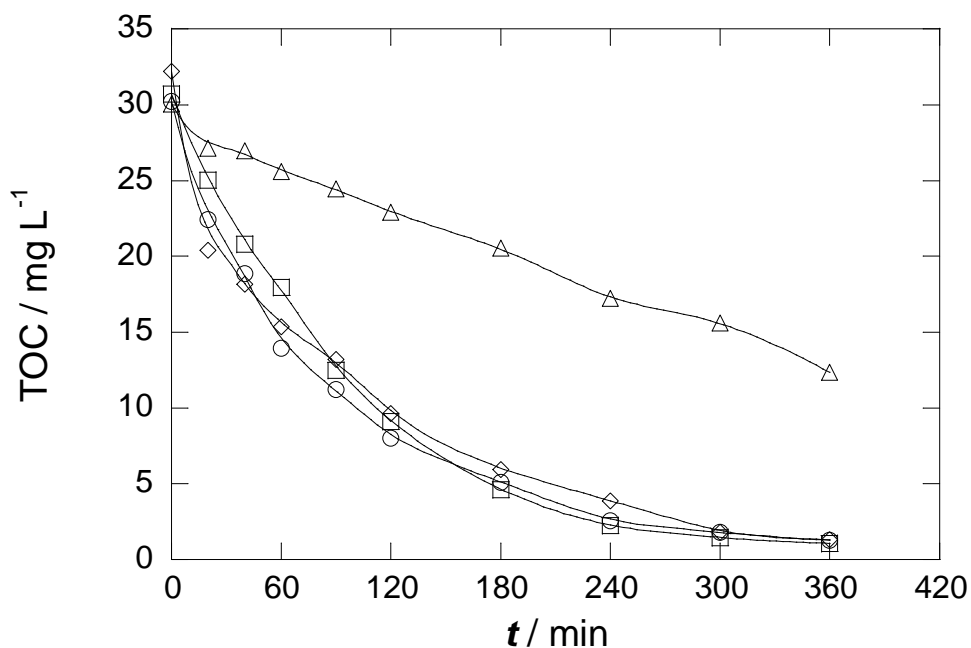


Figure 6.41. TOC decay profiles for 41 mg L⁻¹ ibuprofen solutions containing 0.05 M Na₂SO₄ at 25.0 °C electrolyzed at 33 mA cm⁻² using a BDD anode coupled with a stainless steel cathode at: (○) pH 3.0; (□) pH 3.0 + UVA irradiation; (◇) pH 3.0 + 1.0 mM Fe²⁺ + UVA irradiation; (△) pH 6.0.

Also an increase of the current density was tested for anodic oxidation treatments with BDD anode, which however only led to insignificant increases in the extent of mineralization of this compound.

After these results, treatments based on the oxygen diffusion cathode (electro-Fenton methods) on solutions containing Fe²⁺ have been tested. As these methods supply an extra amount of [•]OH in the bulk solution due to its generation on the carbon black – PTFE surface (reaction (1.2)) and its reaction with Fe²⁺ present in the solution through the Fenton reaction (reaction (1.3)), better results are expected for the mineralization of ibuprofen.

The oxidation power of several indirect electrooxidation methods was comparatively studied with the electrolysis at 33 mA cm⁻² of a concentrated solution containing 41 mg L⁻¹ of sodium salt ibuprofen with 0.5 mM Fe²⁺ as metallic ion catalyst and 0.05 M Na₂SO₄ as electrolyte at pH 3.0 and 25.0 °C (Figure 6.42). The electro-Fenton (EF) and photoelectro-Fenton (PEF) methods were prolonged up to 6 hours, whereas the solar photoelectro-Fenton (SPEF) treatments, for which solar radiation was used instead of the 6 W UVA emitting black light blue tube, were applied for 4 h. In all these experiments the treated solution remained colourless and its pH dropped slightly to a final value close to 2.6 – 2.7. The formation of

aliphatic carboxylic acids as degradation intermediates of this drug is the cause of this slight pH drop.

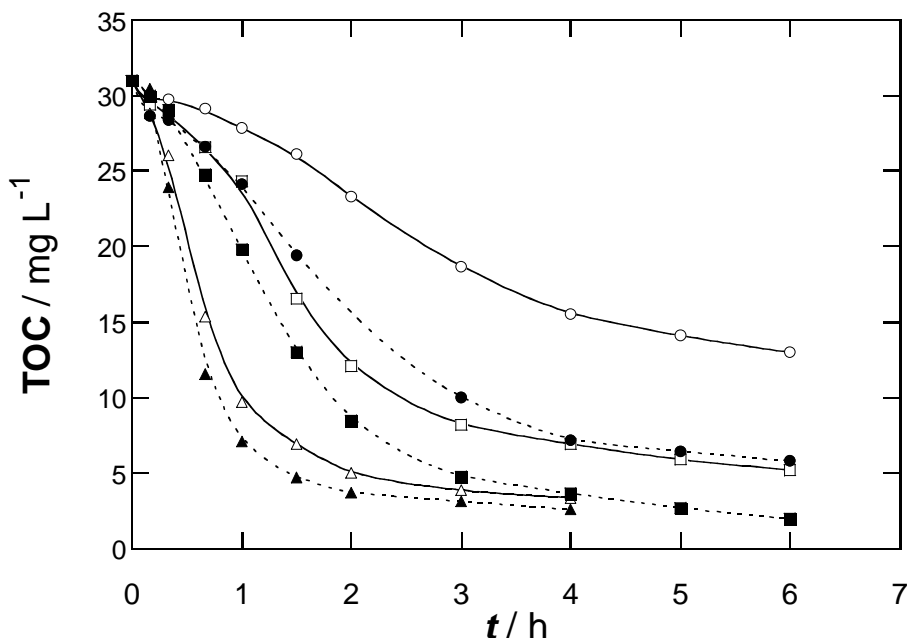


Figure 6.42. TOC decay with time for the electrolysis of 100 mL of a solution containing 41 mg L⁻¹ ibuprofen, 0.5 mM Fe²⁺ and 0.05 M Na₂SO₄ at pH 3.0 using a 3 cm² O₂-diffusion cathode at 33.3 mA cm⁻² and 25.0 °C. Method: (a,○) electro-Fenton with a 3 cm² Pt anode (Pt-EF); (b,●) electro-Fenton with a 3 cm² BDD anode (BDD-EF); (c,□) photoelectro-Fenton with Pt under irradiation with a 6 W UVA light of λ_{max} = 360 nm (Pt-PEF); (d,■) photoelectro-Fenton with BDD under UVA irradiation (BDD-PEF); (e,△) solar photoelectro-Fenton with Pt (Pt-SPEF) and (f,▲) solar photoelectro-Fenton with BDD (BDD-SPEF).

The replacement of the stainless steel cathode for an oxygen diffusion one and the addition of 1 mM Fe²⁺ has a negative effect on the mineralization efficiency when the platinum anode is used, since only 58% mineralization is reached, whereas for the Pt-AO treatment a higher 81% is attained. The implementation of the oxygen diffusion cathode supplies •OH radicals in the bulk of the solution, but the added Fe²⁺ is oxidized to Fe³⁺, which interacts with many aliphatic carboxylic acid intermediates (mainly with oxalic acid), leading to carboxylate complexes, difficult to destroy even for •OH. When the platinum anode is replaced by the BDD one, the mineralization of ibuprofen reaches 81%. The ability of BDD to produce more reactive •OH radicals, capable of oxidizing oxalic acid explains this improvement, but this result still lies far from that attained using the BDD anode coupled with the stainless steel cathode (96%), because again many of the formed Fe³⁺ – oxalato complexes resist the attack of •OH radicals.

When UVA radiation from a 6 W black light blue tube is supplied, the photolysis of Fe^{3+} – oxalato complexes can take place to a certain extent and the TOC decay profile for ibuprofen solutions is expected to sharpen. Curves *c* and *d* in Figure 6.42 are consistent with this, since the supply of UVA irradiation leads the TOC concentration to undergo a faster decay and the final total organic carbon removal reaches 83% when platinum is used (Pt-PEF) and 94% for the BDD-based photoelectro-Fenton treatment (BDD-PEF).

The supply of UVA radiation significantly accelerates the TOC mineralization. However faster mineralization rates indicating an important photolysis of oxalato and other possible Fe^{3+} – carboxylato complexes are pursued. For this reason two further experiments were done, in which the UVA radiation from the lamp was replaced by direct sunlight, exposing the experiment to the sun: solar photoelectro-Fenton experiments. Curves *e* and *f* in Figure 6.42 show much sharper decay profiles for Pt-SPEF and BDD-SPEF, with 88% and 92% mineralization after only 3 hours of electrolysis, respectively. This proves that the higher supplied radiation intensity by the sun leads to a much more important photolysis of oxalato and other arisen Fe^{3+} – complexes.

For these methods, current efficiencies have been calculated. The electrochemical mineralization of ibuprofen can be stoichiometrically written as:



Current efficiency of mineralization or MCE (mineralization current efficiency) is defined as the quotient between the amount of mineralized pollutant (given by the measured variation of TOC, ΔTOC_{exp}) and the amount of theoretically mineralized pollutant (given by the theoretical variation of TOC, ΔTOC_{theor}) under ideal conditions of 100% efficiency, i.e. with no side reactions involving a loss of current:

$$\text{MCE} \equiv \frac{\Delta\text{TOC}_{exp}}{\Delta\text{TOC}_{theor}} \quad (6.19)$$

On the basis of the stoichiometric information from reaction (6.18) for the ibuprofen electrochemical mineralization and applying Faraday's law, this expression can be written as

$$\text{MCE} \equiv \frac{\Delta\text{TOC}_{exp}}{\frac{ItM}{nFV_s}} \quad (6.20)$$

where I is the current intensity, t , the time, M , the molar mass of ibuprofen ($156.143 \text{ g mol}^{-1}$), F , the Faraday constant (96485 C mol^{-1}), n , the number of electron mols involved for the stoichiometrical mineralization of ibuprofen (56) and V_s is the solution volume (0.1 L).

Using expression (6.20), curves for the mineralization current efficiency were calculated from the data in Figure 6.42 and appear displayed in Figure 6.43.

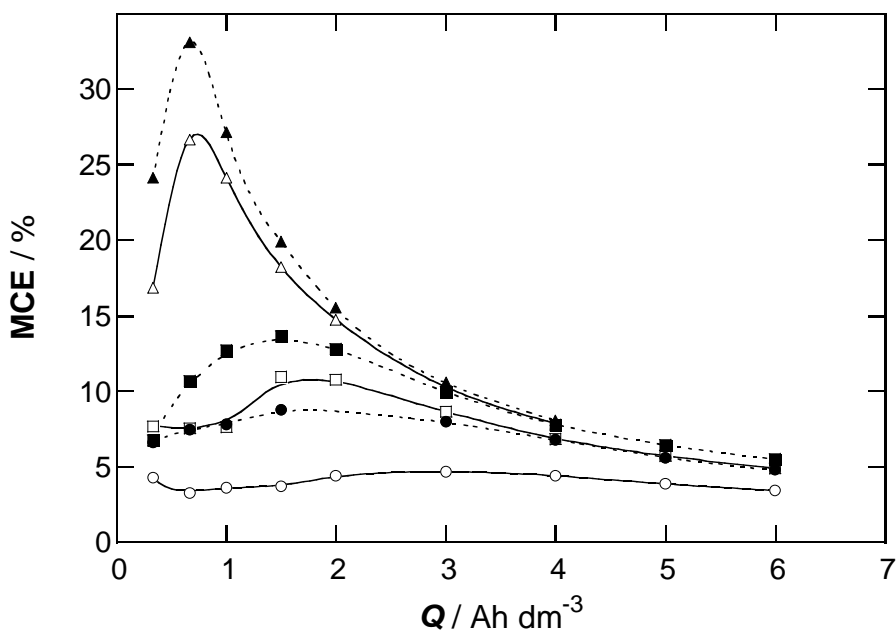


Figure 6.43. Mineralization current efficiency calculated from expression (6.20) vs. consumed specific charge for the electrochemical degradation of 100 mL of a solution containing 41 mg L^{-1} at the same conditions and methods described under Figure 6.42. Applied method: (a, \circ) Pt-EF; (b, \bullet) BDD-EF; (c, \square) Pt-PEF; (d, \blacksquare) BDD-PEF; (e, \triangle) Pt-SPEF and (f, \blacktriangle) BDD-SPEF.

The maximum values of the mineralization current efficiency exhibit the same trend as the TOC abatement sharpness of the curves for these treatments in Figure 6.42: Pt-EF < BDD-EF < Pt-PEF < BDD-PEF < Pt-SPEF < BDD-SPEF.

The influence of dissolved Fe^{2+} concentration on the efficiency of the mineralization of ibuprofen was tested for the electrolysis using the BDD-PEF method at 33.3 mA cm^{-2} . This method was applied to solutions containing 41 mg L^{-1} ibuprofen in $0.05 \text{ M Na}_2\text{SO}_4$ at pH 3.0 and $25.0 \text{ }^\circ\text{C}$.

The best mineralization efficiency was obtained for experiments with added concentrations of Fe^{2+} between 0.2 and 0.5 mM. The mineralization of ibuprofen for added concentrations below this interval was slightly less efficient suggesting that a minimum of 0.2 mM Fe^{2+} is necessary in order to optimally stimulate the mineralization of ibuprofen, especially to boost Fenton and photo-Fenton processes (reactions (1.3) and (6.3)), which most strongly enhance the production of the $\bullet\text{OH}$ radicals.

On the other hand, Fe^{2+} concentrations above 0.5 mM not only did not accelerate the mineralization of ibuprofen, but they even produced a slight decrease on its mineralization rate, as can be seen in Figure 6.44 for the decay curves at 1.0 and 2.0 mM Fe^{2+} . This mineralization inhibition for Fe^{2+} concentrations above 0.5 mM can be explained by the consumption of $\bullet\text{OH}$ radicals with Fe^{2+} by reaction (6.17) [160].

To sum up, concentrations of the Fe^{2+} catalyst between 0.2 and 0.5 mM have been found to be optimal for a most efficient mineralization of ibuprofen by the photoelectro-Fenton method based on the BDD anode.

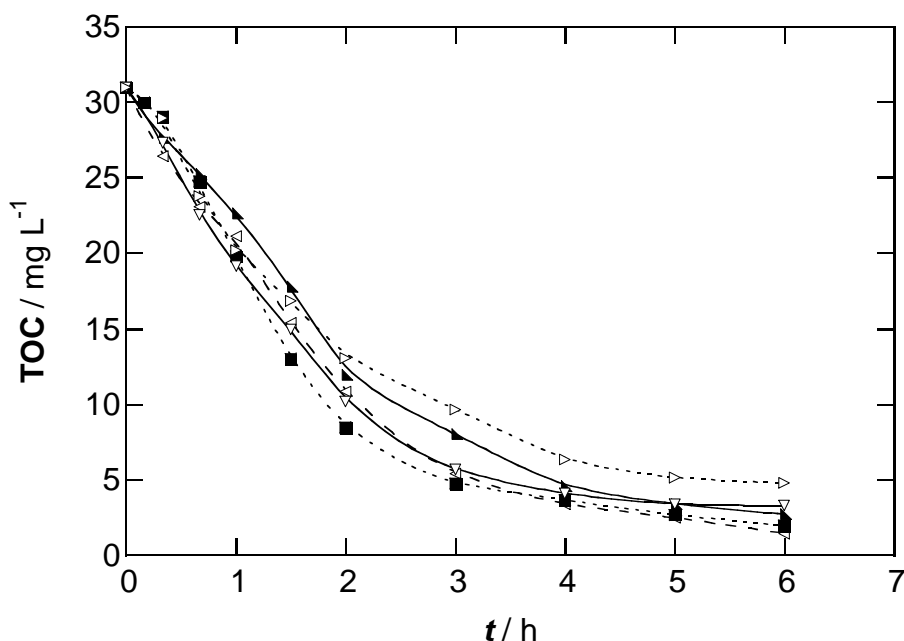


Figure 6.44. Influence of Fe^{2+} concentration on the TOC abatement for 100 mL of a 41 mg L^{-1} ibuprofen solution containing $0.05 \text{ M Na}_2\text{SO}_4$ at pH 3.0 and $25.0 \text{ }^\circ\text{C}$ electrolyzed at 33.3 mA cm^{-2} by the BDD-PEF method. Initial Fe^{2+} concentration: (▲) 0.1 mM; (◁) 0.2 mM; (■) 0.5 mM; (▽) 1.0 mM and (▷) 2.0 mM.

The effect of pH on the mineralization of ibuprofen was also studied for the BDD-PEF treatment working at a current density of 33.3 mA cm^{-2} with ibuprofen solutions containing 0.5 mM Fe^{2+} .

Figure 6.45 shows that ibuprofen is fastest mineralized at a start pH 3.0. Working at pH 4.0, a similar mineralization extent is obtained at the end of the trial, but the mineralization rate during the first 2 hours of experiment is clearly lower. At pH 2.0 and 6.0 poor mineralization values are obtained (79% and 82% respectively). Since reactions (6.2) and (6.3) take place in their greatest extent at pH near 3.0 [160], these results confirm that the hydroxyl radical, mostly arisen from Fenton and photo-Fenton processes, accounts for most of the mineralization of ibuprofen.

These results lead to conclude that pH 3.0 is the optimal one in order to mineralize ibuprofen dissolved in water by the EAOPs.

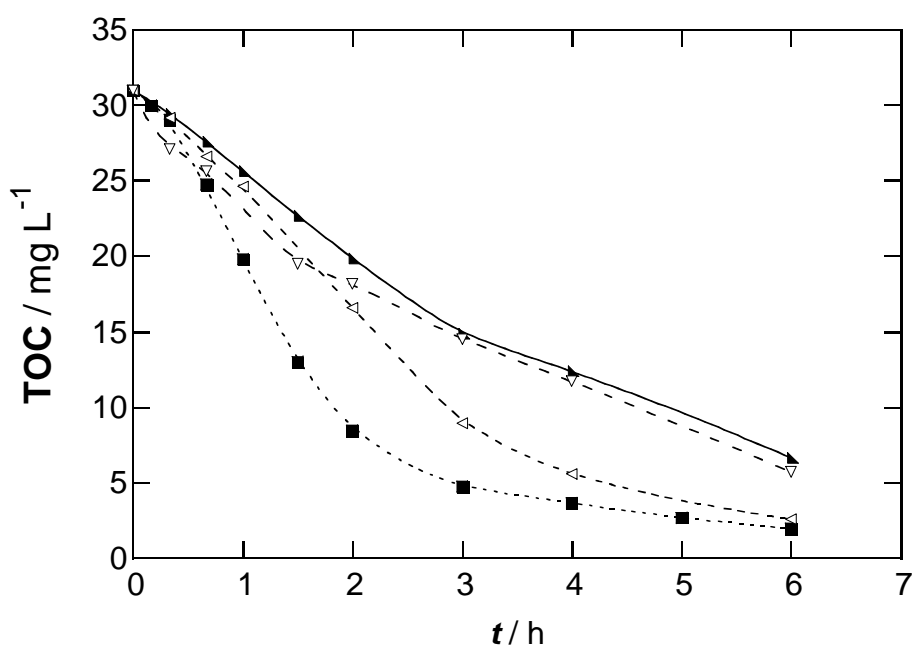


Figure 6.45. pH effect on TOC abatement for 100 mL of a 41 mg L^{-1} ibuprofen solution containing 0.5 mM Fe^{2+} and $0.05 \text{ M Na}_2\text{SO}_4$ at $25.0 \text{ }^\circ\text{C}$ and electrolyzed at 33.3 mA cm^{-2} by the BDD-PEF method. pH: (▲) 2.0; (■) 3.0; (◁) 4.0 and (▽) 6.0.

The influence of the applied current density on the ibuprofen mineralization rate and its efficiency has also been studied. For this reason, a series of electrolyses has been carried out applying the BDD-PEF treatment to ibuprofen solutions containing 0.5 mM Fe^{2+} at pH 3.0 and 25.0 °C. The results of these experiments are shown in Figure 6.46.

During the first 4h of treatment, the increase in the current density from 6.6 mA cm^{-2} to 33.3 mA cm^{-2} brings about a slight enhancement of the TOC abatement. However, for longer trial times, very similar values are obtained for all applied current densities. The raise of j from 33.3 mA cm^{-2} to 100 mA cm^{-2} does not improve the mineralization rate, thus suggesting a kinetic limitation by mass transport of the organics towards the anode.

Although an increase in current density brings a slight enhancement of TOC mineralization rate, their efficiency goes down. Thus, after 1.5 h of electrolysis, 52%, 55%, 58% and 59% of mineralization is reached at 6.6, 13.3, 33.3 and 100 mA cm^{-2} , respectively, but at the expense of increasing the applied charge Q from 0.3, 0.6, 1.5 to 4.5 A h dm^{-3} . The greatest MCE values were found for the lowest current density (6.6 mA cm^{-2}), with a maximum value of 52% at 1.5 h of treatment (0.3 A h dm^{-3}).

This slight improvement in the mineralization rate of ibuprofen with time up to 4 h of treatment with raising j from 6.6 to 33.3 mA cm^{-2} is explained by a higher formation of $\bullet\text{OH}_{(\text{BDD})}$ from the oxidation of water on the BDD surface (reaction (1.1)) and also by an improved generation of H_2O_2 at the oxygen diffusion cathode (reaction (1.2)) as a bigger charge is applied, what leads to a greater production of $\bullet\text{OH}$ radical through the Fenton and photo-Fenton processes (reactions (1.3) and (6.2)).

However, the higher consumption of Q and, thus, the loss of efficiency with increasing values of j suggests the existence of waste reactions involving side-reactions of the hydroxyl radical which do not lead to the oxidation of organics. Some of these waste reactions are the evolution of oxygen from adsorbed $\bullet\text{OH}$ radicals (reaction (6.12)), the dimerization of $\bullet\text{OH}$ radicals to form hydrogen peroxide (reaction (6.13)), the loss of $\bullet\text{OH}$ when reacting with Fe^{2+} according to reaction (6.17) or its loss when reacting with H_2O_2 (reaction (6.16)) [160].

Apart from this, the j raise also favours the formation of weak oxidants like $\text{S}_2\text{O}_8^{2-}$ and ozone (reactions (6.14) and (6.15)) in detriment of the generation of $\bullet\text{OH}$ at the anode surface (reaction (1.1)).

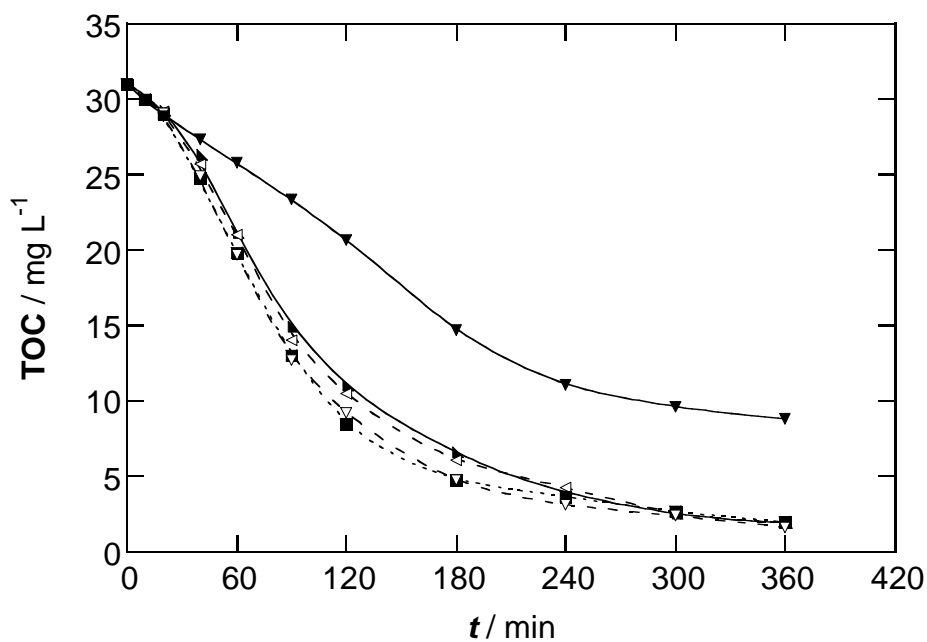


Figure 6.46. Influence of current density on the TOC removal for a 41 mg L^{-1} ibuprofen solution containing, 0.5 mM Fe^{2+} and $0.05 \text{ M Na}_2\text{SO}_4$ at pH 3.0 and $25.0 \text{ }^\circ\text{C}$ electrolyzed applying the BDD-PEF treatment. Applied current density: (▼) 3.3 mA cm^{-2} ; (▲) 6.6 mA cm^{-2} ; (◁) 13.3 mA cm^{-2} ; (■) 33.3 mA cm^{-2} and (▽) 100 mA cm^{-2} .

The results from this series of trials at different current densities allow concluding that the mineralization of ibuprofen is effectively reached even at very low current densities, which are optimal as a much lower charge must be wasted and a higher efficiency for the mineralization of ibuprofen is attained.

6.3.2 Study of ibuprofen and its degradation intermediates time-course / *Estudi de l'evolució de l'ibuprofè i dels seus intermedis de degradació*

The concentration of ibuprofen was monitored to study its abatement kinetics with $\bullet\text{OH}_{(\text{Pt})}$ and $\bullet\text{OH}_{(\text{BDD})}$. To do this, a 41 mg L^{-1} ibuprofen solution at $25.0 \text{ }^\circ\text{C}$ and pH 3.0 was electrolyzed by Pt-AO and BDD-AO methods applying a current density of 33.3 mA cm^{-2} .

In Figure 6.47 both curves for both methods are represented, showing a total elimination of ibuprofen in about 4 hours of treatment for the Pt-AO method, and after 2 hours of electrolysis for the BDD-AO method. These results show that the drug molecule reacts more quickly with $\bullet\text{OH}_{(\text{BDD})}$ than with $\bullet\text{OH}_{(\text{Pt})}$, which is not surprising, since the hydroxyl radical adsorbed on the platinum surface is strongly chemisorbed to it, whereas that adsorbed on the BDD surface is only physisorbed and it is not prevented from reacting with surrounding ibuprofen and other oxidizable molecules.

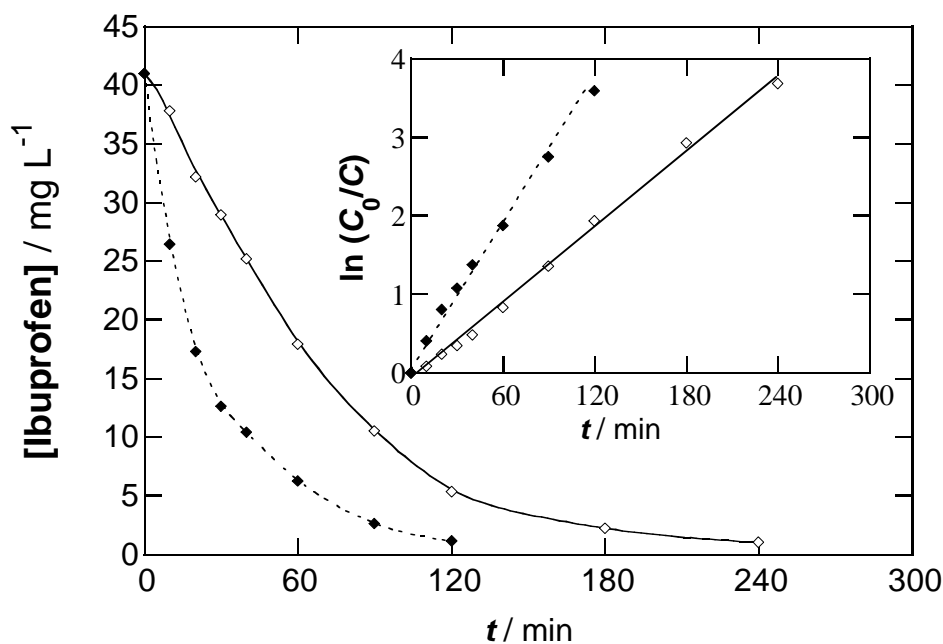


Figure 6.47. Decay of ibuprofen concentration with electrolysis time during the degradation of 100 mL of a 41 mg L^{-1} drug solution in $0.05 \text{ M Na}_2\text{SO}_4$ at pH 3.0 using a cell with a 3 cm^2 (◇) Pt or (◆) BDD anode and a 3 cm^2 stainless steel cathode at 33.3 mA cm^{-2} and at $25.0 \text{ }^\circ\text{C}$. The inset panel gives the corresponding kinetic analysis considering a pseudo-first-order reaction for ibuprofen.

The assumption of a pseudo-first-order reaction for ibuprofen leads to the obtention of good straight curves (see inset in Figure 6.47). From these correlations, apparent first-order rate constants (k_1) of $2.67 \cdot 10^{-4} \text{ s}^{-1}$ for Pt-stainless steel treatment (Pt-AO) and $4.86 \cdot 10^{-4} \text{ s}^{-1}$ for BDD-stainless steel treatment (BDD-AO) were found.

The ibuprofen concentration was also monitored for several electrolyses involving the use of the oxygen diffusion cathode (electro-Fenton methods). All 41 mg L^{-1} ibuprofen solutions containing 0.5 mM Fe^{2+} were electrolyzed at $25.0 \text{ }^\circ\text{C}$, pH 3.0 and a current density of 33.3 mA cm^{-2} . Ibuprofen was completely eliminated in about 40 minutes for all experiments. The small influence of UVA irradiation rules out a direct photolysis of ibuprofen or its iron complexes.

The contrast between the much faster abatement of ibuprofen in the trials involving the use of the oxygen diffusion cathode in comparison with the latter experiments, where a stainless steel cathode was used, leads to the conclusion that the electrogenerated H_2O_2 combined with the present Fe^{2+} yields a much bigger amount of $\bullet\text{OH}$ than that attained on the surface of the platinum or BDD anodes.

Again, the assumption of pseudo-first-order kinetics allowed very good linear correlations. From the analysis in the inset panel of Figure 6.48, k_1 values of $1.86 \cdot 10^{-3} \text{ s}^{-1}$ for Pt-EF, $2.00 \cdot 10^{-3} \text{ s}^{-1}$ for Pt-PEF, $2.06 \cdot 10^{-3} \text{ s}^{-1}$ for BDD-EF, and $2.08 \cdot 10^{-3} \text{ s}^{-1}$ for BDD-PEF are obtained. This trend suggests that there is a steady production of $\bullet\text{OH}$ from Fenton reaction in the electro-Fenton methods and a small influence of photo-Fenton reaction in the photo-electro-Fenton trials. However, the curves in Figure 6.48, corresponding to Pt-SPEF and BDD-SPEF treatments, show a much quicker removal of ibuprofen in comparison with the other four curves, where no sunlight is involved. Thus, solar radiation accounts for the generation of a much larger amount of oxidant $\bullet\text{OH}$. This is possible, since the UV intensity from the sunlight is much greater than that coming from the used 6 W black light blue tube.

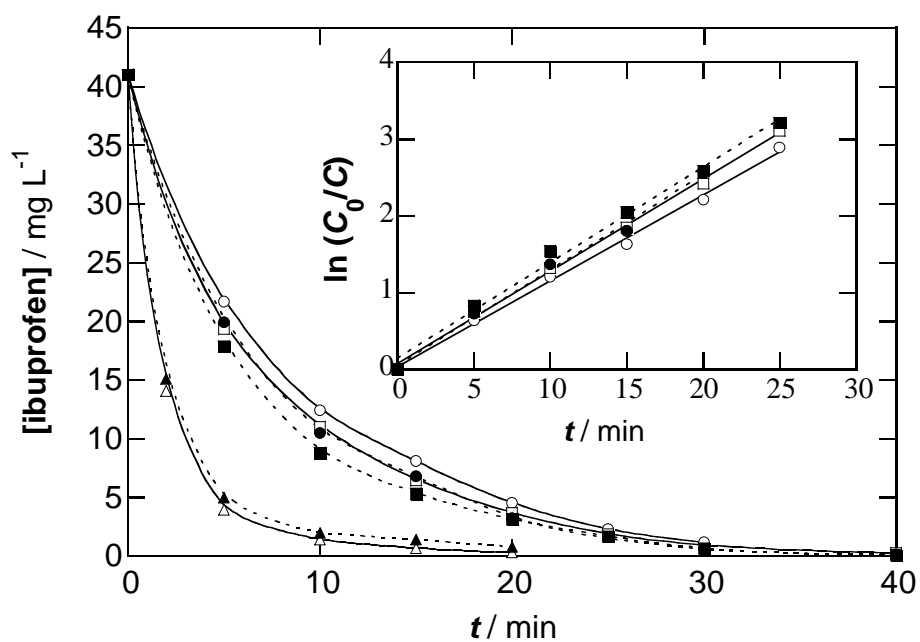


Figure 6.48. Time-course of ibuprofen concentration during the mineralization of 100 mL of a 41 mg L⁻¹ ibuprofen solution treated by (○) Pt-EF; (●) BDD-EF; (□) Pt-PEF; (■) BDD-PEF; (△) Pt-SPEF and (▲) BDD-SPEF methods under the same conditions as reported in Figure 6.47.

- Effect of the applied current density on ibuprofen abatement rate / *Efecte de la densitat de corrent aplicada a la velocitat de desaparició de l'ibuprofè*

The influence of current density on ibuprofen abatement was studied for the BDD-PEF treatment. As can be observed in Figure 6.49, the drug is removed faster at higher j values, disappearing after ca. 60, 50 and 40 min at 6.6, 13.3 and 33.3 mA cm⁻², respectively. Their concentration decays follow a pseudo-first order reaction (see inset panel of Figure 6.49) with increasing k_1 values of $1.32 \cdot 10^{-3} \text{ s}^{-1}$, $1.52 \cdot 10^{-3} \text{ s}^{-1}$ and $2.08 \cdot 10^{-2}$, respectively. This trend is not surprising, since higher applied current densities are expected to yield a larger amount of H₂O₂, which will yield $\bullet\text{OH}$ radicals through Fenton reaction with the Fe²⁺ ion.

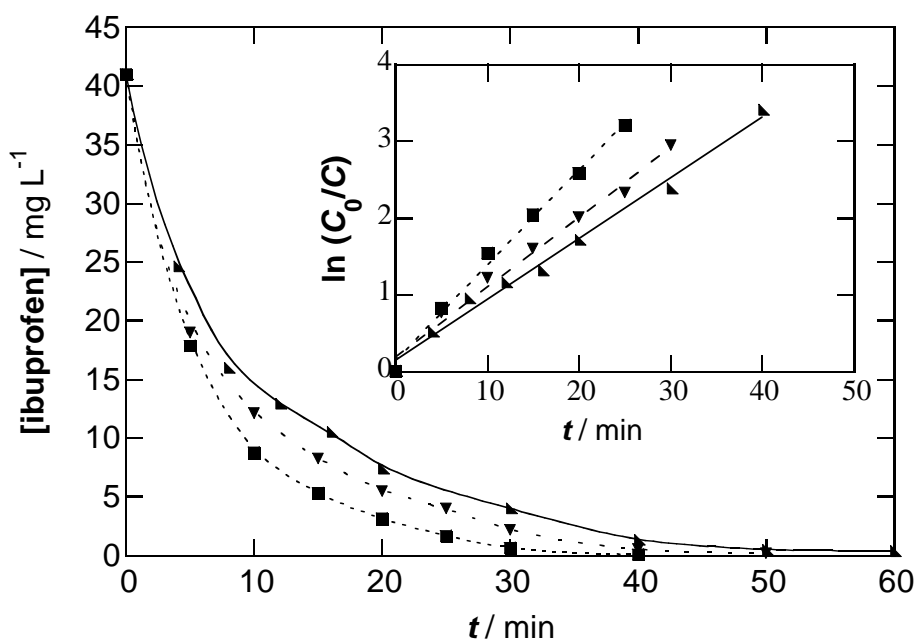


Figure 6.49. Effect of current density on ibuprofen decay for the BDD-PEF process at (▲) 6.6 mA cm⁻²; (▼) 13.3 mA cm⁻² and (■) 33.3 mA cm⁻². The inset panels give the kinetic analysis for the EF and PEF treatments assuming that the drug follows a pseudo-first-order reaction.

- Time-course of 4-isobutylacetophenone / *Evolució de la 4-isobutilacetofenona*

The aromatic intermediate 4-isobutylacetophenone was identified by GC-MS and detected in all treated solutions by reversed-phase HPLC, which allowed its monitoring for all treatments at 33.3 mA cm^{-2} .

The curves on Figure 6.50 show that 4-isobutylacetophenone is more quickly eliminated under more powerful oxidizing methods (EF < PEF < SPEF). For Pt-EF and BDD-EF, the concentration of this intermediate attains a maximum of $1.3 - 1.4 \text{ mg L}^{-1}$ at 15 – 25 min and disappears in 50 – 60 min, whereas the removal of the parent drug ibuprofen takes only 40 min (Figure 6.49). This indicates that 4-isobutylacetophenone is more slowly oxidized by $\bullet\text{OH}$ radicals adsorbed at the anode ($\bullet\text{OH}_{(\text{Pt})}$ or $\bullet\text{OH}_{(\text{BDD})}$) or present in the bulk solution. However, this intermediate suffered a significantly quicker removal under Pt-PEF and BDD-PEF treatments, disappearing in 30 min after reaching a maximum concentration of 1.3 mg L^{-1} at

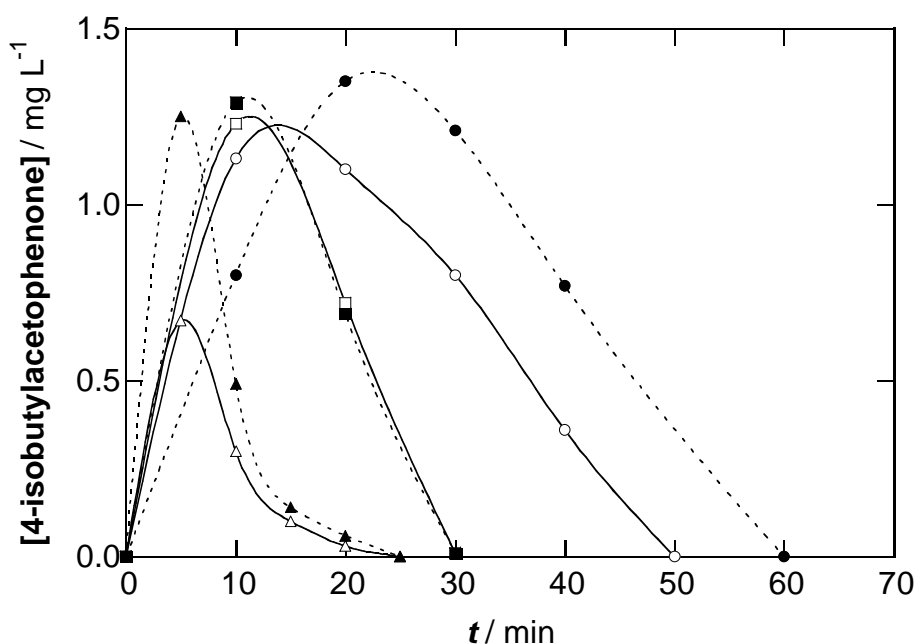


Figure 6.50. Evolution of 4-isobutylacetophenone concentration detected as the main aromatic intermediate during the electrochemical degradation of a 41 mg L^{-1} ibuprofen solution for the same trials as Figure 6.47. Method: (○) Pt-EF; (●) BDD-EF; (□) Pt-PEF; (■) BDD-PEF; (△) Pt-SPEF and (▲) BDD-SPEF.

10 min. These results suggest a possible photodecarboxylation which would lead to an acceleration of its degradation process. The enhancement of this photodecarboxylation along

with the generation of a larger amount of $\bullet\text{OH}$ induced by photo-Fenton reaction under solar irradiation explains the fastest removal of 4-isobutylacetophenone in about 25 min under the SPEF treatment.

- Evolution of aliphatic carboxylic acid intermediates / *Evolució d'intermedis carboxílics alifàtics*

Several carboxylic aliphatic acids were detected as intermediates formed from ibuprofen mineralization for the different oxidation treatments. Amongst them, pyruvic, acetic, oxalic and formic acids were detected. Pyruvic acid was found up to about 90 min, with a maximum content of ca. 2.5 mg L^{-1} at 15 – 20 min. Acetic acid, which would arise from pyruvic acid degradation and was detected at a maximum concentration of $10 - 12 \text{ mg L}^{-1}$ disappeared after 120 min. Traces of formic acid were also observed for the treatments with Pt anode.

On the contrary, a significant amount of oxalic acid was generated from acetic acid oxidation and mainly, from the oxidative breaking of the aryl moiety of aromatics [161 – 164]. Oxalic acid is the ultimate carboxylic acid, which is degraded to yield CO_2 .

Both Figures 6.51 and 6.52 show that the elimination of oxalic acid is significantly enhanced when the ibuprofen solution is irradiated with UVA (either from a UV lamp or from natural sunlight), as oxalic acid complexes with Fe^{3+} undergo a quick photodecomposition [150]. A steady accumulation of oxalic acid up to attain 17.6 mg L^{-1} (4.7 mg L^{-1} TOC) at the end of Pt-EF can be observed in Figure 6.51, indicating that neither $\bullet\text{OH}$ adsorbed on the platinum surface nor $\bullet\text{OH}$ present in the bulk solution are able to remove the Fe(III) – oxalato complexes formed in the solution. Thus the major components of Pt-EF final treated solution, having 13.0 mg L^{-1} TOC (Figure 6.48) correspond to undetected intermediates (8.3 mg L^{-1} TOC), probably polymeric compounds, which are also hardly mineralized. When the BDD-EF treatment is applied, accumulation of Fe(III) – oxalato complexes for 180 min is observed (Figure 6.51), with a very slow destruction by $\bullet\text{OH}_{(\text{BDD})}$ to yield 14.8 mg L^{-1} oxalic acid (3.9 mg L^{-1} TOC) at the end of the trial. Since this solution contains 5.9 mg L^{-1} TOC (Figure 6.48), a content of only 2.0 mg L^{-1} TOC corresponding to undetected compounds is formed, indicating that these undetected species are able to be slowly mineralized by $\bullet\text{OH}$ adsorbed at the surface of BDD anode, but

not by $\bullet\text{OH}$ present in the bulk solution. Figure 6.51 evidences a fast photodecarboxylation of Fe(III) – oxalato complexes under the Pt-PEF and BDD-PEF treatments, giving rise to their total disappearance in 300 – 360 min. Under these conditions, the remaining TOC of 5.2 mg L⁻¹ for Pt-PEF and 2.0 mg L⁻¹ for BDD-PEF (Figure 6.48) can only be ascribed to the presence of persistent undetected species.

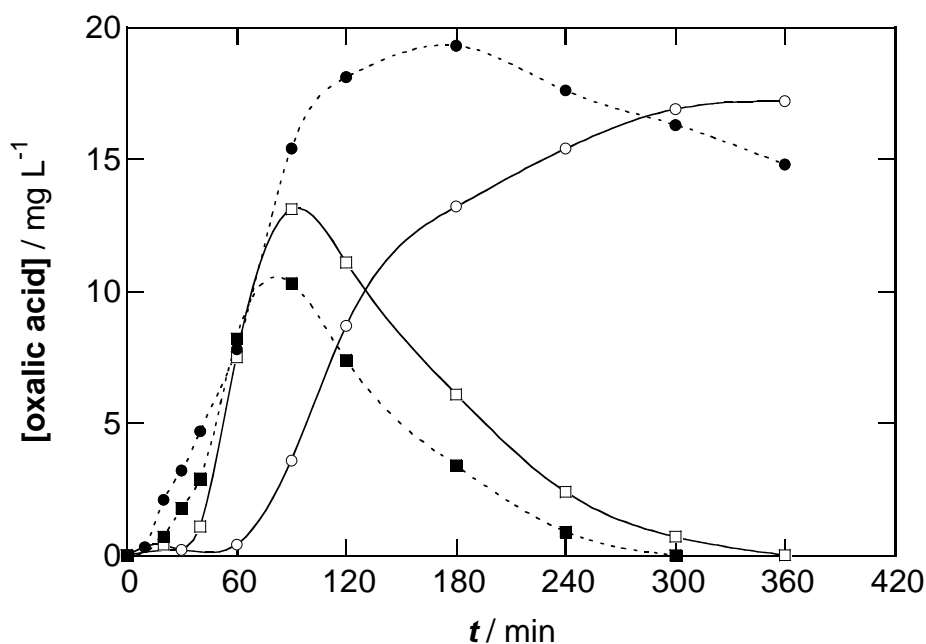


Figure 6.51. Time-course of the concentration of oxalic acid detected as final carboxylic acid for the degradation of 41 mg L⁻¹ of ibuprofen in the trials of Figure 6.47. In plot (a), (○) Pt-EF; (●) BDD-EF; (□) Pt-PEF and (■) BDD-PEF.

A very similar behavior can be observed in Figure 6.52 for Pt-SPEF and BDD-SPEF. For these latter treatments, however, the Fe(III) – oxalate complexes undergo a complete photolysis in a shorter time (60 – 75 min) because of the higher UV intensity of sunlight, which causes a much greater generation of $\bullet\text{OH}$ induced by photo-Fenton reaction thus strongly increasing the degradation rate of the intermediates whose degradation yields oxalic acid. However, from 120 min for both methods, the effect of solar irradiation is rather inefficient and the small proportion of remaining compounds related to 5.0 and 3.7 mg L⁻¹ TOC for Pt-SPEF and BDD-SPEF, respectively (see Figure 6.48) is only very slowly removed by $\bullet\text{OH}_{(\text{Pt})}$ and

$\bullet\text{OH}_{(\text{BDD})}$, the $\bullet\text{OH}$ radical in the bulk solution being incapable of degrading the final species formed during ibuprofen mineralization.

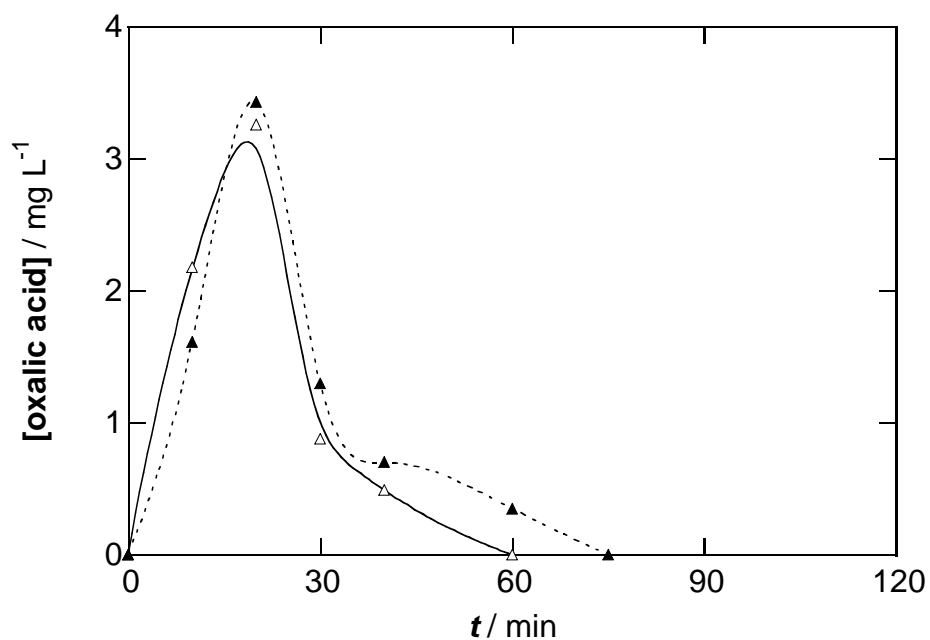


Figure 6.52. Time-course of the concentration of oxalic acid detected as final carboxylic acid for the degradation of 100 mL of a 41 mg L⁻¹ ibuprofen solution in the SPEF trials of Figure 6.48. In plot: (Δ) Pt-SPEF and (\blacktriangle) BDD-SPEF.

6.3.3 Proposal of a degradation pathway for Ibuprofen mineralization by AEOPs
 / Proposta d'una ruta de degradació per a la mineralització de l'Ibuprofè mitjançant AEOPs

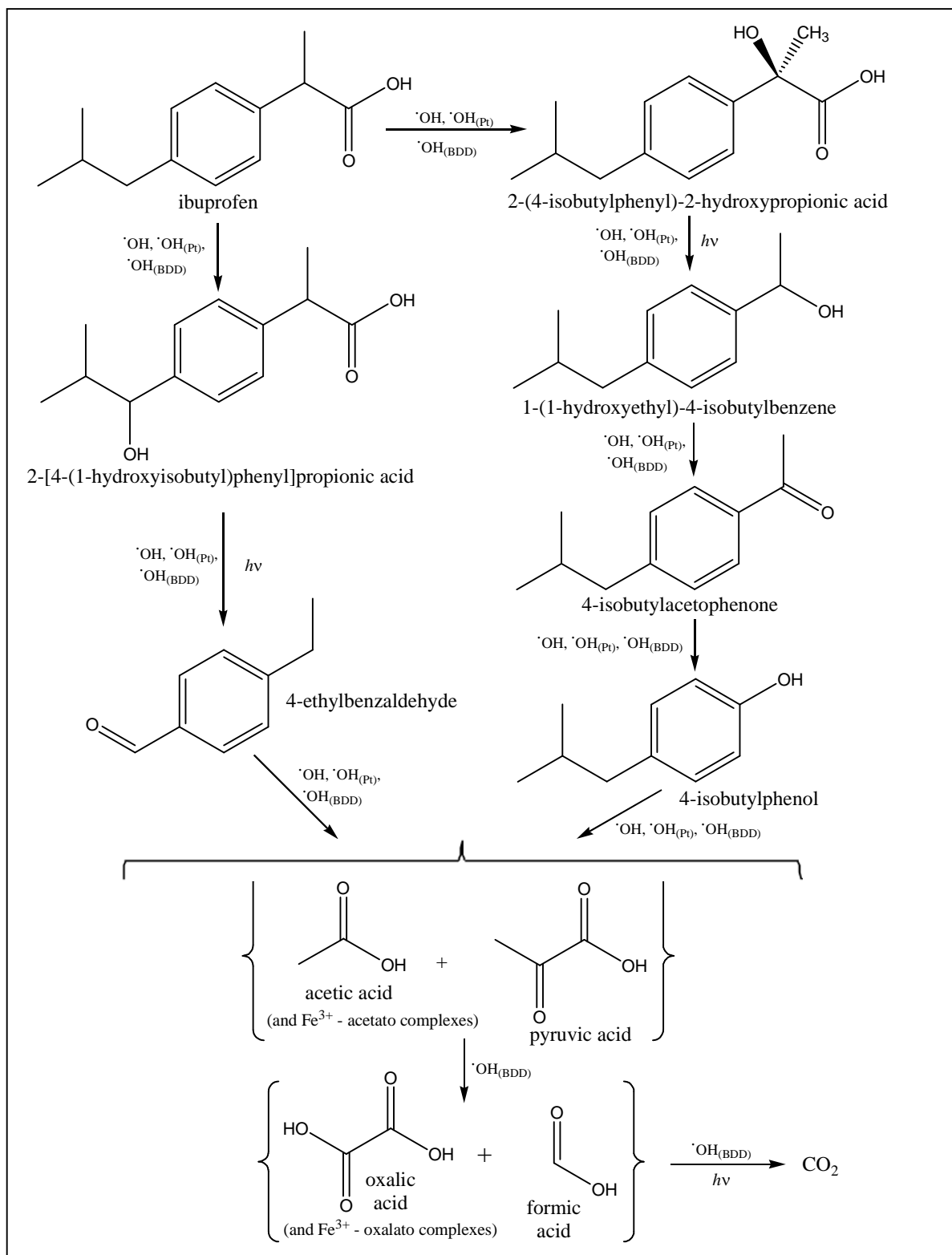


Figure 6.53. Proposed pathway for the degradation of ibuprofen in acidic medium by EAOPs.

The ibuprofen molecule undergoes an hydroxylation in position 1 of its lateral isobutyl chain as a result of the oxidation by $\bullet\text{OH}$ radicals from either the bulk solution $\bullet\text{OH}_{(\text{bulk})}$ or those adsorbed on the Pt or BDD anode surface ($\bullet\text{OH}_{(\text{Pt})}$ and $\bullet\text{OH}_{(\text{BDD})}$, respectively). This hydroxylation yields 2-[4-(1-hydroxyisobutyl)phenyl]propionic acid, which undergoes further oxidation and decarboxylations up to yield 4-ethylbenzaldehyde.

Ibuprofen can also suffer an hydroxylation in position 2 of its propionic acid group yielding 2-(4-isobutylphenyl)-2-hydroxypropionic acid. This latter species undergoes a decarboxilation leading to 1-(1-hydroxyethyl)-4-isobutylbenzene, whose hydroxyl group is oxidated yielding 4-isobutylacetophenone, which still loses its acetyl group followed by an hydroxylation and 4-isobutylphenol arises.

The breakdown of the formed aromatic intermediates leads to acetic and pyruvic acids, which are subsequently oxidized yielding oxalic and formic acids. These latter compounds are eventually mineralized into carbon dioxide.

6.4 Study of diclofenac mineralization by electrochemical advanced oxidation processes / Estudi de la mineralització del diclofenac mitjançant mètodes electroquímics d'oxidació avançada

In this section, the elimination of the antiinflammatory drug diclofenac is studied. The influence of several parameters on the mineralization efficiency of EAOPs, such as the nature of electrodes (platinum vs BDD) and their structure (mesh electrodes vs bulk electrodes), the applied current density and the effect of pH are first discussed. Finally, the concentration evolution of the antiinflammatory and the several arisen intermediates are shown and discussed for the several parameters.

6.4.1 Effect of experimental parameters on diclofenac mineralization / *Efecte de parameters experimental a la mineralització del diclofenac*

The mineralization of sodium diclofenac salt was studied using only anodic oxidation-based methods. Electro-Fenton and photoelectron-Fenton treatments were not used for the mineralization of diclofenac because the low pH needed for the good operation of these treatments would convert the diclofenac sodium salt into its neutral form ($pK_a = 4.7$) [165], which would immediately precipitate as it has a water solubility of only 2.37 mg L^{-1} [166].

At pH values below 5.0 the formation of a white turbidity indicates the precipitation of the neutral form of diclofenac. Also, pH values above 7.0 involve the dissolution of CO_2 arisen from the drug mineralization, which has to be removed prior to TOC analysis by a method based on acidification which would make the drug precipitate. Because of this fact, an operation pH 6.0 was selected after making sure that at this pH no significant amount of CO_2 was dissolved and that diclofenac sodium salt solutions were stable during several days.

In the first experiments, the electrolysis of 100 mg L^{-1} diclofenac sodium salt solutions with $0.05 \text{ M Na}_2\text{SO}_4$ as background electrolyte, at pH 6.0 and $35.0 \text{ }^\circ\text{C}$ was studied under anodic

oxidation-based treatments in which 3 cm² BDD or platinum anodes operated at a current intensity of 300 mA with a stainless steel cathode of the same surface area.

The expected main oxidant species for these mineralization treatments is the $\bullet\text{OH}$ radical, adsorbed on the anode surface and arisen from the oxidation of water (reaction (1.1)).

Figure 6.54 shows that the treatment using the Pt anode is capable of mineralizing only half of diclofenac from solution after 6 hours, getting practically stopped after the 2 first hours of trial. This stop can be explained by the formation of aliphatic carboxylic intermediates, which would be resist oxidation at the platinum anode. The much more reactive $\bullet\text{OH}$ radicals, electrochemically generated on the BDD anode surface, enable it to oxidize even these more recalcitrant intermediates up to attain a mineralization of 92% at the end of the trial.

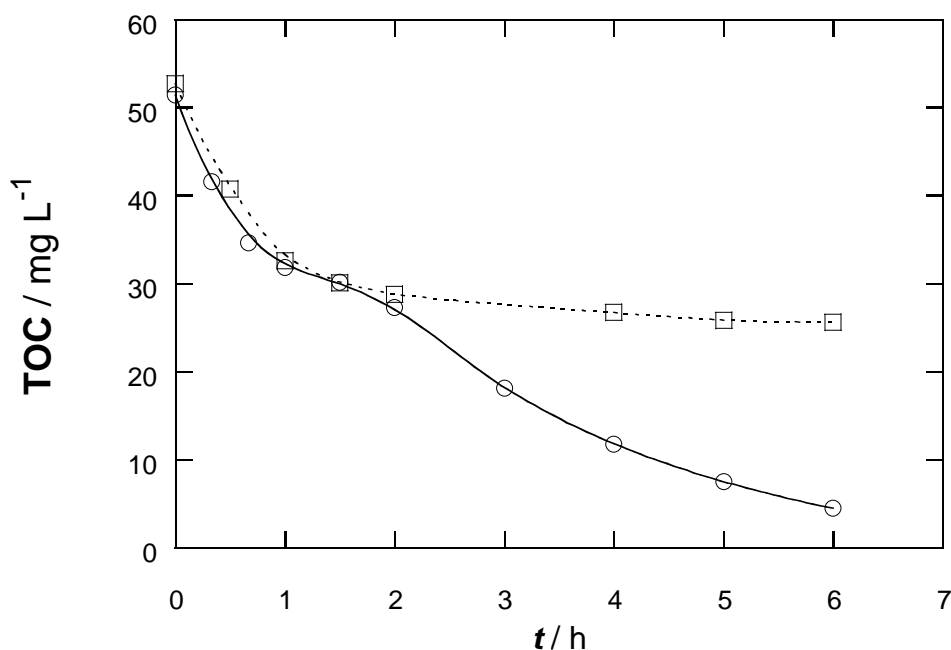
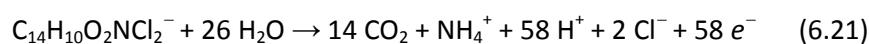


Figure 6.54. TOC abatement during electrolyses at 100 mA cm⁻² for 100 mg L⁻¹ of a 100 mg L⁻¹ diclofenac sodium salt solutions containing 0.05 M Na₂SO₄ at pH 6.0 and 35.0 °C. Anodic oxidation involving a stainless steel cathode coupled to a: (○) BDD anode, (□) platinum anode.

The mineralization process of diclofenac can be stoichiometrically written as



considering that NH_4^+ ion is formed instead of NO_3^- or NO_2^- .

The mineralization current efficiency (MCE) for the electrolysis of diclofenac can be calculated by equation (6.20) where n takes the value of 58 from reaction (6.21).

From expression (6.20) MCE values are calculated and plotted in Figure 6.55.

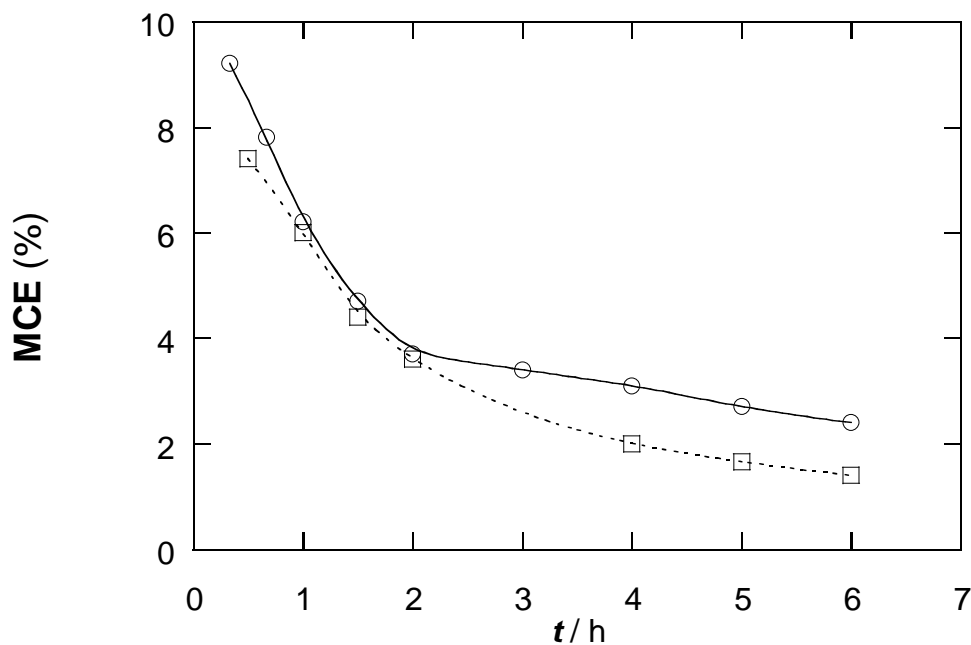


Figure 6.55. Mineralization Current Efficiency for electrolyses of 100 mL of a 100 mg L^{-1} diclofenac sodium salt solution containing $0.05 \text{ M Na}_2\text{SO}_4$ at 100 mA cm^{-2} , pH 6.0 and $35.0 \text{ }^\circ\text{C}$. The applied method is an anodic oxidation with a stainless steel cathode coupled to a: (○) BDD anode, (□) platinum anode.

During the first 2 h of electrolysis both treatments, Pt-AO and BDD-AO display a similar mineralization current efficiency. It is only after that point that the lower degradation efficiency of $\bullet\text{OH}$ radicals chemisorbed at the platinum anode is observed.

New electrodic configurations

Since the low solubility of the diclofenac sodium salt at acidic pH prevents the application of electro-Fenton treatments, another type of electrode is implemented: a niobium-based mesh BDD electrode which is active on its both sides.

Niobium-based mesh BDD electrodes (NbMBDD) can be assembled in a stack in which one of these electrodes works as anode and the other as cathode, and between them a conducting polymeric membrane which works as an electrolyte (SPE or solid polymer electrolyte) can be integrated (see Figures 5.5 – 5.7). The integration of such membrane makes the addition of a salt as support electrolyte unnecessary and makes feasible the electrolysis of the drug without addition of any background electrolyte. The membrane used in this MEA (membrane electrode assembly) is a Nafion[®] 324 membrane.

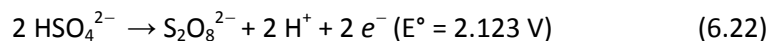
The new configurations used for the mineralization of diclofenac are described:

NbMBDD/NbMBDD	Anodic oxidation using two assembled Niobium-based BDD mesh electrodes, one acting as a cathode and the other the anode. The solution to be treated contains 0.05 M Na ₂ SO ₄ as background electrolyte.
NbMBDD/SPE/NbMBDD	Anodic oxidation using two assembled Niobium-based BDD mesh electrodes with a Nafion [®] 324 membrane between them, acting as electrolyte. The solution to be treated contains 0.05 M Na ₂ SO ₄ .
NbMBDD/SPE/NbMBDD-NS	Anodic oxidation using two assembled Niobium-based BDD mesh electrodes with a Nafion [®] 324 membrane between them. The treated solution does not contain any background electrolyte. (NS states for <i>No Sulfate</i>).

In the first experiments, 26.8 cm² Niobium-based mesh BDD electrodes were used to treat 0.5 L of 100 mg L⁻¹ diclofenac sodium salt solutions. The electrolyses took place at pH 6.0 and 35.0 °C. These trials were carried out at a current density of 100 mA cm⁻².

Figure 6.56 shows the TOC evolution of the mineralization trials using the Niobium-based mesh BDD electrodes. The use of these electrodes assembled with a Nafion[®] membrane for the mineralization of a solution of diclofenac containing 0.05 M Na₂SO₄ (NbMBDD/SPE/NbMBDD method) gave very poor results, obtaining only 55% mineralization after 6 hours of treatment. The oxidation power of the NbMBDD electrodes when their most active face is covered by the Nafion[®] membrane hindering the drug molecules from approaching the adsorbed •OH radicals is based in the generation of ozone (reaction (6.15)), which is then released into the solution and reacts with diclofenac and its degradation intermediates.

The reason explaining the bad performance of this electrode when assembled with the Nafion[®] membrane is the presence of the background electrolyte Na₂SO₄. The formation of peroxodisulfate anion, which is a competitive process in front of the oxidation of water to yield ozone (E° = 2.076 V) takes place according to



Thus, the presence of sulfate from the background electrolyte diminishes the rate in which ozone is produced, thus limiting the main oxidative process and leading the system composed by niobium-meshed BDD assembled with Nafion[®] to attain a very poor mineralization of only about the half of the treated drug.

If the Nafion[®] membrane is removed (NbMBDD/NbMBDD method), a far better mineralization is attained, reaching 89% of mineralization. With no solid polymer electrolyte present, the most active inner sides of the electrodes are not blocked and diclofenac is not hindered from entering in contact with the slightly adsorbed hydroxyl radicals, thus leading to a much efficient mineralization of the treated drug.

If instead of removing the Nafion[®] membrane the cell operates in a solution without background electrolyte, the mineralization of diclofenac also attains 89% mineralization after the end of the experiment. In this case the mineralization acceleration is explained by the enhancement of the reaction (6.15), thus allowing a much more significant production of ozone, which would account for most of the mineralization of the drug.

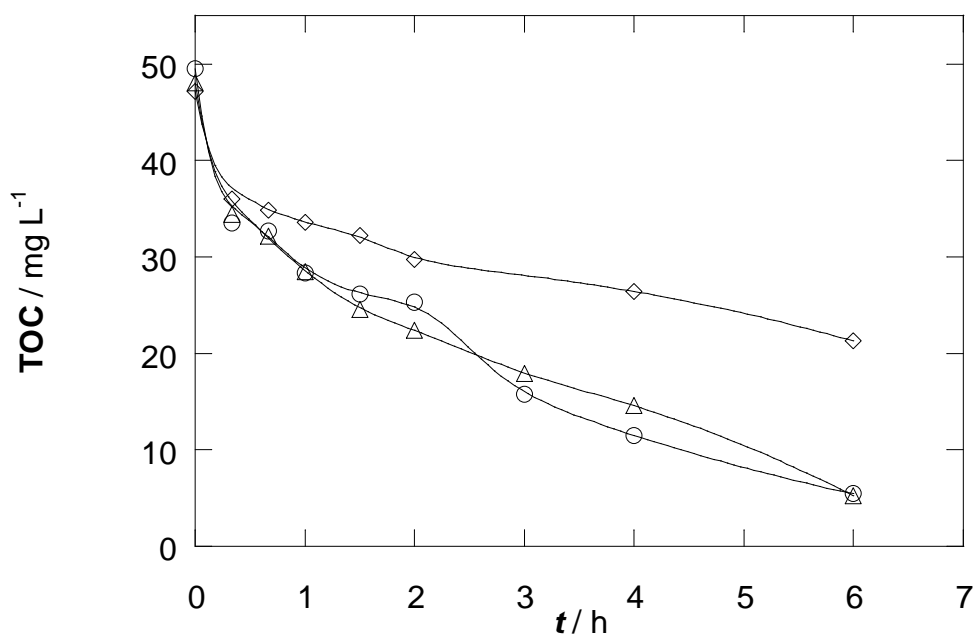


Figure 6.56. TOC abatement during electrolysis at 100 mA cm^{-2} for 500 mL of a 100 mg L^{-1} diclofenac sodium salt solution containing $0.05 \text{ M Na}_2\text{SO}_4$ at pH 6.0 and $35.0 \text{ }^\circ\text{C}$. The electrodes have an area of 26.8 cm^2 . (○) NbMBDD/NbMBDD, (△) NbMBDD/SPE/NbMBDD-NS, (◇) NbMBDD/SPE/NbMBDD.

The mineralization current efficiencies for the treatments with niobium-based mesh BDD electrodes were also calculated and plotted in Figure 6.57.

As expected, the poorest current efficiency obtained is that for the NbMBDD/SPE/NbMBDD treatment where the simultaneous presence of both, the Nafion[®] membrane, which prevents the drug molecules to approach the more active inner anode side, where most part of $\bullet\text{OH}$ adsorbed radicals are present, and the Na_2SO_4 background electrolyte, which reacts at the anode competing against the generation of ozone, causes an inefficient mineralization.

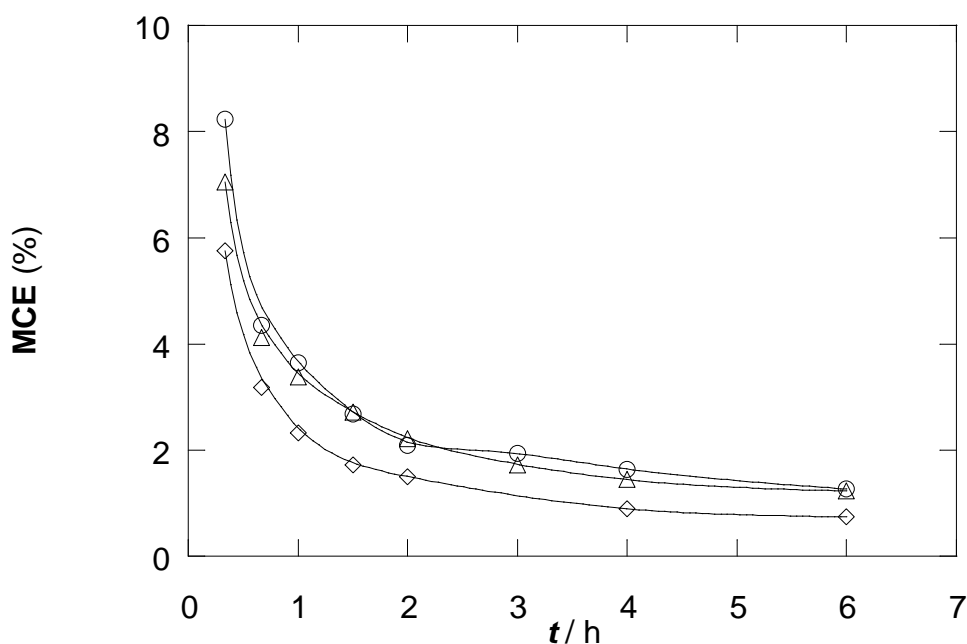


Figure 6.57. Mineralization current efficiency for electrolyses of 500 mL of 100 mg L^{-1} diclofenac sodium salt solutions containing $0.05 \text{ M Na}_2\text{SO}_4$ at 100 mA cm^{-2} at pH 6.0 and $35.0 \text{ }^\circ\text{C}$. The area of the electrodes was 26.8 cm^2 . (O) NbMBDD/NbMBDD, (◇) NbMBDD/SPE/NbMBDD, (△) NbMBDD/SPE/NbMBDD-NS.

The current efficiency for the experiments with the assembled mesh electrodes suffers a much steeper drop when compared to those using a 100 mL cell and BDD or platinum coupled with stainless steel cathode without assembling the electrodes. As this could possibly be caused by the important differences in size of the electrodes (3 cm^2 area of platinum and BDD electrodes vs. 26.8 cm^2 for NbMBDD) and the treatment vessel, further experiments were carried out in a 100 mL cell and using NbMBDD assembled electrodes of 3 cm^2 of area, so that the regime conditions are identical.

A series of experiments, then, were carried out for the same treatments based on the assembled NbMBDD electrodes with 3 cm^2 electrodes and a working cell of 100 mL capacity. The mineralization curves of these experiments, displayed on Figure 6.58, show less powerful TOC decays in comparison with their larger counterparts because the ratio between the volume of treated solution and the electrode surface has been increased when going from 500 mL treated by 26.8 cm^2 electrodes to 100 mL treated by 3 cm^2 electrodes at the same applied current density. However, the mineralization current efficiency is increased (Figure 6.59). This increase is explained by the better stirring conditions inherent to the 100 mL capacity vessel, which allow diclofenac and its intermediates to easily reach the electrode surface.

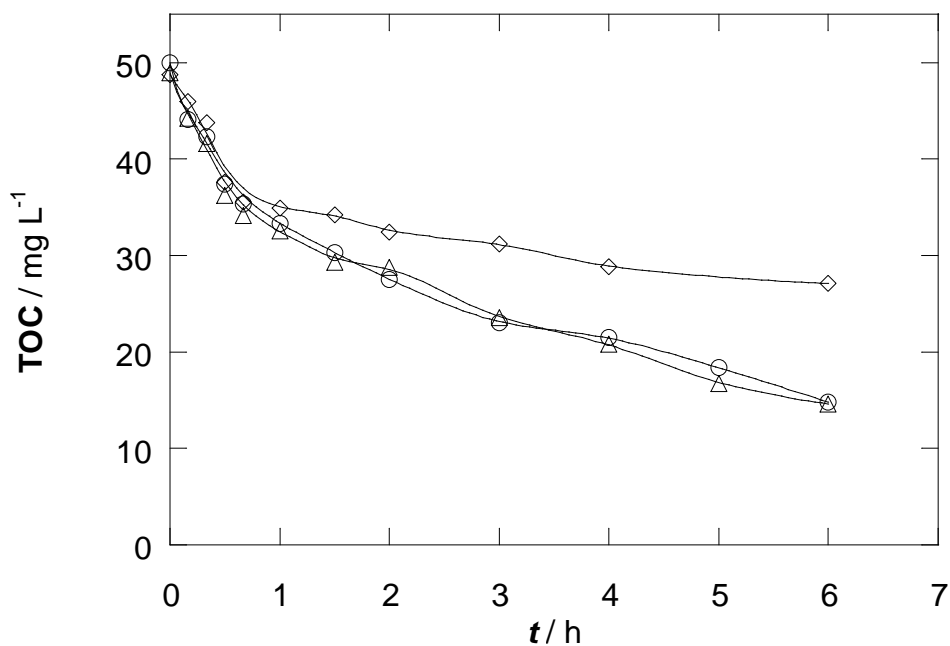


Figure 6.58. TOC abatement during electrolysis at 100 mA cm^{-2} for 100 mL of 100 mg L^{-1} diclofenac sodium salt solutions containing $0.05 \text{ M Na}_2\text{SO}_4$ at pH 6.0 and $35.0 \text{ }^\circ\text{C}$. The electrodes had a geometrical area of 3 cm^2 . (O) NbMBDD/NbMBDD, (Δ) NbMBDD/SPE/NbMBDD-NS, (\diamond) NbMBDD/SPE/NbMBDD.

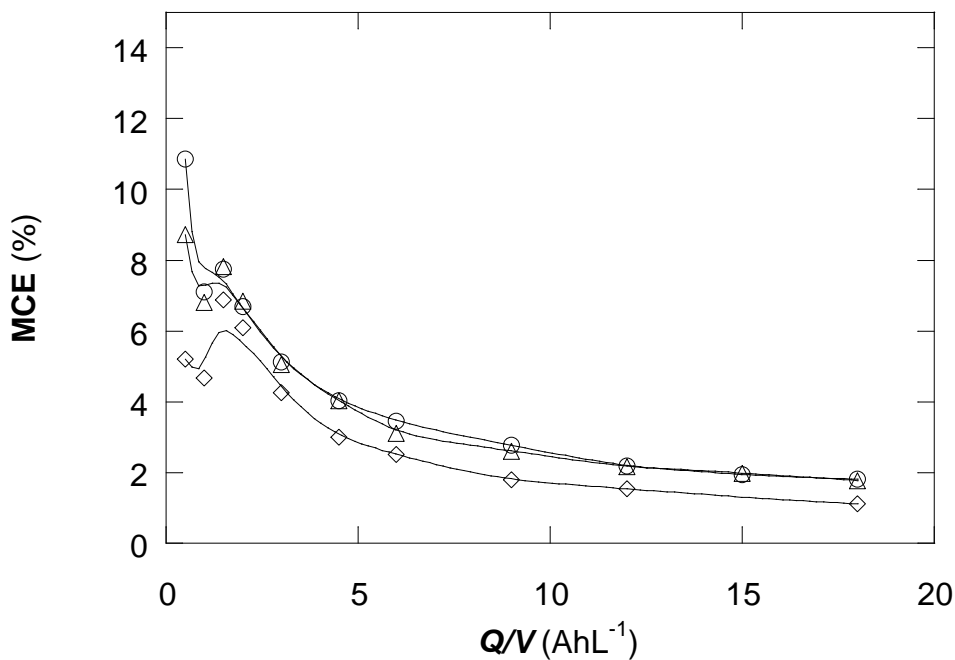


Figure 6.59. Mineralization current efficiency for electrolyses of 100 mL of 100 mg L^{-1} diclofenac sodium salt solutions containing $0.05 \text{ M Na}_2\text{SO}_4$ at 100 mA cm^{-2} at pH 6.0 and $35.0 \text{ }^\circ\text{C}$. The area of the electrodes is 3 cm^2 . (O) NbMBDD/NbMBDD, (\diamond) NbMBDD/SPE/NbMBDD, (Δ) NbMBDD/SPE/NbMBDD-NS.

As in the previous experiments using Nafion[®] based NbMBDD electrodes, NbMBDD/NbMBDD and NbMBDD/SPE/NbMBDD-NS treatments are those attaining a higher mineralization percentage of diclofenac, even though this extent is not very high (only 72% each one). The absence of the Nafion[®] membrane in NbMBDD/NbMBDD treatment has as a result better interaction possibilities between the $\bullet\text{OH}$ radicals physisorbed on the BDD surface and the dissolved diclofenac, since there is no Nafion[®] membrane to hinder such interactions as in the NbMBDD/SPE/NbMBDD treatment, where the mineralization extent only attains a poor 45%. Although the Nafion[®] membrane is also present in NbMBDD/SPE/NbMBDD-NS treatment, the absence of background Na_2SO_4 electrolyte favours the generation of ozone. O_3 can destroy species with aromatic rings very quickly and the elimination of such compounds leads to a relatively important TOC abatement despite the presence of the $\bullet\text{OH}$ oxidation-hindering Nafion[®] membrane.

6.4.2 Identification of diclofenac and its mineralization intermediates time-course / *Estudi de l'evolució del diclofenac i dels seus intermedis de mineralització*

The concentration of diclofenac was monitored during the several mineralization experiments by means of reversed-phase liquid chromatography.

Figure 6.60 shows that under Pt-AO treatment it takes diclofenac 6 hours before being totally removed from the treated solution. When replacing the platinum anode by a BDD anode (BDD-AO treatment), the destruction of diclofenac is greatly enhanced thanks to the highly reactive $\bullet\text{OH}$ radicals formed on the BDD surface, resulting in the practically total elimination of diclofenac in 4 hours of treatment. NbMBDD/SPE/NbMBDD treatment shows a similar effect to that of BDD-AO, removing over 90% of diclofenac after 4 hours of electrolysis. NbMBDD/NbMBDD treatment shows a slightly faster removal of the drug than both BDD-AO and NbMBDD/SPE/NbMBDD treatments during the first 2 hours of treatment. After this point, it slows down, but also reaches the total removal of diclofenac at 4 hours of time.

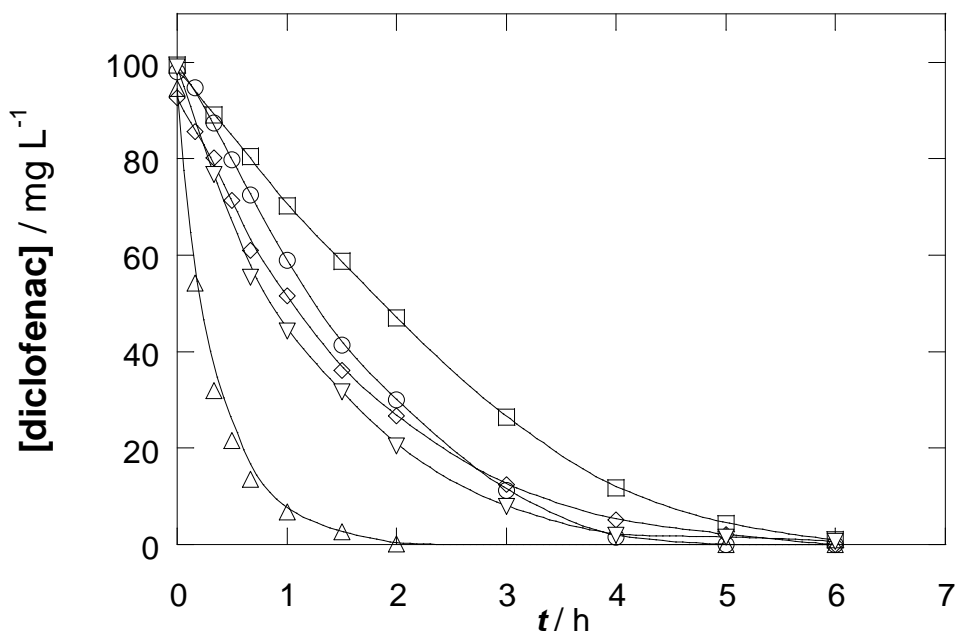


Figure 6.60. Monitoring of the concentration of diclofenac during the electrolysis at 100 mA cm^{-2} for 100 mL of 100 mg L^{-1} diclofenac sodium salt solutions containing $0.05 \text{ M Na}_2\text{SO}_4$ at $\text{pH } 6.0$ and $35.0 \text{ }^\circ\text{C}$. The electrodes had a geometrical area of 3 cm^2 . (∇) NbMBDD/NbMBDD, (\triangle) NbMBDD/SPE/NbMBDD-NS, (\diamond) NbMBDD/SPE/NbMBDD, (\circ) BDD-AO, (\square) Pt-AO.

Yet the most spectacular enhancement occurs when diclofenac is treated with niobium-based mesh BDD electrodes assembled with a Nafion[®] membrane between them acting as a solid polymer electrolyte and in the absence of Na₂SO₄ in the solution (NbMBDD/SPE/NbMBDD-NS treatment). Under this degradation treatment the drug only stays 2 hours in the solution. In this treatment, the inner side of the anode, where most significant amount of •OH radicals are generated, is covered with a Nafion[®] membrane which prevents diclofenac molecules from approaching the anode surface. That suggests that •OH radicals would not account for most of the elimination of diclofenac. Another fact that supports this possibility is the much poorer mineralization efficiency of diclofenac molecule under the NbMBDD/NbMBDD treatment (only 72% after 6 hours, Figure 6.58), where there is no membrane present, and the most active inner anode side is not hindered, allowing the adsorbed •OH radicals present at its surface to come in contact with dissolved diclofenac.

Figure 6.61 shows concentrations of ozone generated during the several diclofenac mineralization treatments.

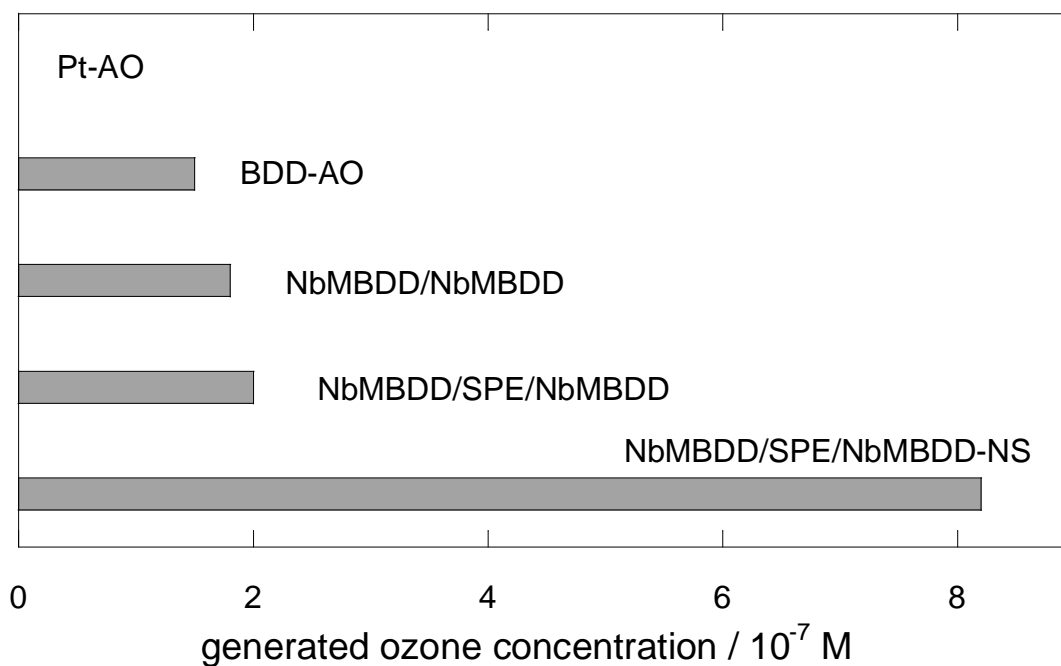


Figure 6.61. Detected concentrations of ozone during several treatments applied for the mineralization of 100 mg L⁻¹ diclofenac sodium salt solutions with 3 cm² electrodes at a current density of 100 mA cm⁻², 35.0 °C and pH 6.0. All solutions contained 0.05 M Na₂SO₄ except that treated with the NbMBDD/SPE/NbMBDD-NS method, which did not contain any background electrolyte.

When operating under the NbMBDD/SPE/NbMBDD-NS treatment, a strong smell of ozone can be felt. This smell, as indicator of ozone presence, was not perceived during the other treatments, suggesting that this oxidant molecule would be generated to a lesser extent in them. In order to evaluate the generated concentration of ozone for the different applied treatments the indigo method was used [167].

The results of the measurements displayed on Figure 6.61 show a significantly much bigger generated concentration of ozone when the Nafion[®] membrane was working as a solid polymer electrolyte because of the absence of Na₂SO₄ electrolyte in the solution, where a concentration of $8.2 \cdot 10^{-7} \text{ mol L}^{-1}$ was generated against concentrations below $2.0 \cdot 10^{-7} \text{ mol L}^{-1}$ for all other mineralization treatments. The fact that the NbMBDD/SPE/NbMBDD-NS treatment also registered the fastest decay for diclofenac strongly suggests that ozone is the responsible for this faster destruction, since ozone can break aromatic rings very quickly, as observed in paracetamol ozonation treatments. The much lower values of generated ozone for the other treatments would explain the much longer presence of diclofenac in solution when those treatments were applied.

- Aromatic intermediates / *Intermedis aromàtics*

2,6-Dichloroaniline

Small concentrations of 2,6-dichloroaniline were detected for all mineralization treatments except the Pt-AO one. Figure 6.62 shows the evolution of this intermediate for all applied treatments. This haloaromatic amine is less accumulated and faster removed from the medium under the NbMBDD/SPE/NbMBDD-NS method, where it does not even reach 0.5 mg L⁻¹ of maximum concentration and is totally eliminated after 3 hours of electrolysis. This is consistent with the higher generation of ozone associated to its treatment, as ozone can oxidize aromatic compounds faster than adsorbed •OH radicals.

Much less efficient is the NbMBDD/NbMBDD treatment, where a Na₂SO₄ background electrolyte is used instead of the Nafion[®] SPE. These conditions lead to a much smaller generation of ozone, which result in a similar maximum attained concentration for this haloaromatic compound (slightly above 0.5 mg L⁻¹), but the time needed to completely remove this intermediate from the solution is doubled.

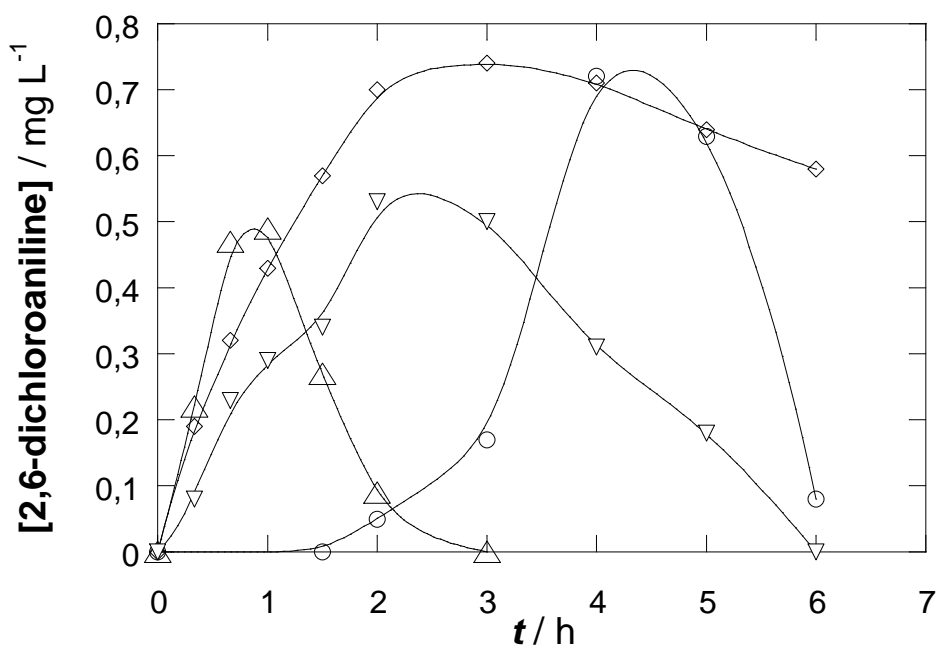


Figure 6.62. Monitoring of the concentration of the intermediate 2,6-dichloroaniline during the electrolysis at 100 mA cm⁻² for 100 mL of a 100 mg L⁻¹ diclofenac sodium salt solution containing 0.05 M Na₂SO₄ at pH 6.0 and 35.0 °C. The electrodes had a geometrical area of 3 cm². (○) BDD-AO, (▽) NbMBDD/NbMBDD, (△) NbMBDD/SPE/NbMBDD-NS, (◇) NbMBDD/SPE/NbMBDD.

This result shows again that the oxidant activity of O_3 accounts for most of the elimination of the aromatic intermediates and diclofenac itself, in comparison with the activity of $\bullet OH$ radicals. Under the NbMBDD/SPE/NbMBDD method, a much higher concentration above 0.7 mg L^{-1} 2,6-dichloroaniline is accumulated, and most of it remains in the solution after 6 hours of the trial. The poor performance of this method to eliminate aromatic compounds is explained by the combination of two effects. First, the presence of the background electrolyte prevents the system from generating an important amount of ozone, which would lead to a faster removal of the aromatic degradation intermediates such as 2,6-dichloroaniline. Secondly, the presence of the Nafion[®] membrane between the two electrodes prevents the aromatic molecules from reacting with most of $\bullet OH$ radicals, which are mostly adsorbed on the inner part of the anode surface, thus hindering the oxidation of aromatic species.

Under the BDD-AO treatment also a big amount of 2,6-dichloroaniline is accumulated (near 0.7 mg L^{-1}), but it is rapidly eliminated from solution. Taking into account that under the BDD-AO treatment small concentrations of ozone are generated, the sharp decay of the concentration of this intermediate can only be ascribed to the activity of the $\bullet OH$ radicals adsorbed at the BDD surface, which are not hindered at all.

2,6-Dichloroaniline could not be detected under Pt-AO treatment. As the detected concentrations of this intermediate are so low for the other treatments, the possibility that a certain amount under the LOD of this substance may have arisen is not ruled out.

2,6-Dichlorohydroquinone

2,6-Dichlorohydroquinone was detected as an intermediate formed from the degradation of diclofenac for all of the applied mineralization methods.

The evolution of 2,6-dichlorohydroquinone is displayed in Figure 6.63. The curves associated to BDD-AO and Pt-AO treatments show a remarkably small accumulation of this haloaromatic intermediate in comparison with the other applied mineralization treatments.

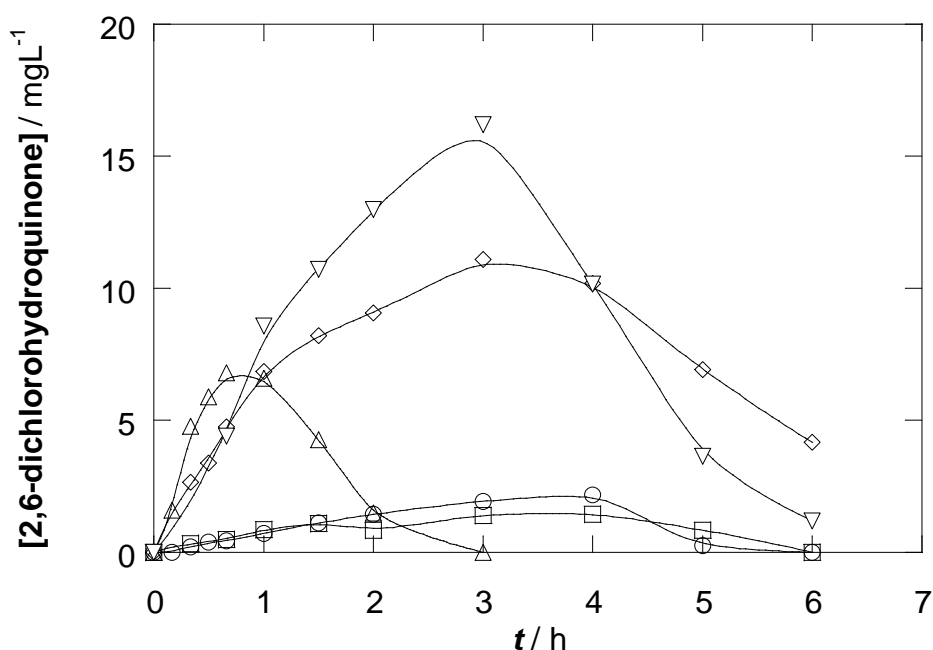


Figure 6.63. Monitoring of the concentration of the intermediate 2,6-dichlorohydroquinone during the electrolysis at 100 mA cm^{-2} for 100 mL of 100 mg L^{-1} diclofenac sodium salt solutions containing $0.05 \text{ M Na}_2\text{SO}_4$ at pH 6.0 and $35.0 \text{ }^\circ\text{C}$. The electrodes had a geometrical area of 3 cm^2 . (○) BDD-AO, (□) Pt-AO, (▽) NbMBDD/NbMBDD, (△) NbMBDD/SPE/NbMBDD-NS, (◇) NbMBDD/SPE/NbMBDD.

The high reactivity and oxidation efficiency of the weakly physisorbed $\bullet\text{OH}$ radicals of the silicon-based BDD anode would account for the low accumulation of 2,6-dichlorohydroquinone. The low accumulated amount of this product when applying the Pt-AO treatment is not surprising, as the slow destruction of the parent compound, diclofenac, limits the rate of generation of its degradation intermediates, this haloaromatic compound being one amongst them.

The treatments based on the NbMBDD electrodes show a higher accumulated concentration for this intermediate. These results again suggest the less efficient generation of $\bullet\text{OH}$ radicals on the surface of this electrode. Among them, only for the NbMBDD/SPE/NbMBDD-NS treatment does the concentration of 2,6-dichlorohydroquinone go down to zero as a result of the breaking of its aromatic ring by ozone, which is not present in significant amounts in NbMBDD/SPE/NbMBDD and NbMBDD/NbMBDD treatments.

- Aliphatic carboxylic intermediates / *Intermedis carboxilics alifàtics*

Oxalic acid has been detected and its concentration has been monitored for all of applied oxidation treatments on diclofenac, as shown in Figure 6.64.

Oxalic acid is only completely eliminated after 6 hours of trial by the BDD-AO treatment. Under this treatment, the concentration of oxalic acid attains a maximum concentration near 8 mg L^{-1} before disappearing. This treatment had already proven to be very effective to remove oxalic acid by the action of the weakly adsorbed $\bullet\text{OH}$ radicals on the surface of the silicon based BDD electrode. The weak physisorption of these radicals allow them to react freely with surrounding oxalic acid molecules. The Pt-AO treatment follows a very different pattern for the concentration of oxalic acid. Under this treatment, oxalic acid experiences a slow steady increase in its concentration which does not revert at the end of trial. The slow destruction of diclofenac under this treatment only leads to a slow formation of aromatic and aliphatic carboxylic acids. The formation of oxalic acid, along with the other degradation intermediates of diclofenac is kinetically limited by the slow elimination of diclofenac.

Oxalic acid accumulates up to 11.7 and 15.3 mg L^{-1} under NbMBDD/NbMBDD and NbMBDD/SPE/NbMBDD treatments, respectively. These values are comparatively higher than the maximum 8 mg L^{-1} attained under the BDD-AO treatment, and none of the treatments with the niobium-based BDD electrode is able to get the concentration of oxalic acid down to zero after 6 hours of electrolysis. These results show a clear better performance of the silicon-based BDD – stainless steel electrodic pair in comparison with the niobium-based mesh BDD (with or without Nafion[®] membrane) pair. A lower superficial concentration of $\bullet\text{OH}$ on the surface of the niobium-based BDD anode ($\bullet\text{OH}_{(\text{BDD})}$) than that on the surface of the silicon-based BDD one would explain the poorer performance of these treatments in comparison with that using the silicon-based BDD anode. When the electrolysis of diclofenac was carried out in the absence of background Na_2SO_4 electrolyte using NbMBDD as both anode and cathode with a Nafion[®] membrane between them working as a SPE, a very high maximum concentration of this acid is attained (22.8 mg L^{-1}). Since during this treatment a very large amount of O_3 is generated (as shown in Figure 6.61), the poor efficiency in the mineralization of oxalic acid can be explained by the generation of ozone (reaction (6.15)) in detriment of the generation of $\bullet\text{OH}$ radicals. Whereas $\bullet\text{OH}_{(\text{BDD})}$ can mineralize oxalic acid, O_3 has proven incapable of doing it.

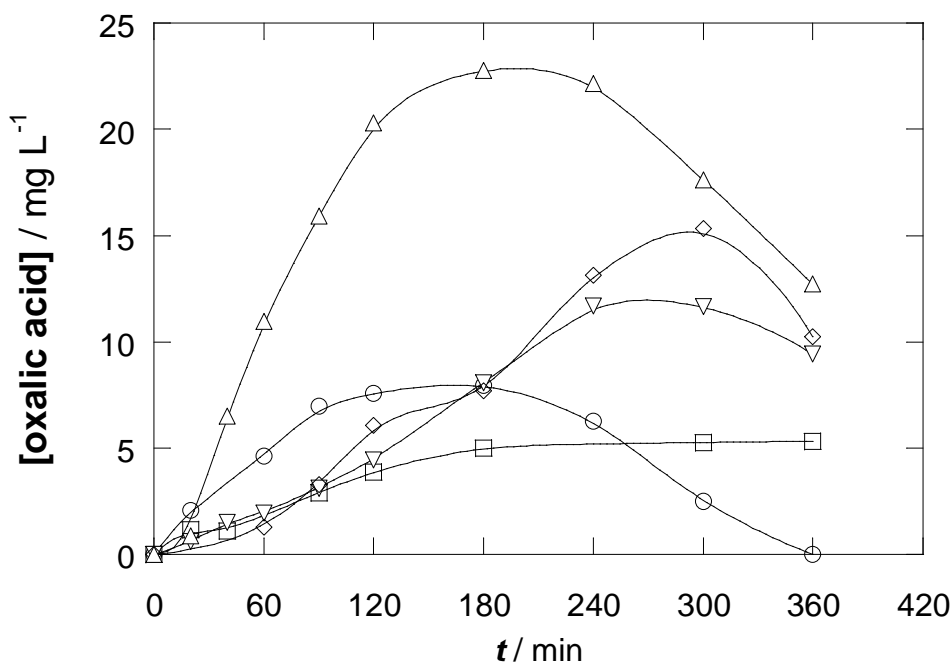


Figure 6.64. Monitoring of the concentration of oxalic acid during the electrolysis at 100 mA cm^{-2} for 0.1 L of 100 mg L^{-1} diclofenac sodium salt solutions containing $0.05 \text{ M Na}_2\text{SO}_4$ at $\text{pH } 6.0$ and $35.0 \text{ }^\circ\text{C}$. The electrodes had a geometrical area of 3 cm^2 . (○) BDD-AO, (□) Pt-AO, (▽) NbMBDD/NbMBDD, (△) NbMBDD/SPE/NbMBDD-NS, (◇)NbMBDD/SPE/NbMBDD.

Also formic acid has been detected for most of tested treatments, but in most of cases the low molar extinction quotient of formic acid did not allow a proper quantification of its concentration.

The highest concentrations of formic acid have been registered for the NbMBDD/SPE/NbMBDD-NS treatment, where its concentration reached about 9 mg L^{-1} after 5 hours of trial and stayed in solution after the end of the electrolysis at 6 hours. The strong ozone smell which can be felt when applying this treatment indicates that in this oxidation method the generation of ozone takes place at a significant extent, in detriment of the generation of other oxidant species, such as $\bullet\text{OH}$ radicals and, since ozonation without catalysts can only achieve a limited mineralization of formic acid, since its ozonation rate constant is as low as $5 \cdot 10^{-2} \text{ M}^{-1}\text{s}^{-1}$ [168], this result is understandable. For the other treatments, with the exception of Pt-AO and BDD-AO for which this intermediate is not detected, formic acid is detected in much lower concentrations under the limit of quantification.

- Time-course of ions during diclofenac mineralization / *Evolució dels ions durant la mineralització del diclofenac*

The concentration of chloride was followed with time by means of ion exchange chromatography and a conductivity detector. Chloride anion displayed a peak at $t_R = 3.45$ min.

The results of this study are shown in Figure 6.65.

Under the Pt-AO method, the chloride concentration steadily increases up to 19.4 mg L^{-1} after 6 hours of electrolysis. This is a 87% of conversion from the chlorine atoms in diclofenac molecule to free chloride ion. Under all of the other oxidation treatments the concentration of free chloride ion does not even reach 5.7 mg L^{-1} (25% of diclofenac chlorine to chloride conversion). These results show again, as in the former case with chloroxylenol, that the BDD anode is able to oxidize the Cl^- which is released after the breakdown of degradation intermediates containing chlorine to Cl_2 .

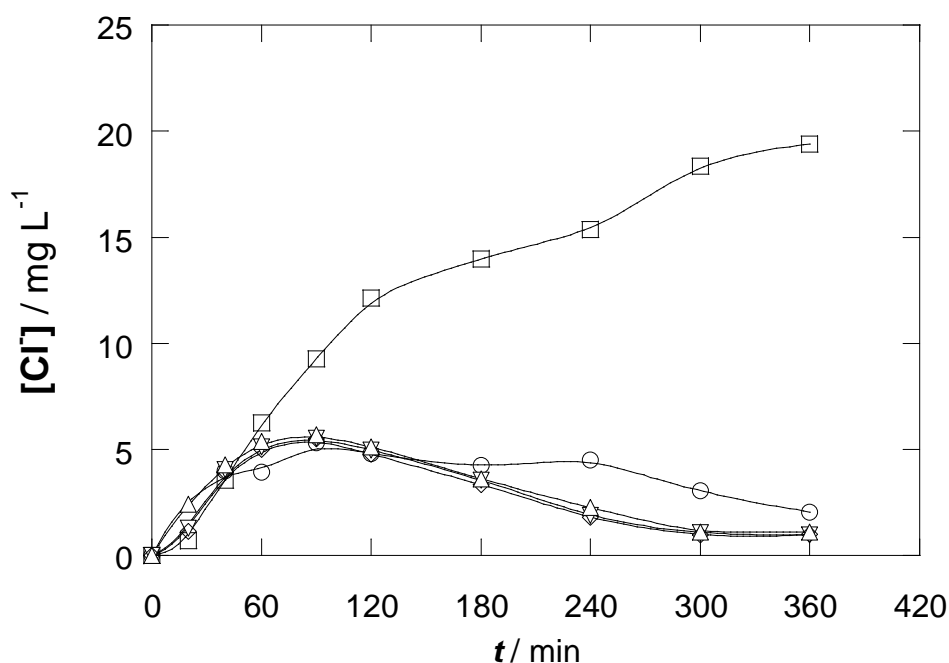


Figure 6.65. Monitoring of the concentration of chloride during the electrolysis at 100 mA cm^{-2} for 100 mL of a 100 mg L^{-1} diclofenac sodium salt solution containing $0.05 \text{ M Na}_2\text{SO}_4$ at $\text{pH } 6.0$ and $35.0 \text{ }^\circ\text{C}$. The electrodes had a geometrical area of 3 cm^2 . (○) BDD-AO, (□) Pt-AO, (▽) NbMBDD/NbMBDD, (△) NbMBDD/SPE/NbMBDD-NS, (◇) NbMBDD/SPE/NbMBDD.

Also the concentration of nitrate was followed during the application of EAOPs. The nitrate concentration profiles are plotted in Figure 6.66.

In all of treatments, the generated amount of nitrate is far away from the 100% of conversion from diclofenac amino group to nitrate ($4.55 \text{ mg L}^{-1} \text{ NO}_3^-$), which means that for all of these treatments a significant amount of nitrogen still stays in the solution. Part of this is expected to be NH_4^+ , which could not be analyzed and has been detected as a product in other diclofenac degradation treatments [169].

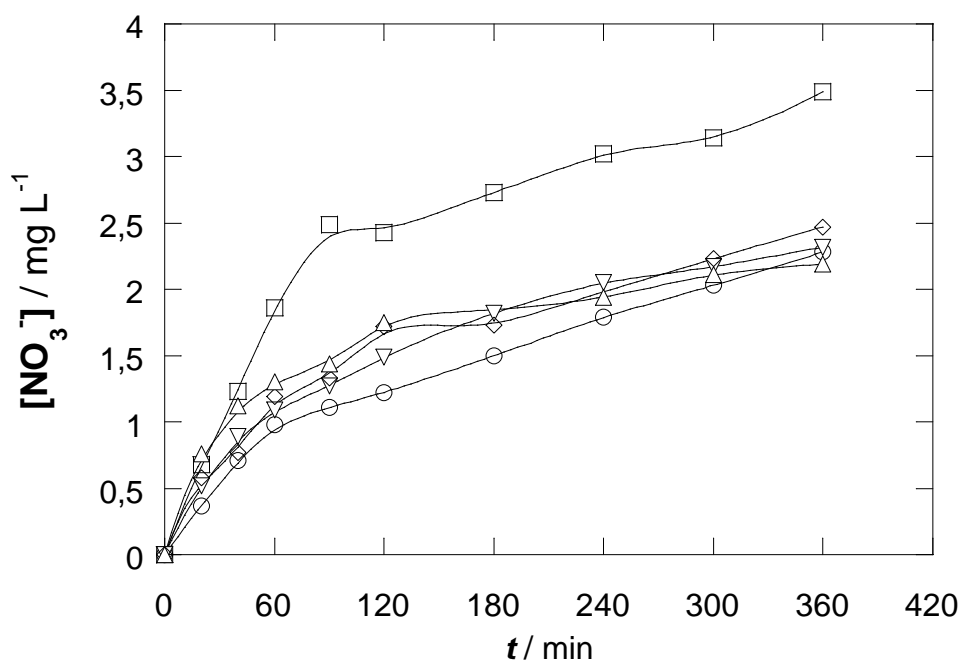


Figure 6.66. Monitoring of the concentration of nitrate during the electrolysis at 100 mA cm^{-2} for 100 mL of a 100 mg L^{-1} diclofenac sodium salt solution containing $0.05 \text{ M Na}_2\text{SO}_4$ at $\text{pH } 6.0$ and $35.0 \text{ }^\circ\text{C}$. The electrodes had a geometrical area of 3 cm^2 . (○) BDD-AO, (□) Pt-AO, (▽) NbMBDD/NbMBDD, (△) NbMBDD/SPE/NbMBDD-NS, (◇) NbMBDD/SPE/NbMBDD.

6.4.3 Proposal of a degradation pathway for the mineralization of diclofenac /
 Proposta d'un camí de degradació per a la mineralització del diclofenac

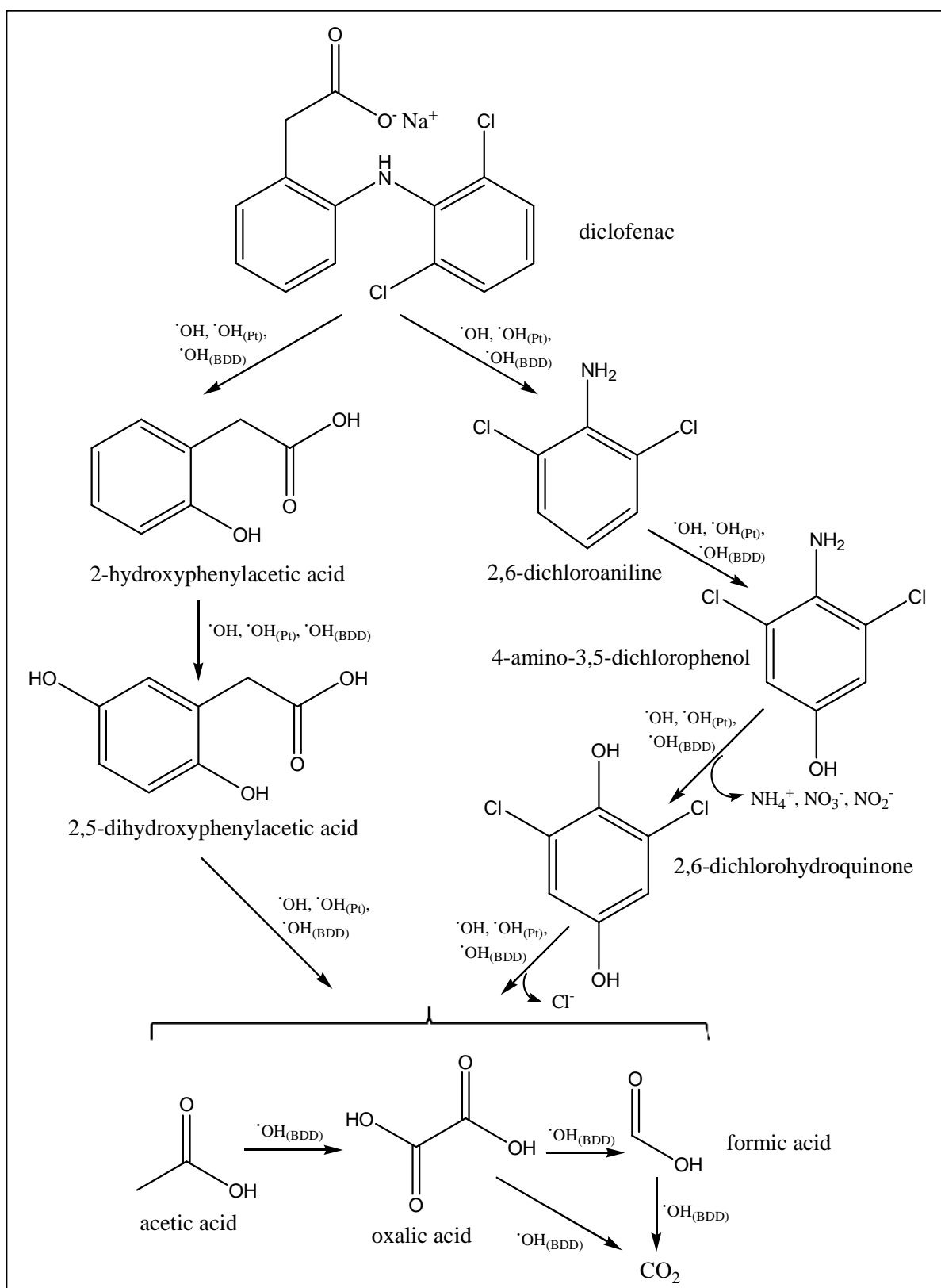


Figure 6.67. Proposed pathway for the degradation of diclofenac by EAOPs.

Diclofenac first degradation step would be the attack by $\bullet\text{OH}$ adsorbed on BDD, Pt or in the bulk solution to the amino group of the drug, which would lead to the splitting of the molecule into 2-hydroxyphenylacetic acid and 2,6-dichloroaniline.

2-Hydroxyphenylacetic acid undergoes an hydroxylation in position 5 of the aromatic ring yielding 2,5-dihydroxyphenylacetic acid. The aromatic ring of this molecule would be broken by a further attack of hydroxyl radical from which acetic and oxalic acids would arise.

Para-hydroxylation of 2,6-dichloroaniline leads to 4-amino-3,5-dichlorophenol, which would undergo further hydrolysis yielding 2,6-dichlorohydroquinone. The breakdown of the aromatic ring of 2,6-dichlorohydroquinone leads to the formation of acetic and oxalic acids.

Acetic acid hydroxylated by $\bullet\text{OH}$ adsorbed on the BDD surface also yield oxalic acid, which under further oxidation by the same $\bullet\text{OH}_{(\text{BDD})}$ degrades to formic acid. Both oxalic and formic acid are further degraded into CO_2 .